

Status of thesis

Title of thesis

Prediction of CO₂ Corrosion with the Presence of Low Concentrations Acetic Acid in Turbulent Flow Conditions

I MARTIN CHOIRUL FATAH

hereby allow my thesis to be placed at the Information Resource Center (IRC) of Universiti Teknologi PETRONAS (UTP) with the following conditions:

1. The thesis becomes the property of UTP.
2. The IRC of UTP may make copies of the thesis for academic purposes only.
3. This thesis is classified as

☐

Confidential

☒

Non-confidential

If this thesis is confidential, please state the reason:

The contents of the thesis will remain confidential for _____ years.

Remarks on disclosure:

Endorsed by

Signature of Author

Komplek LAPAN, B 11, No. 30,

Pekayon, Jakarta, Indonesia

Date: _____

Signature of Supervisor

Date: _____

UNIVERSITI TEKNOLOGI PETRONAS

Approval by Supervisors

The undersigned certify that have read, and recommend to The Postgraduate Studies Programme for acceptance, a thesis entitled **“Prediction of CO₂ Corrosion with the Presence of Low Concentrations Acetic Acid in Turbulent Flow Conditions”** submitted by **Martin Choirul Fatah** for the fulfillment of the requirements for the DEGREE OF MASTER OF SCIENCE IN MECHANICAL ENGINEERING

April 15th, 2009

Date

Signature : _____

Main Supervisor : _____

Date : _____

Co- Supervisor : _____

UNIVERSITI TEKNOLOGI PETRONAS

Prediction of CO₂ Corrosion with the Presence of Low Concentrations Acetic Acid in
Turbulent Flow Conditions

By

Martin Choirul Fatah

A THESIS

SUBMITTED TO THE POSTGRADUATE STUDIES PROGRAMME

AS A REQUIREMENT FOR THE
DEGREE OF MASTER OF SCIENCE IN
MECHANICAL ENGINEERING

BANDAR SERI ISKANDAR,

PERAK

APRIL, 2009

DECLARATION

I hereby declare that the thesis is based on my original work except for quotations and citations which have been duly acknowledged. I also declare that it has not been previously or concurrently submitted for any other degree at UTP or other institutions.

Signature : _____

Name : Martin Choirul Fatah

Date : _____

DEDICATION

Above all I want to dedicate this work

To My Parents for their loving care

To my Wife for her caring love

To my Children the fruit of love

ACKNOWLEDGEMENTS

I would like to express my sincere appreciation to my supervisor AP. Ir. Dr. Mokhtar Che Ismail, who has never given up correcting the mistakes I made, has encouraged me to broaden my viewpoint, and taught me the meaning of the life. His patience and dedication in directing us students on the way to success, and his goal of providing a reliable research working environment encouraged me to keep going. Under his supervision, I grew professionally and he helped me prepare for the new challenges in my career.

Great thanks go to my co-supervisor, Mr. Kamal Arif, who were always very confident in me and gave me full support and direction both in my daily life and academic work. Great thanks also go to AP. Dr. Bambang Ari Wahjoedi for his critiques and suggestion for my work and Dr. Khairul Fuad for his encouragement so I can be optimistic in face the world.

Furthermore I would like also to give a special word of appreciation, to all the mechanical engineering lecturers, all the mechanical engineering technicians, especially Mr. Anuar and Mr. Faisal, and all postgraduate officers.

I would like to acknowledge Mr. Yuli Panca Asmara and Mr. Budi Agung Kurniawan for their invaluable advice, critiques and true friendship. Special thanks also given to Indonesia Community in Bandar-U, V4D-T3 and PPI UTP. I feel living in my country with their presence.

I am very grateful to my parents, who taught me the meaning of struggle in this life. I would like to express my deep indebtedness to my wife and my children (Azahra Zeita Zavira, Indana Zulfa and Hasby Asad Bil Fathi) for their true love and support. Their loves is the power in my life and always make my life more colorful.

I would like also to acknowledge my Institution, Indonesia Institute of Sciences (LIPI) for the opportunity of postgraduate study.

Finally, I would like to acknowledge the scholarship granted by Universiti Teknologi PETRONAS.

ABSTRACT

CO₂ corrosion of mild steel with the presence of organic acids typically acetic acid (HAc) is a current concern in the oil and gas industry. However, this problem received relatively little attention in the corrosion analysis of oil and gas systems. Most of CO₂ corrosion prediction models do not consider the effect of acetic acid species in corrosivity analysis which strictly limits the prediction to CO₂ corrosion only. Recent studies have shown significant effect of acetic acid on CO₂ corrosion but contribution of low concentration up to 60 ppm is not addressed. Thus, the objective of this research is to study the kinetics and mechanism of CO₂ corrosion with the presence of low concentration of acetic acid in turbulent flow conditions at fixed pH and various temperatures. The electrochemical studies are based on linear polarization resistance (LPR) and potentiodynamic polarization. Rotating Cylinder Electrode (RCE) apparatus was used to simulate turbulent conditions producing shear stress representing pipe-flow condition. The experimental results are compared with the prediction by three openly available models: Norsok, Cassandra and de Waard Milliams models. Based on LPR results, low concentration of HAc below 40 ppm does not contribute much to corrosion rates. An appreciable increase in corrosion rate is observed for HAc concentration more than 40 ppm, whereby a maximum increase of 68 % at pH 5 and 120 % at pH 6 depending on temperatures. HAc increases corrosion rate by extra cathodic reaction which originated from the direct reduction and dissociation reactions. It is also observed that corrosion rate increases with increasing temperature. This is due to acceleration of anodic and cathodic reaction when temperature increases, also this is related with availability of more HAc species at higher temperature. Furthermore, an increase in corrosion rate due to the increase of rotational velocity is recorded in this study until 2000 rpm, beyond this not much effect of rotational velocity is observed. Flow effect is related to the transport of species towards and away from metal surface. Potentiodynamic polarization sweeps showed that the cathodic limiting current slightly increases with the presence of low concentration of HAc. There is no change in the mechanism of anodic reaction. The overall corrosion process is mainly controlled by a charge transfer process. It is indicated by corrosion current (i_{corr}) value lower than limiting current (i_{lim}). The

empirical prediction equation that considers the effect of low concentration of acetic acid is proposed based on LPR tests at pH 5 in turbulent conditions.

Keywords

CO₂ corrosion, acetic acid, turbulent flow conditions, extra cathodic reaction, prediction equation.

ABSTRAK

Pengakisan CO₂ keluli ringan yang disebabkan oleh asid organik lazimnya asid asetik (HAc) adalah perkara yang dihadapi oleh industri minyak dan gas pada masa ini. Namun, masalah ini tidak mendapat perhatian secukupnya dalam analisis pengakisan sistem minyak dan gas. Sebahagian besar model ramalan pengakisan CO₂ tidak mengambil kira kesan dari spesies asid asetik dalam analisis kepenghakisannya hanya menghadkan kepada ramalan pengakisan CO₂ sahaja. Kajian terkini hanya menunjukkan kesan ketara asid asetik di dalam pengakisan CO₂, namun fungsi penumpuan rendah sehingga 60 ppm tidak diuraikan. Oleh itu, objektif penyelidikan ini ialah mengkaji kinetik dan mekanisme pengakisan CO₂ dengan menggunakan penumpuan rendah asid asetik dalam keadaan aliran gelora pada pH tetap dan suhu pelbagai. Kajian elektrokimia diasaskan pada kerintangan pengutuban linear (LPR) dan pengutuban potensiodinamik. Alat elektrod silinder berputar (RCE) digunakan untuk mensimulasikan keadaan bergelora yang mengeluarkan tekanan kuat mewakili keadaan alir-paip. Keputusan ujikaji dibandingkan dengan ramalan daripada tiga model terbuka sedia ada: NORSOK, Cassandra dan de Waard Milliams. Ujian LPR menunjukkan tidak banyak kesan dari asid asetik di bawah 40 ppm terhadap kadar pengakisan. Kesan paling ketara dari kadar asid asetik dicerap lebih dari 40 ppm, di mana maximum 68 % pada pH 5 dan 100 % pada pH 6 bergantung kepada penumpuan suhu. HAc menaikkan kadar pengakisan dengan reaksi katodik tambahan yang berasal dari pengurangan dan penceraian langsung. Juga didapati bahawa kadar pengakisan meningkat seiring dengan meningkatnya suhu. Hal ini disebabkan oleh pencepatan reaksi anodik dan katodik apabila suhu meningkat, juga berkait dengan ketersediaan spesies HAc yang lebih banyak pada suhu yang lebih tinggi. Selain itu, kenaikan kadar pengakisan yang disebabkan oleh kenaikan kadar putaran turut direkodkan dalam kajian ini. Kesan paling ketara dari kadar putaran dicerap hingga 2000 rpm, lebih dari itu tidak banyak kesan daripada kadar putaran dapat dicerap. Kesan aliran juga berkait dengan pengangkutan spesies-spesies kearah dan meninggalkan permukaan logam. Pengutuban potensiodinamik menunjukkan bahawa arus pembatasan katodik meningkat dengan kewujudan penumpuan rendah HAc.

Tiada sebarang perubahan berlaku dalam mekanisme reaksi anodik. Proses pengakisan secara keseluruhan dikawal sepenuhnya oleh proses pemindahan cas. Hal ini ditunjukkan dengan nilai arus pengakisan (i_{corr}) yang lebih rendah dari arus pembatasan (i_{lim}). Persamaan ramalan empirik yang mengambil kira kesan dari pada penumpuan rendah asid asetik dicadangkan berasaskan kepada ujian LPR pada pH 5 dalam keadaan bergelora.

Kata kunci

Pengakisan CO_2 , asid asetik, keadaan aliran bergelora, reaksi katodik tambahan, persamaan ramalan.

TABLE OF CONTENTS

STATUS OF THESIS	i
APPROVAL PAGE	ii
TITLE PAGE	iii
DECLARATION	iv
DEDICATION	v
ACKNOWLEDGEMENTS	vi
ABSTRACT	viii
ABSTRAK	x
TABLE OF CONTENTS	xii
LIST OF TABLES	xv
LIST OF FIGURES	xvii
NOMENCALTURE	xxiii
1 INTRODUCTION	1
1.1 Overview	1
2 LITERATURE REVIEW	5
2.1 Carbon dioxide (CO₂) Corrosion	5
2.1.1 Type of CO ₂ Corrosion Damage.....	8
2.1.2 Key Factors Influencing CO ₂ Corrosion.....	9
2.2 CO₂ Corrosion Prediction Models	11
2.3 Acetic Acid	14
2.4 Iron Carbonate Scale Formation	19
2.5 Flow Effect	21
2.5.1 Flow Effects on Corrosion	22
2.5.1.1 Flow Effects on CO ₂ Corrosion	23
2.5.2 Rotating Cylinder Electrode (RCE).....	26
2.5.2.1 Mass Transfer Expressions for the Rotating Cylinder Electrode (RCE)	28
2.5.2.2 Wall Shear Stress	29

3	METHODOLOGY	31
3.1	Introduction.....	31
3.2	Electrochemical Test Methods.....	31
3.2.1	Linear Polarization Resistance (LPR).....	31
3.2.2	Potentiodynamic Polarization Curves.....	32
3.3	Experimental set-up.....	32
3.3.1	Static Test Set-up.....	34
3.3.2	Dynamic Experiments.....	35
3.4	Materials	37
3.5	Test environment	37
3.5.1	Preparation of Solutions.....	37
3.5.2	Addition of Acetic Acid and Acetate.....	38
3.6	Solution Composition.....	38
3.7	Experimental Procedure	41
3.7.1	Linear Polarization Resistance Measurements (LPR).....	41
3.7.2	Potentiodynamic Polarization Curves.....	42
3.8	Corrosion Prediction	42
4	RESULTS AND DISCUSSION	43
4.1	Linear Polarization Resistance (LPR) Tests.....	43
4.1.1	Effect of HAc concentration.....	45
4.1.1.1	Effect of HAc at pH 5	45
4.1.1.1.1	Temperature 25°C.....	45
4.1.1.1.2	Temperature 40°C.....	46
4.1.1.1.3	Temperature 60°C.....	48
4.1.1.2	Effect of HAc at pH 6	49
4.1.1.2.1	Temperature 25°C.....	49
4.1.1.2.2	Temperature 40°C.....	50
4.1.1.2.3	Temperature 60°C.....	52
4.1.2	Effect of rotational velocity.....	54
4.1.2.1	Effect of rotational velocity at pH 5	54
4.1.2.1.1	Effect of rotational velocity at pH 5, Temperature 25°C.....	54
4.1.2.1.2	Effect of rotational velocity at pH 5, Temperature 40°C.....	55
4.1.2.1.3	Effect of rotational velocity at pH 5, Temperature 60°C.....	56
4.1.2.2	Effect of rotational velocity at pH 6	57
4.1.2.2.1	Effect of rotational velocity at pH 6, Temperature 25°C.....	57
4.1.2.2.2	Effect of rotational velocity at pH 6, Temperature 40°C.....	58
4.1.2.2.3	Effect of rotational velocity at pH 6, Temperature 60°C.....	59

4.1.3	Effect of Temperature.....	61
4.1.3.1	Effect of temperature at pH 5.....	61
4.1.3.2	Effect of temperature at pH 6.....	65
4.2	Potentiodynamic Polarization Test	69
4.2.1	Cathodic Polarization Tests.....	69
4.2.1.1	Cathodic Polarization Tests at 25°C.	69
4.2.1.2	Cathodic Polarization Tests at 60°C.	71
4.2.1.3	Flow Effect in CO ₂ Corrosion and with the Presence of HAc.....	74
4.2.2	Cathodic Polarization Behavior.....	77
4.2.2.1	Flow-independent Limiting Current Component or ‘Chemical Reaction’ Limiting Current.....	77
4.2.2.2	Flow-dependent Limiting Current Density.....	80
4.2.2.2.1	Limiting Current due to Hydrogen Ion (H ⁺) and Carbonic Acid (H ₂ CO ₃) Species.....	81
4.2.2.2.2	Limiting Current Density due to Acetic Acid.....	82
4.2.2.2.3	The Effect of HAc Concentration on Limiting Current (i _{lim}) ..	87
4.2.3	Anodic Polarization Tests	89
4.2.4	Corrosion Rate Behavior based on LPR Tests.....	90
4.3	Comparison between Experimental Corrosion Rates and Open Available Predictive Models.....	94
4.3.1	Comparison at pH 5.....	95
4.3.2	Comparison at pH 6.....	96
5	CO₂ CORROSION PREDICTION WITH THE PRESENCE OF LOW CONCENTRATION OF HAC AT TURBULENT FLOW CONDITIONS.....	99
5.1	Empirical Prediction Equation.....	99
5.1.1	RCE Tests at 25°C.....	99
5.1.2	RCE Tests at 40°C.....	101
5.1.3	RCE Tests at 60°C.....	103
5.2	Comparison of Prediction Equation and Commercial Prediction Model.....	107
5.2.1	Comparison at pH 5.....	107
5.2.2	Comparison at pH 6.....	109
6	CONCLUSION	112
6.1	Conclusions.....	112
6.2	Future Work.....	113
7	REFERENCES.....	115

LIST OF TABLES

Table 1.1:	Summarized effect of HAc on CO ₂ Corrosion at 1 bar CO ₂	3
Table 2.1:	An overview of the parameters treated in the various predictive models.	12
Table 2.2:	Brief description of various models used in the oil and gas industry.	13
Table 2.3:	Acetic Acid Species Distribution at Various pH Values, 80°C	15
Table 2.4:	The common dimensionless numbers	25
Table 2.5:	Advantages and Disadvantages for Corrosion Measurements using RCE ..	26
Table 2.6:	Merits and Limitations of Measuring Techniques for Corrosion Rates under Flow Conditions Using Rotating Cylinder Electrode	27
Table 3.1:	Test matrix for the research.	33
Table 3.2:	Wall shear stress at different rotational speeds for turbulent conditions for 12 mm diameter x 8 mm length of electrode.	37
Table 3.3:	Composition of steel 080A15 (% wt).	37
Table 3.4:	Calculated ratio of base and acid.	38
Table 3.5:	Chemical Reactions and Their Equilibrium Constants.	39
Table 3.6:	Concentration of acetic acid species (ppm) in the solution.	41
Table 3.7:	Vapor pressure of water	42
Table 4.1:	Average Corrosion Rates at pH 5 and temperature 25°C, 40°C and 60°C with various rotational velocity	43
Table 4.2:	Average Corrosion Rates at pH 6 and temperature 25°C, 40°C and 60°C with various rotational velocity	44
Table 4.3:	Percentage increase in corrosion rates with the increase in HAc concentration at pH 5, 25°C.....	46
Table 4.4:	Percentage increase in corrosion rates with the increase in HAc concentration at pH 5, 40°C.....	47
Table 4.5:	Percentage increase in corrosion rates with the increase in HAc concentration at pH 5, 60°C.....	49

Table 4.6: Percentage increase in corrosion rates with the increase in HAc concentration at pH 6, 25°C.....	50
Table 4.7: Percentage increase in corrosion rates with the increase in HAc concentration at pH 6, 40°C.....	51
Table 4.8: Percentage increase in corrosion rates with the increase in HAc concentration at pH 6, 60°C.....	53
Table 4.9: Percentage increase in corrosion rates with the increase in rotational velocity at pH 5, 25°C.....	55
Table 4.10: Percentage increase in corrosion rates with the increase in rotational velocity at pH 5, 40°C.....	56
Table 4.11: Percentage increase in corrosion rates with the increase in rotational velocity at pH 5, 60°C.....	57
Table 4.12: Percentage increase in corrosion rates with the increase in rotational velocity at pH 6, 25°C.....	58
Table 4.13: Percentage increase in corrosion rates with the increase in rotational velocity at pH 6, 40°C.....	59
Table 4.14: Percentage increase in corrosion rates with the increase in rotational velocity at pH 6, 60°C.....	60
Table 4.15: Percentage increase of corrosion rate at pH 5 with the increasing of temperature as compared to corrosion rate at temperature 25°C.....	64
Table 4.16: Percentage increase of corrosion rate at pH 6 with the increasing of temperature as compared to corrosion rate at temperature 25°C.....	68
Table 4.17: Intercept values at 25°C and 60°C of the chemical reaction limiting-current calculated versus experimental values.....	79
Table 4.18: Experimental and calculated limiting current densities.....	88

LIST OF FIGURES

Figure 2.1:	Simple Model for CO ₂ Corrosion Process under Multiphase Flow.....	7
Figure 3.1:	Schematic diagram for both static and dynamic experimental set-up	33
Figure 3.2:	Experimental arrangement for static test.	34
Figure 3.3:	Experimental set-up for RCE test.	36
Figure 3.4:	Details of the RCE specimen assembly with electrode diameter of 12 mm and length 8 mm.	36
Figure 3.5:	Concentration of carbonic species in water, as a function of pH, at 1 bar CO ₂ and 25°C.....	40
Figure 3.6:	Concentration of carbonic species in water, as a function of pH, at 1 bar CO ₂ and 60°C.....	40
Figure 4.1:	Corrosion trend at pH 5 and 25°C.	45
Figure 4.2:	Corrosion trend at pH 5 and 40°C.	46
Figure 4.3:	Corrosion trend at pH 5 and 60°C.	48
Figure 4.4:	Corrosion trend at pH 6 and 25°C.	49
Figure 4.5:	Corrosion trend at pH 6 and 40°C.	51
Figure 4.6:	Corrosion trend at pH 6 and 60°C.	52
Figure 4.7:	Effect of rotational velocity at pH 5, 25°C with different acetic acid concentrations.	54
Figure 4.8:	Effect of rotational velocity at pH 5, 40°C with different acetic acid concentrations.	55
Figure 4.9:	Effect of rotational velocity at pH 5, 60°C with different acetic acid concentrations.	56
Figure 4.10:	Effect of rotational velocity at pH 6, 25°C with different acetic acid concentrations.	57
Figure 4.11:	Effect of rotational velocity at pH 6, 40°C with different acetic acid concentrations.	58

Figure 4.12: Effect of rotational velocity at pH 6, 60°C with different acetic acid concentrations.	59
Figure 4.13: Average corrosion rates at different temperature with blank solution.....	61
Figure 4.14: Average corrosion rates at different temperature with 10 ppm HAc.....	61
Figure 4.15: Average corrosion rates at different temperature with 20 ppm HAc.....	62
Figure 4.16: Average corrosion rates at different temperature with 40 ppm HAc.....	62
Figure 4.17: Average corrosion rates at different temperature with 60 ppm HAc.....	63
Figure 4.18: Average corrosion rates at different temperature with blank solution.....	65
Figure 4.19: Average corrosion rates at different temperature with 10 ppm HAc.....	65
Figure 4.20: Average corrosion rates at different temperature with 20 ppm HAc.....	66
Figure 4.21: Average corrosion rates at different temperature with 40 ppm HAc.....	66
Figure 4.22: Average corrosion rates at different temperature with 60 ppm HAc.....	67
Figure 4.23: Cathodic polarization curves for different HAc concentrations at pH 5, 25°C and 1000 rpm.	69
Figure 4.24: Cathodic polarization curves for different HAc concentrations at pH 5, 25°C and 2000 rpm.	70
Figure 4.25: Cathodic polarization curves for different HAc concentrations at pH 5, 25°C and 4000 rpm.	70
Figure 4.26: Cathodic polarization curves for different HAc concentrations at pH 5, 60°C and 1000 rpm.	71
Figure 4.27: Cathodic polarization curves for different HAc concentrations at pH 5, 60°C and 2000 rpm.	72
Figure 4.28: Cathodic polarization curves for different HAc concentrations at pH 5, 60°C and 4000 rpm.	72
Figure 4.29: Cathodic polarization curves for different HAc concentrations at pH 5, 60°C and 6000 rpm.	73
Figure 4.30: Cathodic polarization test at pH 5, 25°C, blank solutions (0 ppm HAc) with various rotation speeds.....	74

Figure 4.31: Cathodic polarization test at pH 5, 25°C, 10 ppm HAc with various rotation speeds.	74
Figure 4.32: Cathodic polarization test at pH 5, 25°C, 40 ppm HAc with various rotation speeds.	75
Figure 4.33: Cathodic polarization test at pH 6, 25°C, blank solutions (0 ppm HAc) with various rotation speeds.....	75
Figure 4.34: Cathodic polarization test at pH 6, 25°C, 10 ppm HAc with various rotation speeds.	76
Figure 4.35: Cathodic polarization test at pH 6, 25°C, 40 ppm HAc with various rotation speeds.	76
Figure 4.36: Limiting current densities (i_{lim}) as a function of the peripheral velocity (U) to the power of 0.7, 25 °C, pH 5.	78
Figure 4.37: Limiting current densities (i_{lim}) as a function of the peripheral velocity (U) to the power of 0.7, 60°C, pH 5.	78
Figure 4.38: Comparison of the limiting current due to H^+ and H_2CO_3 species at 25°C.	81
Figure 4.39: Comparison of the limiting current due to H^+ and H_2CO_3 species at 60°C.	82
Figure 4.40: Calculated limiting current density due to 10 ppm HAc vs experimental i_{lim} at 25°C.....	83
Figure 4.41: Calculated limiting current density due to 40 ppm HAc vs experimental i_{lim} at 25°C.....	83
Figure 4.42: Calculated limiting current density due to 10 ppm HAc vs experimental i_{lim} at 60°C.....	84
Figure 4.43: Calculated limiting current density due to 40 ppm HAc vs experimental i_{lim} at 60°C.....	84
Figure 4.44: Comparing calculated total limiting current to experimental i_{lim} , 10 ppm HAc, 25°C.....	85
Figure 4.45: Comparing calculated total limiting current to experimental i_{lim} , 40 ppm HAc, 25°C.....	86
Figure 4.46: Comparing calculated total limiting current to experimental i_{lim} , 10 ppm HAc, 60°C.....	86

Figure 4.47: Comparing calculated total limiting current to experimental i_{lim} , 40 ppm HAc, 60°C.....	87
Figure 4.48: Cathodic polarization tests at pH 5, 60°C, 4000 rpm with various HAc concentrations.	88
Figure 4.49: Flow effect on anodic sweeps at pH 5, 60°C, 40 ppm HAc.	89
Figure 4.50: The effect of HAc concentrations on the anodic sweeps in bubbling CO ₂ solutions at 4000 rpm, pH 5 and 60°C.....	89
Figure 4.51: Comparison of the measured limiting current density (i_{lim}) with the corrosion current density (i_{corr}) at different peripheral velocity, pH 5, blank, 25°C.	91
Figure 4.52: Comparison of the measured limiting current density (i_{lim}) with the corrosion current density (i_{corr}) at different peripheral velocity, pH 5, 10 ppm HAc, 25°C.....	92
Figure 4.53: Comparison of the measured limiting current density (i_{lim}) with the corrosion current density (i_{corr}) at different peripheral velocity, pH 5, 40 ppm HAc, 25°C.....	92
Figure 4.54: Comparison of the measured limiting current density (i_{lim}) with the corrosion current density (i_{corr}) at different peripheral velocity, pH 5, blank, 60°C.	93
Figure 4.55: Comparison of the measured limiting current density (i_{lim}) with the corrosion current density (i_{corr}) at different peripheral velocity, pH 5, 10 ppm HAc, 60°C.....	93
Figure 4.56: Comparison of the measured limiting current density (i_{lim}) with the corrosion current density (i_{corr}) at different peripheral velocity, pH 5, 40 ppm HAc, 60°C.....	94
Figure 4.57: Comparison between experimental corrosion rates and predictive models at 25°C.....	95
Figure 4.58: Comparison between experimental corrosion rates and predictive models at 40°C.....	95
Figure 4.59: Comparison between experimental corrosion rates and predictive models at 60°C.....	96
Figure 4.60: Comparison between experimental corrosion rates and predictive models at 25°C.....	96

Figure 4.61: Comparison between experimental corrosion rates and predictive models at 40°C.....	97
Figure 4.62: Comparison between experimental corrosion rates and predictive models at 60°C.....	97
Figure 5.1: RCE tests at 25°C.	99
Figure 5.2: Prediction based on RCE tests at 25°C.....	100
Figure 5.3: The variation of slopes with the rotation rate.	101
Figure 5.4: Relationship between corrosion rate and HAc concentration as plotted at different rotation rates at 40°C.....	102
Figure 5.5: Best-fit equations for relationship between corrosion rate and HAc concentration as plotted at different rotation rates at 40°C.....	102
Figure 5.6: The variation of slopes with rotation rate.	103
Figure 5.7: Relationship between corrosion rate and HAc concentration as plotted at different rotation rates at 60°C.....	104
Figure 5.8: Best-fit equations for relationship between corrosion rate and HAc concentration as plotted at different rotation rates at 60°C.....	104
Figure 5.9: The variation of slopes with rotation rate.	105
Figure 5.10: The variation of the constant with the temperature.	106
Figure 5.11: Comparison of prediction equation with experimental data at pH 5, 25°C, 1 bar CO ₂ . Error bars represent 10 % variant of predicted corrosion rate compared to Multicorp version 4 model.....	107
Figure 5.12: Comparison of prediction equation with experimental data at pH 5, 40°C, 1 bar CO ₂ . Error bars represent 10 % variant of predicted corrosion rate compared to Multicorp version 4 model.....	108
Figure 5.13: Comparison of prediction equation with experimental data at pH 5, 60°C, 1 bar CO ₂ . Error bars represent 10 % variant of predicted corrosion rate compared to Multicorp version 4 model.....	109
Figure 5.14: Comparison of prediction equation with experimental data at pH 6, 25°C, 1 bar CO ₂ . Error bars represent 10 % variant of predicted corrosion rate compared to Multicorp version 4 model.....	109

Figure 5.15: Comparison of prediction equation with experimental data at pH 6, 40°C, 1 bar CO ₂ . Error bars represent 10 % variant of predicted corrosion rate compared to Multicorp version 4 model.....	110
Figure 5.16: Comparison of prediction equation with experimental data at pH 6, 60°C, 1 bar CO ₂ . Error bars represent 10 % variant of predicted corrosion rate compared to Multicorp version 4 model.....	111

NOMENCALTURE

A	surface are of the steel in m^2
b_a	anodic curve tafel slope
b_c	cathodic curve tafel slope
B	stern geary constant
$C_{f_{RCE}}$	friction coefficient of rotating cylinder electrode
CR	corrosion rate in mm/yr
C_b	bulk concentrations in mol
$C_{bH_2CO_3}$	bulk aqueous concentration of H_2CO_3
$D_{H_2CO_3}$	aqueous diffusion coefficient of H_2CO_3 in m^2/s
D_{HAc}	aqueous diffusion of HAc in m^2/s
D_{CO_2}	aqueous diffusion of CO_2 in m^2/s
$D_{ref(H^+)}$	reference aqueous diffusion coefficient for H^+ , $D_{ref(H^+)} = 9.31 \times 10^{-9}$, in m^2/s at $25^\circ C$
$D_{ref(H_2CO_3)}$	reference aqueous diffusion coefficient for H_2CO_3 , $D_{ref(H_2CO_3)} = 1.3 \times 10^{-9}$ m^2/s at $25^\circ C$
$D_{ref(HAc)}$	reference aqueous diffusion coefficient for HAc , $D_{ref(HAc)} = 5.0 \times 10^{-10}$ m^2/s at $25^\circ C$
d_{RCE}	diameter of rotating cylinder electrode in m
E_{corr}	corrosion (open circuit) potential

F	Faraday constant, 96.500 C/mole
$[HAc]$	acetic acid concentrations in ppm
HAc	acetic acid
i_{lim}	limiting current density in A/cm ²
i_{corr}	corrosion current density in A/cm ²
K	mass transfer coefficient in m/s
K_{HAc}	equilibrium constant for HAc dissociation
$K_{sp}FeCO_3$	equilibrium constant for iron carbonate film
l	length
n	number of electron
P_{CO_2}	partial pressure of CO ₂ in bar
RCE	rotating cylinder electrode
RC	rotating cylinder
R	a. universal gas constant, $R=8.314 J/(mol K)$ b. rotation rate in rpm
R_{FeCO_3}	rate of the precipitation of iron carbonate
Re	Reynolds number, $Re = \frac{ul}{\nu}$
R_p	Resistance polarization in ohm
SS	super saturation value
Sh	Sherwood number of a given species, $Sh = \frac{k_m l}{D}$
Sc	Schmidt number of a given species, $Sc = \frac{\mu}{\rho D}$

T	temperature
T_{ref}	reference temperature
u	peripheral velocity in m/s
V	solution volume
ν	kinematics viscosity in m/s
Z	atomic weight in g/mol

Greek Characters

μ	water dynamic viscosity in kg/(ms)
μ_{ref}	reference water dynamic viscosity $kg/(ms)$ at reference temperature, $\mu_{ref} = 1.002 \times 10^{-3} kg/(ms)$ at 20°C
ρ	density
$\tau_{w_{RCE}}$	wall shear stress of rotating cylinder electrode

CHAPTER ONE

INTRODUCTION

1.1 Overview

CO₂ corrosion of mild steel pipelines is a serious problem in oil and gas industry since it contributes 28 % to the overall corrosion failure [1]. Corrosivity in oil and gas pipelines and the associated equipment originates from the acid gases in wet gas and crude oil sources such as hydrogen sulfide and organic acid. The most common organic acid is acetic acid (HAc) [2]. CO₂ corrosion is a complex process as it is not only affected by the presence of multi corrosive species but also by other operational parameters such as flow, temperature, pH and material characteristic. The combined effect of these factors can produce a more aggressive environment which could result in higher corrosion rate. Consequently, the survival rate of mild steel pipeline is not guaranteed.

Mild steel is the most common and preferred material of pipelines due to several factors such as availability, cost, and ease of fabrication. Unfortunately, mild steel has lower corrosion resistance in CO₂ environment. However the possibility to use mild steel linepipes instead of corrosion resistant alloy (CRA) linepipes, promises a huge cost saving opportunity.

Carbon dioxide (CO₂) corrosion in the presence of HAc has been the subject of numerous studies since 1983 and particularly in late 1990's. It is found that HAc can significantly increase CO₂ corrosion rate. The CO₂ corrosion rate is known to be flow dependent where flow increases corrosion rates by increasing the mass transfer of corrosion species and/or by damaging protective film in the steel surface [3]. Since almost all of the flow in the field is turbulent, thus it is important to understand CO₂ corrosion behavior in turbulent flow conditions. It is possible to simulate the effect of

flow in the laboratory by applying a similar wall shear stress between real conditions and experimental conditions.

Some experiments had been conducted to study the effect of the presence of HAc in CO₂ corrosion both in static conditions and in dynamic conditions [2, 4, 5–11]. Mixed findings were obtained with regards to the effect of range of HAc concentrations to the CO₂ corrosion rate. Mokhtar [10] has found that at higher HAc concentration more than 400 ppm, HAc shows an inhibitive property. On the contrary, low HAc poses great concern as it increases corrosion rate [4]. However, the experiments were conducted in large range of HAc concentration as shown in Table 1.1 below. Not much work was done below 100 ppm HAc concentrations. The understanding of this discrepancy is important since most study assumes linear correlation between HAc concentration and corrosion rate in the lower concentration. The analysis will be more convincing if the range of HAc concentration is not too large such that more information will be obtained from the missing value in the range.

Table 1.1: Summarized effect of HAc on CO₂ corrosion at 1 bar CO₂.

No	Parameters	Rotational Velocity (1000 x rpm)											Environment Conditions	Authors
	HAc (ppm)	0	0.1	0.5	1	2	3	4	5	6	7	9		
1	0.6, 6, 60, 600, 6000, 60000							•					pH 2.5, 3.8, 4.0, 4.1, 5.0, 5.5, 6.0, 6.2, temperature 22°C	Crolet J.L, 1999 [4]
2	0, 10, 100, 1000, 5000				•								pH 4, temperature 25, 40, 80°C	Yuhua Sun et al., 2003 [6]
3	0, 10, 100, 1000, 5000			•	•	•		•					pH 4, 5, 6 temperature 22, 40, 70, 80°C	Keith S. George, 2003-2004 [5,8]
	0, 100				•									
4	1000, 4000, 10000	•										•	pH 6, 6.3, 6.6, temperature 80°C	O.A Nafday, 2004 [2]
5	0, 18, 72, 180	•											pH 6.6, temperature 80°C	O.A Nafday, 2005 [9]
6	30				•	•	•	•		•			pH 3.8, 5.5, 6 temperature 22, 50, 70, 80°C	Mokhtar C.I, 2005 [10]
	60	•												
	100				•	•	•	•		•				
	120	•												
	200				•	•	•	•		•				
	400				•	•	•	•		•				
	800				•	•		•		•				
7	0, 600					•							temperature 25, 80°C	Egil G, Katherine B, 2006 [11]

Various CO₂ corrosion predictive models were then developed based on studies in the laboratory. These predictive models are used as a tool to predict possible corrosion rate in the system. The predicted data is used as the basis of material selection in the design stage which then provides inputs for maintenance and inspection strategies in the operation stage. Most of CO₂ corrosion predictive models are quite expensive and several publicly available CO₂ corrosion prediction models such as NORSOK [12],

Cassandra [13] and de Waard Milliam [14, 15, 16, 17] do not deliberate on HAc effect in the corrosivity analysis although HAc is known as a hazardous species that give unreliable corrosion prediction as highlighted by Fatah et al. [18] and Woollam et al. [19]. Hence, accurate prediction data is important in the sense that the correct material can be selected and corrosion mitigation method can be implemented to lengthen the design live. This is not only relevant to safety issues but also to cost implications, by avoiding of both under and over designs.

Thus, the objective of the study is to establish the effects of low concentration of HAc on the CO₂ corrosion of mild steel in turbulent flow conditions. The effects are to be incorporated in a predictive model so that reliable prediction of CO₂ corrosion of the carbon steel pipeline with the presence of low concentration HAc can be achieved.

CHAPTER TWO

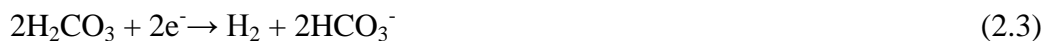
LITERATURE REVIEW

2.1 Carbon dioxide (CO₂) Corrosion

CO₂ corrosion is a great concern in the oil industry. Dry CO₂ gas by itself is not corrosive at the temperatures encountered within oil and gas production. It becomes corrosive when present in water as a dissolved gas under high pressures. The presence of carbon dioxide in solution leads to the formation of a weak carbonic acid (H₂CO₃) which drives CO₂ corrosion reactions. Although a weak acid, carbonic acid is more corrosive than strong acid at same pH due to addition at cathodic reactions. This initiating step is represented by the reaction shown in equation (2.1) and (2.2) [20].



The corrosion process of mild steel is governed by several cathodic reactions and one anodic reaction [21]. The cathodic reactions include the reduction of carbonic acid into bicarbonate ions, the reduction of bicarbonate ions into carbonate ions, and the reduction of hydrogen ions as shown below.



The anodic reaction in CO₂ corrosion is the oxidation of iron to the ferrous (Fe²⁺) ion given in equation (2.6).



There are other models proposed for carbon dioxide corrosion of carbon steel in single-phase full pipe flow such as by Dayalan [22]. The first step is the dissolution of carbon dioxide in the aqueous solution to form the various reactive species, which takes part in the corrosion reaction. The second step is transportation of these reactants to the metal surface. The third step involves anodic and cathodic reactions in the metal surface. The fourth step is the transportation of the corrosion products to the bulk of the solution. These can be shown as:

1. Formation of reactive species in the bulk.



2. Transformation of reactants from bulk to surface.



3. Electrochemical reactants at the surface.



4. Transportation of products from surface to bulk.



For a multiphase flow conditions, Pots [23] has proposed mass transport model for CO_2 corrosion process as shown in Figure 2.1. The protons have to diffuse from the bulk region through the boundary layer to the metal surface, while the transport flux

of carbonic acid needs to reflect both diffusion of H_2CO_3 and hydration of CO_2 in the boundary layer.

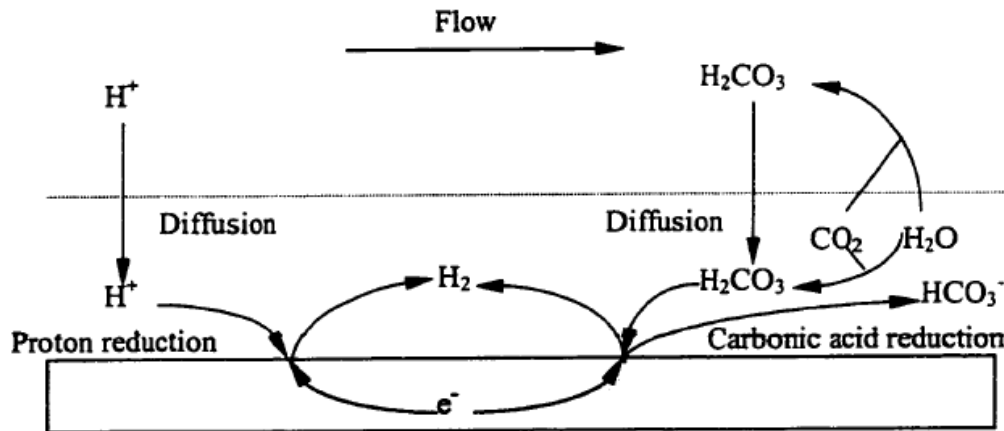


Figure 2.1: Simple Model for CO₂ Corrosion Process under Multiphase Flow [23].

These corrosion reactions provide a chemical environment which promotes the formation of iron carbonate (FeCO_3). FeCO_3 can form along a couple of reaction paths [20]. First, it may form when ferrous ions react directly with carbonate ions as shown in eq. (2.19). Besides that, it can also form by the two step process shown in eq. (2.20, 2.21). When ferrous ions react with bicarbonate ions, a complex of bicarbonate forms which subsequently dissociates into iron carbonate, carbon dioxide and water.



The significance of FeCO_3 formation is that it drops out of solution as a precipitate due to its limited solubility. This precipitate has the potential to form passive films on the surfaces of mild steels which may reduce their corrosion.

2.1.1 Type of CO₂ Corrosion Damage

Typically CO₂ corrosion damages are in the form of general corrosion and three variants of localized corrosion types pitting, mesa attack, and flow induced corrosion [10].

A. Pitting

Pitting occurs at low velocities and around the dew point temperatures in gas producing wells. Temperatures and CO₂ partial pressure can increase the pitting.

B. Mesa Type Attack

Mesa type attack occurs at low to medium flow when the protective iron carbonate film is unstable to withstand the operating regime. The type of this attack most encountered in the area which is has high fluid turbulence such as welds, tubing joints, or ends/constrictions in piping. The corroded areas (mesas) will be elongated in the direction of flow by higher temperature.

C. Flow Induced Corrosion

Flow induced corrosion starts from pits and/or sites of mesa attack above critical flow intensities. It then propagates by local turbulence created by the pits or steps at the mesa attack.

A number of failures have been linked directly to CO₂ corrosion as summarized below [1]:

- Case history I: A 3405 meter deep gas well located in the gulf Mexico was found to have an extremely high corrosion rate, although a regular batch treatment of corrosion inhibitor was employed. The deepest pit approximately 2.54 mm deep was found in the tube. The well contains 1.76 % CO₂ and failure was occurred after 4 months of service.
- Case history II: A 2237 meter deep gas condensate well located in the gulf of Mexico suffered failure in the upper section of the tubing just 23 months after

it began producing. The CO₂ content of the gas was 0.37 % and represents of 3.3 mm/yr of corrosion rate.

The two case histories above were just a small sample problems related to CO₂ corrosion in oil and gas industry. There are many other problems that related to CO₂ corrosion. Therefore, the understanding and the knowledge gathered about CO₂ corrosion of mild steel are very important in oil and gas industry.

2.1.2 Key Factors Influencing CO₂ Corrosion

CO₂ corrosion is influenced by a number of parameters, including environmental, physical, and metallurgical variables. Kermani [24] stated notable parameters that affecting CO₂ corrosion, include:

- Fluid makeup as affected by water chemistry, pH, water wetting, hydrocarbon characteristics and phase ratios.
- CO₂ and H₂S content.
- Temperature.
- Steel surface and corrosion film morphology.
- Fluid dynamics.
- Steel chemistry.

All parameters are interdependent and can interact to influence CO₂ corrosion in many ways. The importance some of these parameters in CO₂ corrosion are summarized as follows:

- Effect of pH

Estimation of the actual pH in the water phase, either the condensed water or formation water, is important in the corrosion of carbon steel. Solution pH has important roles, by influencing both the electrochemical reactions that lead to iron dissolution and the precipitation of protective scales. The actual pH is calculated from

the CO₂ partial pressure, temperature, bicarbonate content in the water, ionic strength and organic acid content. The presence of organic acid decreases the pH value and increasing corrosion rate. Misinterpretation of acetic acid and other organic acids as bicarbonate may lead to an underestimation of corrosion rates. This misinterpretation has been cited by Hedges [25].

- Effect of protective film

Formation of protective carbonate films especially at high temperature can reduce the corrosion rate of carbon steel from several mm/yr to less than 0.1 mm/yr. Protective carbonate films will not form at low temperature, since the iron carbonate solubility is high and the precipitation rate is slow. Protective carbonate films only will form at high temperatures, as the iron carbonate solubility is lower and the precipitation rate much faster. The protective carbonate films would reduce the corrosion rate through several kinds of effects, including: Provision of a diffusion barrier, formation of a low-porosity protective layer, and creation of concentration gradients of the principle chemical species (Fe^{2+} and HCO_3^-) [24].

- Effect of oil wetting

CO₂ corrosion occurs when water is present in the system and wets the steel surface. No corrosion will occur if oil wets the surface. If water in oil emulsion is formed and the water is held in the emulsion, then the water wetting of steel is prevented or greatly reduced, causing the corrosion rate decrease.

- Temperature

The operating temperature strongly affects the nature, characteristics, and morphology of surface film, which, in turn, influences the CO₂ corrosion process [24]. Below scaling temperature (80°C), corrosion rates increase with increasing temperature, and decrease gradually to low values after scaling temperature (Ts) [10].

- Partial pressure

The corrosion rate increase with increasing CO₂ partial pressure. This is due to lower pH, which increases the solubility of the corrosion products.

All the parameters are important in rule to predict possibly CO₂ corrosion rate in the design stage using prediction models. This is important to avoid over design and under design which is related to cost and safety.

2.2 CO₂ Corrosion Prediction Models

Predictive models are developed as an engineering design tool in project development and subsequent operation and maintenance of the plant [10]. Although there are many different models available, basically they were developed from two approaches:

1. Worst case or maximum risk approach, which is based solely on laboratory test data; and
2. Most probable risk approach that is partly based on field data.

Nesic et al. [26] presented a good review of the available models and categorized them into three groups:

- Mechanistic models – Utilizing firm theoretical background to describe the mechanisms of underlying reaction;
- Semi-empirical models - partly based on firm theoretical background and partly based on empirical functions; and
- Empirical models – Based mostly on best-fit parameters from experimental results, hence, relying on minimal theoretical background.

Nyborg [27] highlighted that the main difference in these models is in their treatment of the effect of protective films and the effect oil wetting. The fact that these different models are based on different philosophies and parameters renders them neither

equivalent nor interchangeable. Table 2.1 shows the parameters that are used by different models [10].

Table 2.1: An overview of the parameters treated in the various predictive models.

Parameters	Models					
	DW 95	CASSANDRA	NORSOK	ECE 4	MULTICORP4	HYDROCORR
PCO ₂	√	√	√	?	√	√
Temperature	√	√	√	√	√	√
pH	√	√	√	?	√	√
Flow Rate	√	√	√	√	√	√
Flow regime	√		√			
Scale factor	√		√		√	√
Total Pressure	√		√	√	√	√
Steel	√			√	√	√
Water wetting				√	√	
Ca/HCO ₃		√		√		√
H ₂ S				√	√	
HAc		?		√	√	?
Field Data			√			
Cost (MYR)	Free	Free	Free	40,000 (estimate)	150,000 (estimate)	200,000 (estimate)

√ Parameters considered directly

? Parameters considered indirectly or not considered highly influential

Brief description of these models is presented in Table 2.2 with comment on the HAc input in the model.

Table 2.2: Brief description of various models used in the oil and gas industry.

Models	Brief Description	Comment on HAc
De Waard et al (DW) [14], [15], [16], [17]	First version published in 1975 based only on temperature and PCO_2 . Correction factors for the effect of pH, non-ideality of CO_2 at high pressures and protective film formation introduced in 1991. A new model in 1993 accommodates the effect of flow particularly on the effect of mass transport and fluid velocity. Latest version, in 1995, includes the steel composition and also represents a best fit to the flow loop data generated at IFE. The model was develop primarily for wet gas pipelines	Not Considered
Cassandra [13]	Cassandra is BP's implementation of the de Waard model and based on BP's experience using this model. Spreadsheet on pH calculation module is included which requires CO_2 content, temperature and full water chemistry as inputs. The effect of protective corrosion films is set as a user-option. It gives three corrosion rates based on DW 1993, DW 1995 and the average of the both models setting DW 1993 as the input value.	Acetate determined from water analysis is an input into model for calculation of pH.
NORSOK [12]	This model was developed by the Norwegian oil companies Statoil, Norsk Hydro and Saga Petroleum. It is an empirical model based on laboratory data at low temperature and field data at temperature above 100°C . The model is considerably more sensitive to variation in pH than the de Ward model. The model accounts the effect of protective film, but it does not account for any effect of oil wetting.	The effect of HAc is not direct considered in this model. But, this model still valid to predict the corrosion rate when the total content of organic acids below 100 ppm and the CO_2 partial pressure is less than 0.5 bar.

ECE version 4 [27]	The Electronic Corrosion Engineer model developed by Intetech is based on the de Waard 95 model which added with a module for pH calculation and bicarbonate production. The effect of oil wetting is considered.	Considers the contribution of organic acids in the model. It is more sensitive when account the presence of organic acid on gas system compared to the water system.
MULTICORP [28]	This model was developed by The Institute of Corrosion and Multiphase Technology (ICMT), OHIO University. It was built based on mechanistic model and covers almost key aspects of internal corrosion of mild steel in oil and gas pipelines.	Considers the contribution of organic acid in the model.
HYDROCORR [27,29]	This model was developed by Shell to combine corrosion and fluid flow modeling. It is Shell's preferred tool for CO ₂ corrosion prediction in pipeline. It caters for protective film formation, oil – wetting, H ₂ S content, top-of-line corrosion, oxygen corrosion, micro-bilologically-induced corrosion and organic acid corrosion.	Considers the contribution of organic acid in the model.

Since it was reported that HAc has important role in CO₂ corrosion rate, it is crucial to consider effect of HAc in the corrosivity analysis. Thus, the reliable corrosion prediction will be obtained to avoid failure in the operational stages.

2.3 Acetic Acid

Organic acid, especially HAc, in oil reservoir formation water could be formed from organic matter by thermogenic processes called heterotropic acetogenesis [30]. The presence of organic acids termed as carboxylic acids, and hence their corrosive roles in CO₂ corrosion, have been known since 1940s. This subject has been dormant for thirty years until re-examined in 1980s. The conclusion at that time was that these organic acids played a secondary role in CO₂ corrosion [4]. In early 1983, Crolet and Bonis [31] reported that the presence of HAc in the brine could increase the corrosion

rate of carbon steel significantly. Based on experiment in laboratory, it was found that HAc increase mild steel CO₂ corrosion rate greatly at pH 4 but vanished at pH 6 and higher [9]. This fact can be explained by looking at the dissociation of HAc (which is a weak acid).



The equilibrium constant for HAc dissociation, K_{HAc} is:

$$K_{\text{HAc}} = \frac{[\text{H}^+][\text{Ac}^-]}{[\text{HAc}]} \quad (2.23)$$

And depend on temperature as expressed by Kharaka (1989) [32]:

$$K_{\text{HAc}} = 10^{-(6.66104 - 0.0134916Tk + 2.38756 \times 10^{-5}Tk^2)} \quad (2.24)$$

The concentration of hydrogen ions (H^+), determines the value of pH which affects the distribution of acetic species in the solution. This will determine the amount of undissociated form and acetate ion (Ac^-). Thus, at different pH values, different amounts of undissociated (free) HAc can be found in the solution as shown in Table 2.3.

Table 2.3: Acetic Acid Species Distribution at Various pH Values, 80°C [2].

Total HAc added (ppm)	pH	Free [HAc] (%)	[Ac ⁻] (%)
1000	4	88	12
1000	5	58	42
1000	6	6.8	93.2
1000	6.6	1.8	98.2

It was only recently established that the main cause of mild steel corrosion with the presence of HAc is the undisassociated (free) HAc and not the acetate ion (Ac^-) [7, 33]. From Table 2.3, we can conclude that the presence of organic acids at low pH become a major concern on corrosion because there are many free HAc which increase corrosion rate. However at high pH, such as pH 6.6, there should be no effect on CO_2 corrosion since almost of 98% of the acetic species is present as acetate ion (Ac^-). While this is generally true, there is a concern that the presence of organic acids somehow impairs the formation and protectiveness of iron carbonate (FeCO_3) scales.

Hedges [25] examined the effect of acetate (Ac^-) on CO_2 corrosion. In general, the presence of free HAc increases the corrosion rate substantially, 100 ppm HAc increased the corrosion rate from 3.8 to 9.1 mm/yr and 300 ppm increased the corrosion rate from 2.8 to 14.1 mm/yr. It was concluded that the increase in the corrosion rate is due to Ac^- influence.

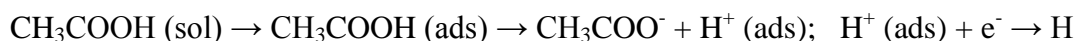
Yuhua Sun et al. [6] investigated the effect of Cl^- and HAc on localized CO_2 corrosion in wet gas flow. They concluded that the corrosion rate of carbon steel in the presence of HAc is not significantly affected by HAc at room temperature, but it is dominated by charge transfer of the H^+ reduction reaction. It also found that the limiting current density at the cathodic reaction was strongly affected by HAc.

Crolet et al. [4] investigated the effect of HAc (0.6 – 60000 ppm) on the anodic dissolution of carbon steel and effect of HAc on the protectiveness of corrosion layers. They concluded that HAc did not influence either the cathodic reduction of H^+ or on the anodic dissolution of iron, but rather affect on the protectiveness of the corrosion layer. Free HAc forming iron acetate which is known very soluble and not protective. Furthermore, it was found that the corrosion rate was inhibited at 180 ppm HAc.

Abarayathna and Naraghi [34] stated that the adding of 50 to 5000 ppm of HAc into CO₂ saturated 3.3 % NaCl environments increased the corrosivity of the environment significantly due to increased acidity and the dissolution of FeCO₃.

Mokhtar [10] in his study showed that the presence of HAc drastically increases the corrosion rate of mild steel in CO₂ corrosion below the scaling temperature and below the inhibitive threshold of HAc concentration. This phenomenon occurs because of extra cathodic reactions and solubilising of ferrous ion (Fe²⁺). The extra cathodic reactions with the presence of HAc are from extra source of hydrogen ion (H⁺) from dissociation and direct reduction of HAc on the electrode surface, where the reactions are:

a. Dissociation of acetic acid



b. Direct reduction of undissociated acetic acid molecules



The solubilising of ferrous ion (Fe²⁺) in the iron carbonate (FeCO₃) corrosion film by HAc, promoting formation of iron acetate film which is known to be soluble and hence not protective.

A good review of the effect of organic acids on CO₂ corrosion was given by Dourghety James [35]. He reviewed the effect of low molecular weight organic acids on corrosion rates. It was observed that as low as 100 ppm concentrations of HAc can cause corrosion attack by thinning the protective film.

Gulbrandsen E and Bilkova K [11] explained the solution chemistry effects on corrosion of carbon steels in the presence of CO₂ and HAc. They also did the experiment to study CO₂ corrosion behavior of X-65 steel in HAc solution (0.1 – 3 % NaCl, 0.5 and 1 bar CO₂, 25 and 80°C, 0-600 ppm HAc, 1900 rpm). Based on the experiment, corrosion rate at 25 °C decreases after 60 ppm HAc, while at 80°C, corrosion rates still increase up to 600 ppm HAc. However, at room temperature, HAc

inhibited general corrosion. In contrast, at 80°C, the average corrosion rate was much higher. It was observed that this is due to inhibition effect at anodic reaction. It could be seen from the anodic polarization curves shifted to higher potentials with increasing HAc. Not only the effect of HAc, but also they investigated the effect of flow on corrosion rate. It was indicating that corrosion rate depended on rotation rate. The flow dependence may mainly be related to the reduction of H^+ and H_2CO_3 , while reduction of HAc was activation controlled.

The mechanism of CO_2 corrosion in the presence of acetic acid was studied by Dugstad A [36]. He concluded that CO_2 has contribution to the cathodic reaction directly or indirectly by affecting the H^+ concentration and the amount of undissociated HAc and H_2CO_3 . It was found that the presence of CO_2 did not effect to the anodic reaction in the range pH 4-6 when the acetate concentration is low.

Furthermore, George and Nesic [8] examined the impact of pH, temperature and velocity to the mechanism of CO_2 corrosion. Polarization, LPR, EIS and weight loss were employed in the experiment. It was observed that the presence of HAc affects the cathodic limiting current, but not charge transfer mechanism of cathodic reaction. However, the anodic reaction was unaffected with increasing HAc concentration at room temperature. As the temperature increases, the HAc effect is more pronounced and it became sensitive to the effect of flow.

A number of failures have been linked directly to acetic acid corrosion. As such based on the open literature, the following concentrations of organic acid have been recorded to cause failure:

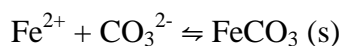
1. Wytch farm oil field failure after 7 years of service. The oilfield brines contained 40 ppm bicarbonate (HCO_3^-) and 64 ppm HAc. Interactions of these species resulted low pH (4.5) which is increasing corrosion rate [38].

2. Elf's field experience shows that fields with CO₂ partial pressure below 5 bar and pH 5.6 are non-corrosive, provided the concentration of free acetic acid is below 6 – 60 ppm [29].
3. Shell also experienced failure due to organic acids as follows [29]:
 - The presence of 700 ppm organic acid caused the failure of a carbon steel inlet nozzle of an offshore flash vessel on a sweet natural gas platform. The nozzle failed in less than two years, which corresponds to a corrosion rate of more than 3 mm/yr. The partial pressure of CO₂ was almost zero.
 - The second field case was due to the presence of 150 ppm organic acid which resulted in the failure (leak) of a water/condensate drainpipe in an onshore sweet natural gas plant. Failure occurred after one year of service, which corresponds to a corrosion rate of about 5 mm/yr.

However, field experience has shown that CO₂ corrosion is reduced at low partial pressure, unless more than 6 to 60 ppm of HAc is present in the water [4]. Since not much work done to study the effect of HAc in the range of 6 – 60 ppm, thus it becomes a challenge in the current study.

2.4 Iron Carbonate Scale Formation

Iron carbonate (FeCO₃) is the main CO₂ corrosion product. FeCO₃ forms on the steel surface if the product of ferrous ion (Fe²⁺) and carbonate ion concentration (CO₃²⁻) exceeds the solubility product limit according to the reaction:



The solubility product limit (K_{sp} FeCO₃) and super saturation (SS) are related via:

$$SS = \frac{[Fe^{2+}][CO_3^{2-}]}{[K_{sp_{FeCO_3}}]} \quad (2.25)$$

The scale will precipitate when the solution is supersaturated or when the SS value exceeds unity. However, the rate of precipitation of iron carbonate can be slow that the precipitation kinetics is more important in determining the protectiveness of the scale rather than the thermodynamics of the process. Johnson and Thomson [37] stated that the most important factors which affect the precipitation of iron carbonate scale are super saturation (SS) and temperature what lead them to propose a rate equation. A similar more frequently used expression for the rate of precipitation of the iron carbonate ($R_{FeCO_3(s)}$) is given by van Hunnik et al [39].

$$R_{FeCO_3(s)} = \frac{A}{V} \cdot f(T) \cdot K_{sp} \cdot f(SS) \quad (2.26)$$

Where A is the surface area of the electrode and V is the solution volume.

The equilibrium constant for iron carbonate film $K_{sp_{FeCO_3}}$ is dependent on temperature ($T^{\circ}C$, *Celsius*) and ionic strength (I) and expressed as

$$K_{sp_{FeCO_3}} = 10^{(-10.13 - 0.0182T_c)} / (0.0115 * I^{-0.6063}) \quad (2.27)$$

$$I = 0.5 * \sum nZ^2$$

Where I represents the number of ions, Z is charge of each ion and n is the molar concentration of each ion.

Nafday [2] concluded that increment of HAc concentration at constant temperature and constant pH does not influence the protectiveness of iron carbonate ($FeCO_3$) scales. These phenomena occur because the rates of iron carbonate precipitation are dependent on the SS value which in turn is a function of Fe^{2+} concentration, pH and $K_{sp_{FeCO_3}}$ as seen from equation below.

$$SS = f(Fe^{2+}, pH, 1/Ksp_{FeCO_3}) \quad (2.28)$$

Whereas Ksp_{FeCO_3} is a function of temperature.

Thus at a fixed pH and temperature the amount of HAc added does not influence the SS and precipitation of Iron Carbonate film.

Iron carbonate precipitates decreases corrosion rate by [2]:

- Presenting a diffusion barrier for the species involved in the corrosion process;
- Blocking a portion of the steel and preventing electrochemical reaction from occurring underneath it.

2.5 Flow Effect

For pipe flow, laminar flow is encountered at Reynold number (Re) below 2300, transition from laminar to turbulent flow occurs between $2000 < Re < 4000$, and turbulent flow will develop at $Re > 4000$.

For a RC (rotating cylinder) geometry, laminar flow typically is encountered for Reynold numbers $Re = v d / \nu < 200$ (where $v = \omega d/2$ is the peripheral velocity of the RC, the rotational (angular) speed in rad/s, and d is the cylinder diameter in m).

There are a large number of empirical mass transfer expressions in open literature for flow in straight, smooth pipe, for example due to Chilton and Colburn expressions [40]. Mass transfer is:

$$Sh = k_m d / D = 0.023 Re^{0.8} Sc^{0.33} \quad (2.29)$$

This can also be expressed in terms of the mass transfer coefficient

$$K = 0.023 D^{0.67} V^{-0.47} u^{0.8} / d^{0.2} \quad (2.30)$$

Berger and Hau [41] gave other empirical but have similar results:

$$Sh = kd/D = 0.017 Re^{0.86} Sc^{0.33} \quad (2.31)$$

Where d is the diameter of the electrode in m, D is the hydrogen diffusion coefficient in m^2/s , u is the fluid velocity (m/s), Re is the Reynolds number Sh is the Sherwood number and Sc is the Schmidt number.

However, in real system the equation which is derived from smooth pipes does not apply, because in real condition pipes are not smooth and straight.

Silverman [42] suggested that the determination of average shear stress is important, because the same mass transfer conditions prevail for systems with the same shear stress magnitude, same flow regime and satisfying the non-slip condition at the all. It is found from the RCE (rotating cylinder electrode) and straight pipe tests, the overall scalar transport rate is identical with mean wall shear stress.

2.5.1 Flow Effects on Corrosion

Bernardus et al. [43] explained the effects of flow on corrosion. They divided the effects of flow into three categories, namely:

1. Distribution of fluid phases

This includes the distribution of the water phase and the wetting of the pipe wall by free water.

2. Mass Transport of Species

Mass transport of corrosive species to the wall across the diffusion boundary layer is the rate-determining step for the corrosion rate. This applies to corrosion by protons, organic acids, and oxygen. When a corrosion product scales forms, the transport of corrosion product away from the wall can be the rate-

determining step. High mass transfer of corrosion products can prevent protective corrosion product scales to form.

3. Mechanical Forces

Impact forces by liquid droplets, as for example:

- Corrosion inhibitor failure caused by high flow, often related to high shear stress.
- Breakdown of corrosion product layers leading to erosion/corrosion.

Poulson [44] explained the spectrum of flow induced corrosion/erosion corrosion process. The sequence process is summarized as follows:

1. Dissolution dominates metal loss.
2. Flow thins protective film to steady-state thickness, which is a function of both mass transfer rate and grow kinetics. In this phase Flow Induced Corrosion/Erosion Corrosion is controlled by the dissolution rate of the protective film.
3. Film is locally removed by dissolution, surface shear stress or particle/bubble impact; but can repassivate.
4. Film is removed and does not reform.
5. Film is removed and underlying metal surface is mechanically damaged which contributes to overall metal loss.
6. Film is removed and mechanical damaged to underlying metal is the dominant damage mechanism.
7. Mechanical damage dominates metal loss.

2.5.1.1 Flow Effects on CO₂ Corrosion

The effects of flow on CO₂ corrosion can be due to cavitation, erosion corrosion and flow accelerated corrosion. In flow-accelerated corrosion, fluid increases the mass transfer of the chemical species to or from the metal surface.

In situation where a reaction is controlled by diffusion of reacting species, the corrosion rate is related to the concentration driving force (C) and the mass transfer coefficient (k). The mass transfer coefficient, k , is defined by

$$I_{lim} = nFkCb \quad (2.32)$$

Where i_{lim} is the limiting current density for cathodic reaction and Cb is the bulk concentration of cathodic reactant. With the knowledge of the mass transfer coefficient (k), we can predict the corrosion rate due to a mass transport-controlled reaction.

There are many different empirical expressions relating mass transfer coefficients to flow rate, fluid flow properties, species properties and system geometry. These empirical relationships are conveniently expressed by dimensionless numbers. The common dimensionless numbers are listed in Table 2.4 [10].

Hydrodynamic analyses have shown that the Re , Sc_i and Sh_i dimensionless numbers can be correlated by the following expression:

$$Sh_i = DRe^x Sc_i^y \quad (2.33)$$

Mendoza and Turgoose [45] have conducted a comprehensive study on the effect of turbulent flow on the localized corrosion of mild steel. Turbulent flow has two possibilities to increasing corrosion rate, by increasing corrosion potential (E_{corr}) value and by increasing wall shear stress. The experiment with different variable was done to assure the factor that governs corrosion. First they investigated the effect of changes E_{corr} at same shear stress and secondly the effect of increasing shear stress without changes in E_{corr} . Finally, they concluded that changes in E_{corr} to more positive values when the rotation speed is increased are more important in removing the electrostatically adsorbed inhibitor from the surface than the increase in shear stress

that is also present. Changing in E_{corr} to more positive values, create a positive charge on the metal surface that forces the inhibitor to remove.

Table 2.4: The common dimensionless numbers [10].

Dimensionless Numbers	Descriptions
<p>The Reynolds number</p> $Re = \frac{ul}{\nu}$ <p>Where u is the mean velocity and ν is the kinematic viscosity of the fluid. The kinematic viscosity is given by the ratio:</p> $\nu = \frac{\mu}{\rho}$ <p>where μ and ρ are the viscosity and density of the fluid, respectively.</p>	<p>Identifying the type of flow occurring in a system, also defines a relative flow velocity in terms of a characteristic length “l”, defined according to the system under study</p>
<p>The Schmidt number, Sc_i, is defined, for a species “i”, as:</p> $Sc_i = \frac{\mu}{\rho D_i} = \frac{\nu}{D_i}$ <p>Where D_i is the diffusion coefficient of the species “i” in the fluid</p>	<p>The Schmidt number, Sc_i, is a dimensionless number associated with the mass-transfer properties of the fluid</p>
<p>The Sherwood number, Sh, is defined, for species “i”, as</p> $Sh_i = \frac{k_i l}{D_i}$ $K_i = \frac{i_{lim_i} I}{n F C_{b_i}}$ <p>Where, C_{b_i} = Bulk concentration</p> <p>Then, the Sherwood number can be rewritten in terms of the limiting current density as:</p> $Sh_i = \frac{i_{lim_i} I}{n F D_i C_{b_i}}$	<p>The Sherwood number, Sh, is a dimensionless group associated with the mass-transfer coefficient, k_i, of a specific species in the fluid.</p>

2.5.2 Rotating Cylinder Electrode (RCE)

Rotating Cylinder Electrode has been widely used as laboratory hydrodynamic test system in corrosion studies because some of its popularity characteristics such as being designed for working in turbulent conditions, its well understood mass transfer properties, its ease of construction and operation, and low cost [46 - 48].

A good review of rotating cylinder electrode was given by Silverman [49]. In this review, he examined several areas important to the use of RCE for examining velocity-sensitive corrosion in single-phase fluids.

Efird K.D [50] gave opinion about advantages and disadvantages of rotating cylinder electrode. The opinion is summarized in Table 2.5.

Table 2.5: Advantages and Disadvantages for Corrosion Measurements using RCE [50].

Advantages	Disadvantages
Equations for mass transfer and wall shear stress well defined	Wall shear stress > 300 Pa is difficult to achieve
Fully developed wall shear stress is uniform over the entire surface	Testing is single phase liquid only for the equations to apply
Electrochemical tests, electrical resistance probes and coupons can be used	Maintaining good electrical contact with the rotating electrodes is difficult
Easy to use with no pumps or valves required	Testing under high pressure is difficult

Other opinion came from G. Schmitt and M. Bakalli [51]. They concluded merits and limitations of rotating cylinder electrode (RCE). The conclusion is given in Table 2.6.

Table 2.6: Merits and Limitations of Measuring Techniques for Corrosion Rates under Flow Conditions Using Rotating Cylinder Electrode [51].

Merits	Limitations
<ul style="list-style-type: none"> • Mechanistic Information <ul style="list-style-type: none"> - Special feature of current density – potential curve - Mass transport control in the corrosion - Changes when going from laminar to turbulent - Influence of wall shear stress on mass transport. <p>This information is obtained by electrochemical experiments</p> <ul style="list-style-type: none"> • Corrosion information <ul style="list-style-type: none"> - Evaluation of maximum corrosion rates under laminar and turbulent flow conditions - Provided sufficiently large surface area of the cylinder coupons • Comparison with other flow system <ul style="list-style-type: none"> - Similarity considerations for flow effects on corrosion rates in other flow systems, e.g. in pipes, are possible, because empirical equations exist which describe flow influenced mass transport at the rotated cylinder. 	<ul style="list-style-type: none"> • Not applicable to get mechanistic and corrosion information on 2-phase and multiphase systems. All mass transport equation are valid only for one-phase flow • No information on localized attack when using small electrodes and linear polarization resistance (LPR).

2.5.2.1 Mass Transfer Expressions for the Rotating Cylinder Electrode (RCE)

In the context of a corrosion study, the rate of mass transport to and from the metal surface is often the factor which governs the rate of corrosion. In 1954, the basic concept on the mass transfer coefficient was published by Eisenberg et al. [52]. The concept was derived based on the electrochemical study of the reduction-oxidation reaction of the $\text{Fe}(\text{CN})_6^{-3} / \text{Fe}(\text{CN})_6^{-4}$ ions. They determined the relationship between the measured limiting current density of an electroactive species “ i ” in solution, (i_{lim_i}) and the rotation rate of the cylindrical electrode (U_{RCE}). The relationship is given by the following equation:

$$i_{\text{lim}_i} = 0.0791nFC_{b_i}d_{\text{RCE}}^{-0.3}\nu^{-0.344}D_i^{0.644}u_{\text{RCE}}^{0.7} \quad (2.34)$$

Which can be simplify:

$$i_{\text{lim}_i} = A.u_{\text{RCE}}^{0.7} \quad (2.35)$$

$$\text{Where } A = 0.0791nFC_{b_i}d_{\text{RCE}}^{-0.3}\nu^{-0.344}D_i^{0.644} \quad (2.36)$$

which can be rearranged to:

$$Sh_{i,\text{RCE}} = 0.0791\text{Re}_{\text{RCE}}^{0.7} Sc_i^{0.356} \quad (2.37)$$

Where n is the number of electrons involved in the electrochemical reaction, F is the Faraday constant, d_{RCE} is the diameter of cylindrical electrode, i.e. the characteristic length “ l ”, C_{b_i} is the concentration in the bulk of the solution of the ionic species “ i ” involved in the electrochemical reaction, ν is the kinematic viscosity of the environment and D_i is the diffusion coefficient of the species “ i ”.

2.5.2.2 Wall Shear Stress

In order to calculate a value of wall shear stress for the RCE ($\tau_{W_{RCE}}$), the following equation is used, developed initially for flow through a pipe [53]:

$$\tau_{W_{RCE}} = c_{f_{RCE}} \frac{1}{2} \rho U_{RCE}^2 \quad (2.38)$$

where ρ is the density of the fluid, U_{RCE} , is the peripheral velocity of the rotating cylinder electrode and $C_{f_{RCE}}$ is the friction coefficient. Eisenberg [52] used the following empirical expression for $C_{f_{RCE}}$ in turbulent regime, between $10^3 < \text{Re}_{RCE} < 10^5$:

$$\frac{C_{f_{RCE}}}{2} = 0.0791 \text{Re}_{RCE}^{-0.3} \quad (2.39)$$

Then, the expression for the wall shear stress can be written as:

$$\frac{\tau_{W_{RCE}}}{\rho u_{RCE}} = 0.0791 \text{Re}_{RCE}^{-0.3} \quad (2.40)$$

This is the common expression used in the calculation of $\tau_{W_{RCE}}$. An alternative expression for the wall shear stress is obtained if the mass-transfer expression proposed by Eisenberg and the universal velocity profile concept are considered:

$$\frac{\tau_{W_{RCE}}}{\rho u_{RCE}} = 1.92 \text{Re}_{RCE}^{-0.6} \quad (2.41)$$

It was concluded that the RCE apparatus under-estimates corrosion rates when compared to a flow loop. However, Turgoose et al. [54] showed that RCE provides

baseline corrosion data comparable with that from an infinitely long pipeline. Silverman [49] stated that the difference in results of several authors may not necessarily reflect that one technique is better than the other. What they may reflect is that the assumptions that underlie the equations are not being met in the same way in the two experiments. Several possible causes the difference are the following:

- The assumptions-hydraulically smooth walls, fully established turbulent flow, or fully established boundary layers-are not fulfilled to the same degree in each piece of equipment.
- Surface roughness from corrosion may have changed the Sherwood number vs Reynolds number relationships differently in each system.
- A subtle difference in the environment between the studies may have caused other types of corrosion to emerge.

Silverman [55] elucidated the conditions of similarity of mass transfer coefficients and fluid shear stress between the RCE and pipes. These parameters have been proposed to establish flow conditions within RCE that could enable to predict flow sensitive corrosion in other geometries such as pipe.

CHAPTER THREE

METHODOLOGY

3.1 Introduction

Electrochemical studies were performed under stagnant and dynamic conditions with the use of static electrodes and the rotating cylinder electrode (RCE) apparatus. Two types of electrochemical measurements were employed in the study, which are Linear Polarization Resistance (LPR) and Potentiodynamic Polarization tests. Reproducibility of the results is ensured by accurate preparation of test samples and test solutions. The tests are repeated at least twice for each case.

3.2 Electrochemical Test Methods

Two types of electrochemical studies, linear polarization resistance (LPR) and potentiodynamic test, were utilized in this study. Linear polarization resistance was used to determine the corrosion rate, while potentiodynamic polarization test was employed to study the mechanism of CO₂ corrosion in the presence of HAc.

3.2.1 Linear Polarization Resistance (LPR)

This method is based on the linear approximation of the polarization behavior at potentials near the corrosion potential. Polarisation resistance (R_p) is given by Stern and Geary [56] equation:

$$R_p = \frac{B}{i_{corr}} = \frac{\Delta E}{\Delta I} \quad (3.1)$$

$$\text{Where, } B = \frac{b_a b_c}{2.303(b_a + b_c)} \quad (3.2)$$

The corrosion current can be related directly to the corrosion rate from Faraday's law:

$$CR(mm/year) = \frac{315 \times Z \times i_{corr}}{\rho \times n \times F} \quad (3.3)$$

Where,

CR = Corrosion rate (mm/year)

i_{corr} = Corrosion current density, $\frac{\mu A}{cm^2}$

ρ = Density of iron, 7.8 g/cm³

F = Faraday's constant, 96.500 C/mole

Z = Atomic weight (g/mol)

n = Electron number

b_a, b_c = The slopes of the logarithmic local anodic and cathodic polarization curves respectively

R_p = Resistance polarization (ohm)

Linear polarization resistance measurements were performed by firstly measuring the corrosion potential of the exposed sample and subsequently sweeping from -10 mV to + 10 mV with the sweep rate 10 mV/min.

3.2.2 Potentiodynamic Polarization Curves

Anodic and cathodic polarization curves were performed on individual coupons in freshly prepared solutions. The sample was polarized either in the anodic or cathodic direction with the scan - 650 mV to + 200 mV from E_{corr} . The sweep rate was 60 mV/min.

3.3 Experimental set-up

The test matrix of the experiment is shown in Table 3.1. While a schematic diagram of the set-up for both static and RCE experiments are shown in Figure 3.1.

Table 3.1: Test matrix for the research.

Parameter	LPR tests	Potentiodynamic Polarization tests
Steel Type	Mild Steel, BS 970	Mild Steel, BS 970
Solution	3 % NaCl	3 % NaCl
De-oxygenation gas	CO ₂	CO ₂
pH	5, 6	5
Total HAc (ppm)	0, 10, 20, 40, 60	0, 10, 40
Temperature (°C)	25, 40, 60	25, 60
Rotational velocity (rpm)	1000, 2000, 4000, 6000	1000, 2000, 4000, 6000

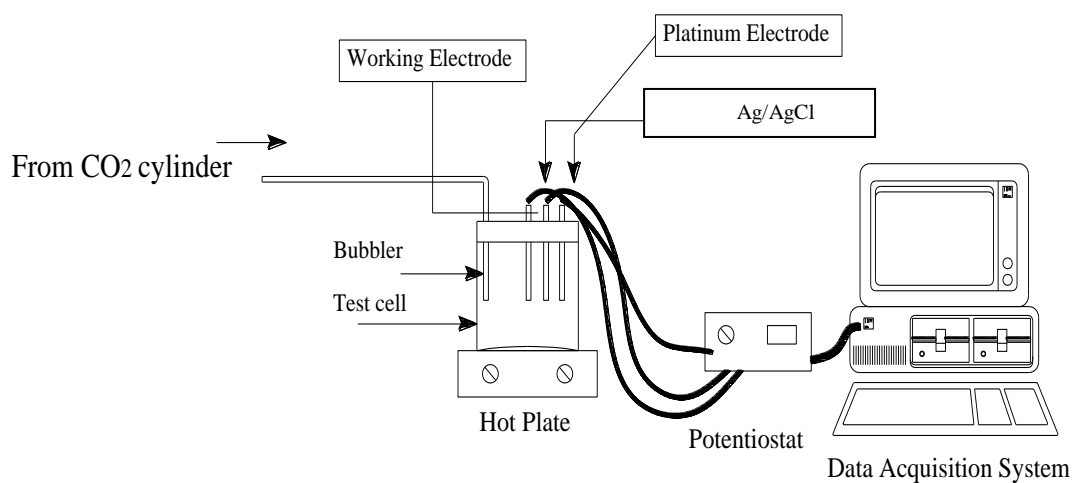
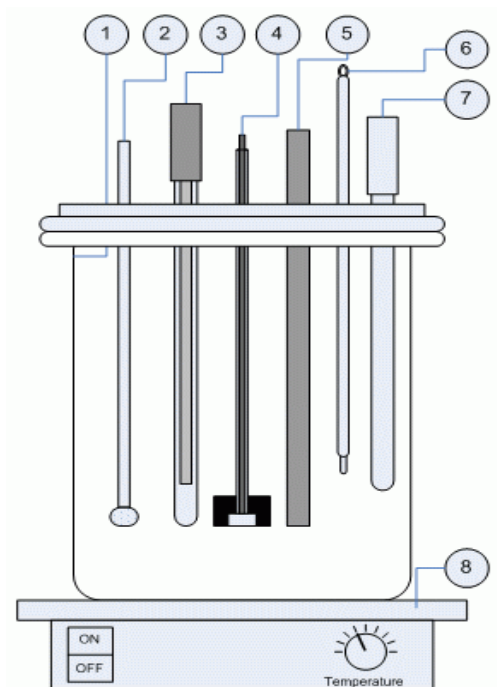


Figure 3.1: Schematic diagram for both static and dynamic experimental set-up

3.3.1 Static Test Set-up

The typical experimental arrangement for the static test is illustrated in Figure 3.2 below.



1. Glass cell; 2. CO₂ bubbler; 3. Reference electrode;
4. Working electrode; 5. Counter electrode; 6. Thermometer;
7. pH meter; 8. Heater

Figure 3.2: Experimental arrangement for static test.

The test assembly consists of one-litre glass cell bubbled with CO₂. The required test temperature is set through a hot plate. The electrochemical measurements are based on a three-electrode system, using a commercially available potentiostat with a computer control system. The reference electrode used is a Ag/AgCl and the auxiliary electrode is a platinum electrode.

The working electrode is prepared from commercial mild steel cylindrical rod with 0.785 cm² cross sectional area. The sample was spot welded with nickel-chromium

wire and mounted in araldite resin. The sample surface is then polished to 600-grade finish using silicon carbide papers. The specimen is degreased and rinsed with ethanol and deionised water before immersion.

3.3.2 Dynamic Experiments

Dynamic experiments were conducted in a 1-litre glass cell with polypropylene cell lids. A three-electrode arrangement was used. The rotating cylinder electrode apparatus used in this research was made by PINE Research Instruments (Model AFMSRCE) with rotation speeds from 50 to 10,000 rpm. The set-up is shown in Figure 3.3 below.

The shaft and the specimen holder of the RCE were made of stainless steel. The cylindrical sample was held in position with the use of PTFE washers and an end cap screwed into the end of the specimen holder. The cylindrical samples used in the RCE apparatus were machined from commercial mild steel grade. The sample surface was then polished to 600-grade finish using silicon carbide papers. The specimen was degreased and rinsed with ethanol and deionised water prior to immersion. A schematic diagram of the specimen assembly, with dimensions of the samples, is shown in Figure 3.4.

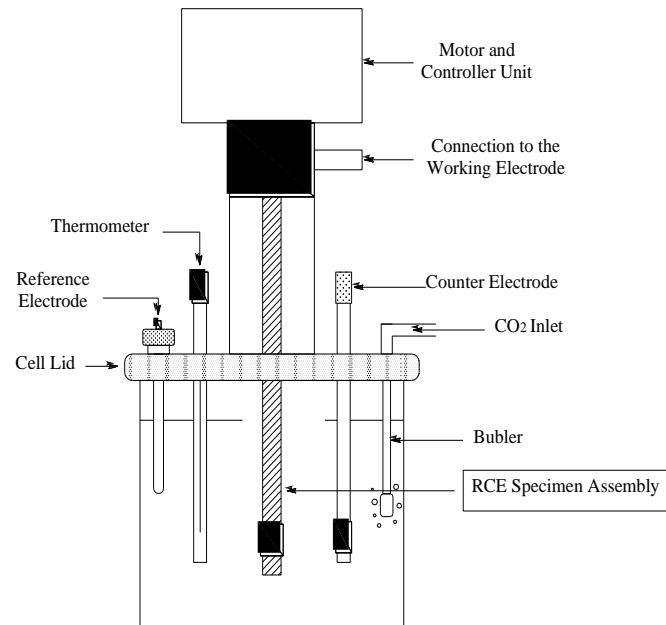


Figure 3.3: Experimental set-up for RCE test.

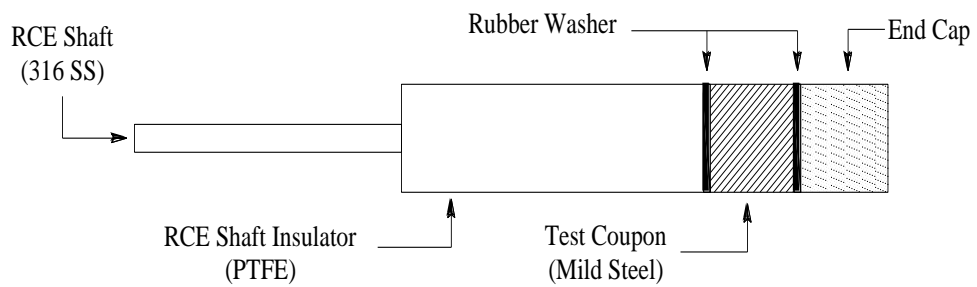


Figure 3.4: Details of the RCE specimen assembly with electrode diameter of 12 mm and length 8 mm.

The corresponding calculated wall shear stress for the dynamic experiment is presented in Table 3.2.

Table 3.2: Wall shear stress at different rotational speeds for turbulent conditions for 12 mm diameter x 8 mm length of electrode.

Rotation Speed (rpm)	Corresponding Wall Shear Stress (Pa)
1000	2.1
2000	7.0
4000	22.6
6000	45

3.4 Materials

Experiments under stagnant and dynamic conditions were conducted with mild steel (BS 970: 080A15) with the following composition:

Table 3.3: Composition of steel 080A15 (% wt).

Steel	C (%)	Si (%)	Mn (%)	P (%)	S (%)	Cr (%)	Mo (%)	Ni (%)	Fe (%)
080A15	0.148	0.175	0.799	0.01	0.032	0.069	0.014	0.065	balance

3.5 Test environment

3.5.1 Preparation of Solutions

The solutions were prepared from the following analytical reagent grade chemicals, namely glacial acetic acid (HAc), sodium acetate (NaAc), and sodium bicarbonate (NaHCO_3).

The 3% NaCl solution is saturated with CO_2 by purging for at least one hour prior to the exposure of electrode. The pH of the solution could be adjusted by adding an amount of 1M NaHCO_3 . The pH value is checked by microcomputer pH-meter

METTLER-TOLEDO Model 320, which had been calibrated using standard buffer solutions.

3.5.2 Addition of Acetic Acid and Acetate

The amount of acetic acid/acetate added is determined by the Handerson-Hasselbach equation ($\text{pH} = \text{pK}_a + \log_{10} [\text{Base}]/[\text{Acid}]$) in order to maintain the required pH.

For acetic buffer, this is given by:

$$\text{pH} = 4.76 + \log_{10} [\text{CH}_3\text{COO}^-]/[\text{CH}_3\text{COOH}]$$

The ratio of acetate ions and acetic acid at each pH is shown in the Table 3.4.

Table 3.4: Calculated ratio of base and acid.

pH Value	Ratio	
	[CH ₃ COO ⁻]	[CH ₃ COOH]
5	2	1
6	17	1

3.6 Solution Composition

The variation of the concentration of carbonic species with temperature is calculated based on the equilibrium constants tabulated in Table 3.5 below.

Table 3.5: Chemical Reactions and Their Equilibrium Constants.

Description	Reaction	Equilibrium Constant	Constant
Dissolution of carbon dioxide	$CO_{2(g)} \leftrightarrow CO_{2(aq)}$	$K_d = \frac{[CO_{2(aq)}]}{P_{CO_{2(g)}}}$	Log $K_d = 108.3865 + 0.01985076T - 6919.53/T - 40.45154 \log T + 669365/T^2$ Source : Plummer [57]
Hydration of carbon dioxide	$CO_{2(aq)} + H_2O \leftrightarrow H_2CO_3$	$K_{hyd} = \frac{[H_2CO_3]}{[CO_2]}$ $K_{hyd} = \frac{k_1}{k_{-1}} = 0.00258$	Log $k_1 = 195.3 - 63.59 \log(T) - 11715.8/T$ Source : Palmer van Eldik [58]
Dissociation of carbonic acid	$H_2CO_3 \leftrightarrow H^+ + HCO_3^-$	$K_{a_1} = \frac{[H^+][HCO_3^-]}{[H_2CO_3]}$ $K_{a_1} = \frac{[H^+][HCO_3^-]}{[H_2CO_3] + [CO_{2(aq)}]}$	Log $K_{a_1} = 29688.2/T + 81.840 \ln(T) - 0.0896488T - 2046790/T^2 - 522.461$ $K_{a_1} = K'_{a_1} (k_{hyd} + 1/k_{hyd})$ Source : Palmer van Eldik [58]
Dissociation of bicarbonate anion	$HCO_3^- \leftrightarrow H^+ + CO_3^{2-}$	$K_{a_2} = \frac{[H^+][CO_3^{2-}]}{[HCO_3^-]}$	Log $K_{a_2} = -2730.7/T - 0.02199T + 5.388$ Source : Palmer van Eldik [58]
Dissociation of acetic acid	$HAc \leftrightarrow H^+ + Ac^-$	$K_{HAC} = [H^+][Ac^-]/[HAc]$	$K_{HAC} = 10^{-(6.66104 - 0.0134916T_K + 2.37856 \times 10^{-5} T_K^2)}$ molar Source : Kharaka [32] $K_f = 3.2 \times 10^5 \text{ s}^{-1}$ Source : Vetter [59]

The calculated concentrations of the carbonic species in solution are shown in Figures 3.5 and 3.6. It is seen that as the temperature of the solution increases, the concentration of dissolved CO_2 decreases and hence the concentration of carbonic acid decreases.

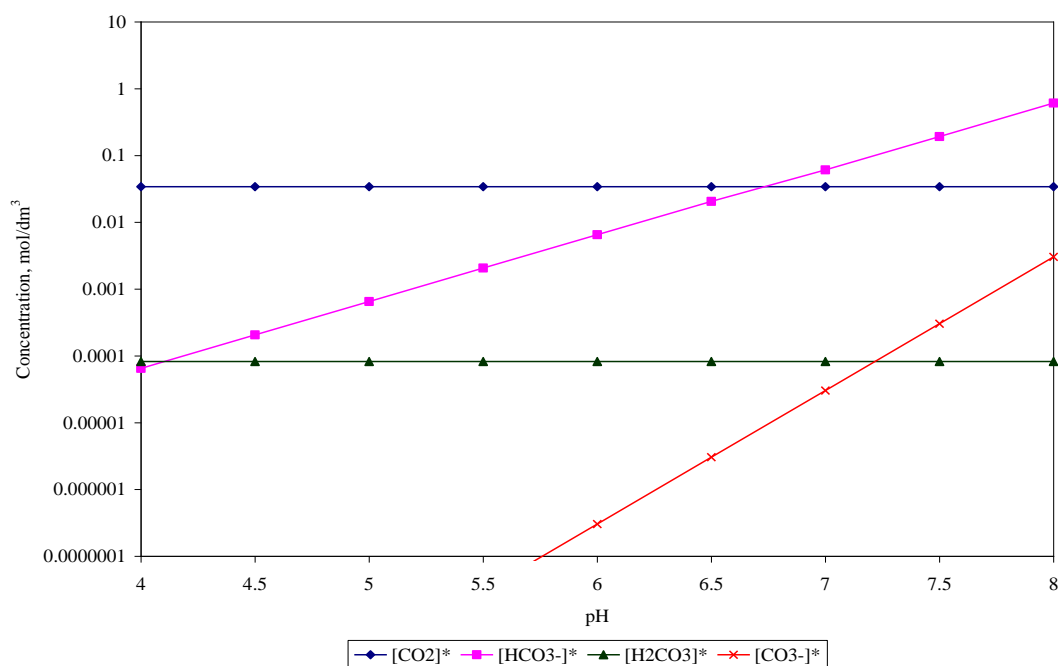


Figure 3.5: Concentration of carbonic species in water, as a function of pH, at 1 bar CO₂ and 25°C.

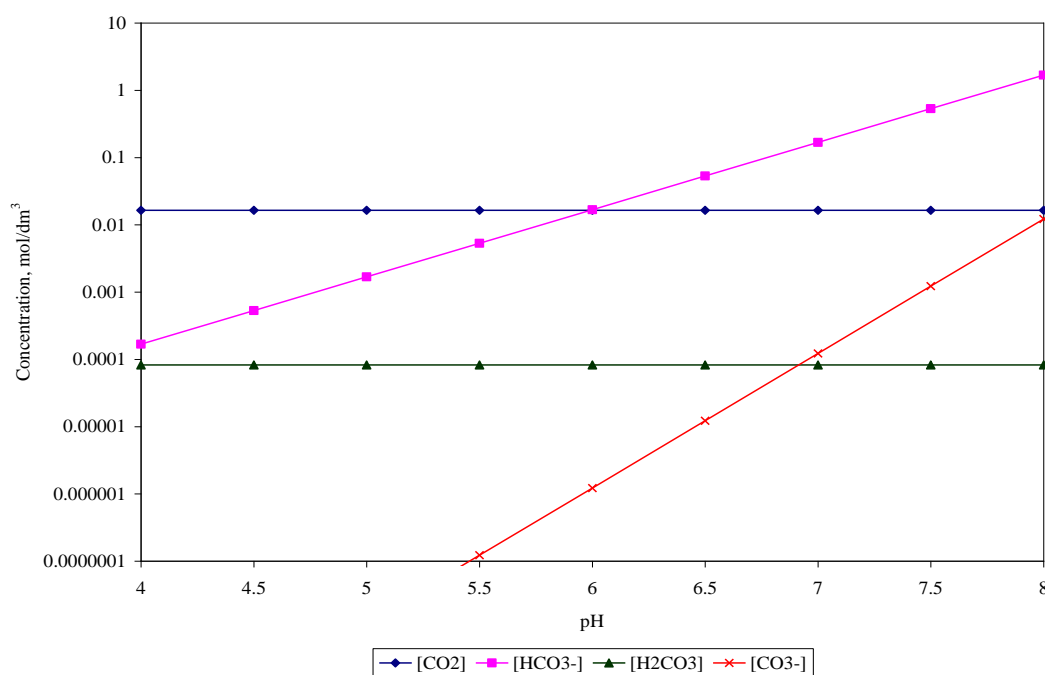


Figure 3.6: Concentration of carbonic species in water, as a function of pH, at 1 bar CO₂ and 60°C.

The calculated concentrations of the acetic acid species in solution are shown in Table 3.6. It is assumed that the concentration of the acetic species remain the same at different temperatures since the equilibrium constant for acetic acid K_{HAc} varies a little with temperature.

Table 3.6: Concentration of acetic acid species (ppm) in the solution.

Species	pH 5				pH 6			
	10 ppm	20 ppm	40 ppm	60 ppm	10 ppm	20 ppm	40 ppm	60 ppm
HAc	3.3	6.6	13.2	19.8	0.56	1.12	2.24	3.36
NaAc	6.7	13.4	26.8	40.2	9.44	18.8	37.76	56.64

3.7 Experimental Procedure

3.7.1 Linear Polarization Resistance Measurements (LPR)

The LPR procedure for RCE test is conducted after sufficient CO_2 gas bubbling, adjusting the solution to the required pH and attaining the set temperature. The bubbling is reduced and maintained throughout the test.

1. Bubble CO_2 through the 1-litre 3% NaCl for at least 1 hour before inserting sample.
2. Adjust pH to the required values by adding solution of 1M NaHCO_3 . pH is measured at room temperature by pH meter.
3. Set the temperature and maintain with an accuracy $\pm 5^\circ\text{C}$.
4. Add the mixture of HAc and Ac accordingly to the required pH values.
5. Insert the polished specimen. For turbulent experiment, set the rotation rate of RCE apparatus.
6. Take readings every 15 minutes for 3 hours.

3.7.2 Potentiodynamic Polarization Curves

1. Bubble CO_2 through the 1-litre 3% NaCl for at least 1 hour before inserting sample.
2. Adjust pH to the required values by adding solution of 1M NaHCO_3 . pH is measured at room temperature by pH meter.
3. Set the temperature and maintain with an accuracy $\pm 5^\circ\text{C}$.
4. Add the mixture of HAc and Ac accordingly to the required pH values.
5. Insert the polished specimen. For turbulent experiment, set the rotation rate of RCE apparatus.
6. Scan from -650 mV to $+200\text{ mV}$ from E_{corr} with the scan rate 60 mV/min

3.8 Corrosion Prediction

Three readily available predictive models were used namely Cassandra, NORSOK and de Waard models. The molar percentage of CO_2 used in the calculation is adjusted to account of the water vapor pressure at respective temperatures as shown in Table 3.7 below.

Table 3.7: Vapor pressure of water [60].

Temperature ($^\circ\text{C}$)	Vapor pressure of water (mm Hg)	Corresponding mole % CO_2
25	23.756	96.9
40	55.234	92.81
60	149.38	76

CHAPTER FOUR

RESULTS AND DISCUSSION

The effects of HAc of various concentrations from 0 ppm to 60 ppm on the corrosion behavior of mild steel in 3 % NaCl solution saturated with CO₂ are presented below in terms of LPR and potentiodynamic polarization tests. The tests in turbulent conditions are conducted at pH 5 and 6 at various temperatures of 25°C, 40°C and 60°C.

4.1 Linear Polarization Resistance (LPR) Tests

The average corrosion rates of mild steel exposed to small HAc concentrations from 0 to 60 ppm in turbulent conditions at pH 5 and 6 with various temperature of 25°C, 40°C and 60°C are summarized in Table 4.1 – 4.2 below.

Table 4.1: Average Corrosion Rates at pH 5 and temperature 25°C, 40°C and 60°C with various rotational velocity.

[HAc]	Temperature (°C)	Average Corrosion Rates at Different Rotational Velocity (mm/yr)				
		0 rpm	1000 rpm	2000 rpm	4000 rpm	6000 rpm
Blank Solution	25°C	1.3	1.4	1.8	1.9	2.1
	40°C	2.1	2.3	2.3	2.3	2.7
	60°C	2.9	3.2	3.8	3.9	3.9
10 ppm	25°C	1.6	1.7	1.8	2.1	2.3
	40°C	2.2	2.3	2.3	2.4	2.7
	60°C	3.0	3.5	4.1	4.1	4.5
20 ppm	25°C	1.8	1.9	2.0	2.2	2.4
	40°C	2.2	2.4	2.5	2.5	3.1
	60°C	3.3	4.1	4.6	4.8	6.2
40 ppm	25°C	1.9	2.0	2.1	2.8	2.9
	40°C	2.6	2.8	2.9	3.5	4.0
	60°C	4.2	5.2	5.3	5.7	6.2
60 ppm	25°C	1.9	2.2	2.2	2.9	3.1
	40°C	2.9	3.2	3.5	3.9	4.2
	60°C	3.8	4.8	4.8	4.8	5.9

Table 4.2: Average Corrosion Rates at pH 6 and temperature 25°C, 40°C and 60°C with various rotational velocity.

[HAc]	Temperature (°C)	Average Corrosion Rates Different Rotational Velocity (mm/yr)				
		0 rpm	1000 rpm	2000 rpm	4000 rpm	6000 rpm
Blank Solution	25°C	0.7	0.9	1.2	1.3	1.5
	40°C	0.9	1.1	1.9	2.0	2.1
	60°C	1.6	1.9	2.2	3.4	3.6
10 ppm	25°C	1.1	1.2	1.4	1.4	1.5
	40°C	1.3	1.9	2.1	2.2	2.8
	60°C	1.8	2.0	3.5	3.5	4.1
20 ppm	25°C	1.2	1.3	1.4	1.5	1.6
	40°C	1.7	2.0	2.2	2.8	2.9
	60°C	2.1	2.5	3.5	3.7	4.1
40 ppm	25°C	1.2	1.4	1.5	1.5	1.7
	40°C	2.0	2.1	2.5	2.9	3.0
	60°C	2.1	2.5	3.6	3.9	4.2
60 ppm	25°C	1.5	1.6	1.8	1.9	2.0
	40°C	2.2	2.5	2.8	3.0	3.1
	60°C	2.4	2.7	3.9	4.2	4.5

From Table 4.1 and 4.2, it is observed that corrosion rate depends on HAc concentrations, rotational velocity and temperature. Thus, the analysis of LPR tests in this study is divided in terms of effect of HAc concentrations, rotational velocity and temperature.

4.1.1 Effect of HAc concentration

The effect of different concentrations of HAc on the corrosion rates as obtained by LPR tests at different rotation rates from static conditions (0 rpm) to 6000 rpm is shown in Figure 4.1 – 4.6 below.

4.1.1.1 Effect of HAc at pH 5

4.1.1.1.1 Temperature 25°C

The effect of different concentrations of HAc on the corrosion rates at various rotation speeds (rpm) as obtained by LPR tests at pH 5, 25°C are shown in Figure 4.1 below.

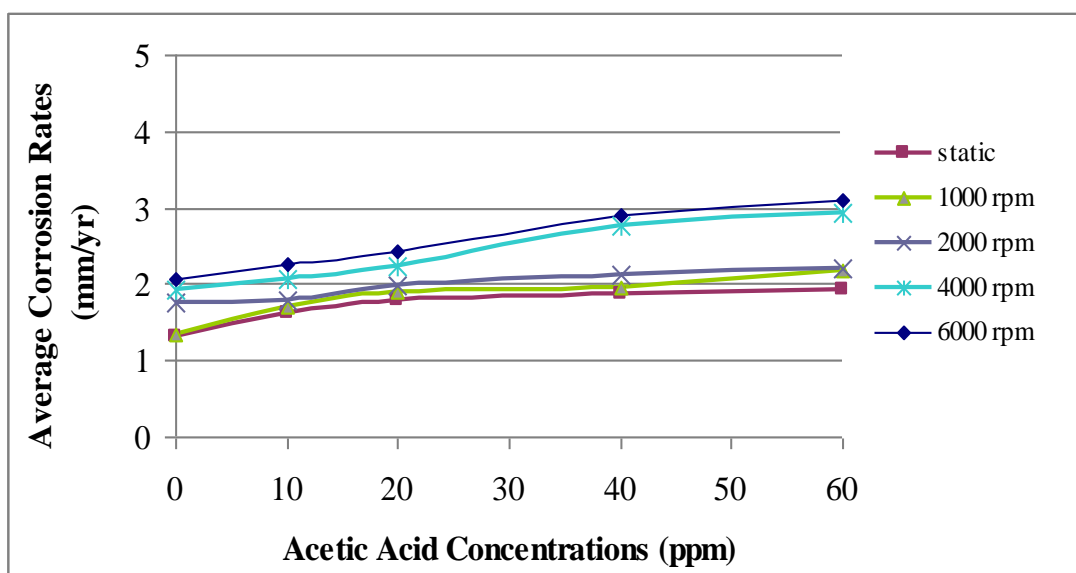


Figure 4.1: Corrosion trend at pH 5 and 25°C.

For both static and turbulent conditions, corrosion rate of mild steel increases with HAc concentrations. It is observed that the significant effect of HAc on turbulent conditions seen at 1000 rpm. At this rotation speed, the corrosion rate increase up to 61%. For 2000, 4000 and 6000 rpm, there is no significant effect of HAc below 40 ppm. The results are summarized in Table 4.3.

Table 4.3: Percentage increase in corrosion rates with the increase in HAc concentration at pH 5, 25°C.

Rotation speed (rpm)	Blank solution (mm/yr)	Percentage difference corrosion rates compared to the blank solution			
		10 ppm	20 ppm	40 ppm	60 ppm
1000	1.4	26%	42%	44%	61%
2000	1.8	1%	12%	21%	26%
4000	1.9	8%	16%	43%	52%
6000	2.1	9%	17%	41%	50%

4.1.1.1.2 Temperature 40°C

The effect of different concentrations of HAc on the corrosion rates as obtained by LPR tests at pH 5, 40°C are shown in Figure 4.2 below.

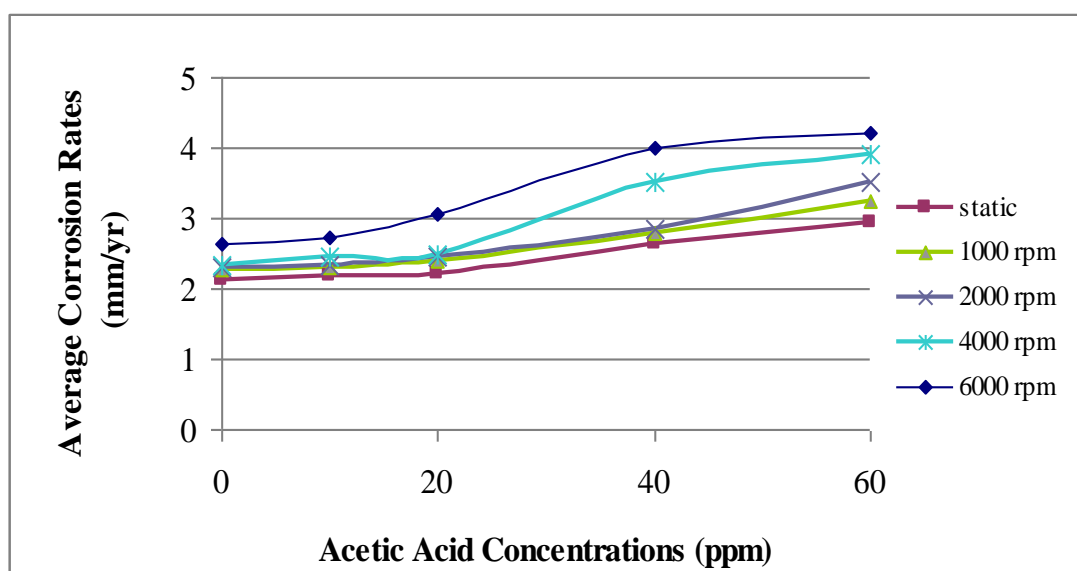


Figure 4.2: Corrosion trend at pH 5 and 40°C.

Generally, the corrosion rates of mild steel at pH 5, 40°C increase with increasing HAc concentrations. This trend is true for both static and turbulent conditions. It is noted at turbulent conditions, there is no significant effect of HAc to the corrosion rate increment below 40 ppm. The significant effect is seen above 40 ppm HAc concentrations. The results are summarized in Table 4.4 below.

Table 4.4: Percentage increase in corrosion rates with the increase in HAc concentration at pH 5, 40°C.

Rotation speed (rpm)	Blank solution (mm/yr)	Percentage difference corrosion rates compared to the blank solution			
		10 ppm	20 ppm	40 ppm	60 ppm
1000	2.26	2%	6%	23%	43%
2000	2.3	2%	7%	24%	53%
4000	2.33	5%	7%	51%	68%
6000	2.65	3%	16%	51%	59%

4.1.1.1.3 Temperature 60°C

The effect of different concentrations of HAc on the corrosion rates as obtained by LPR tests at pH 5, 60°C are shown in Figure 4.3 below.

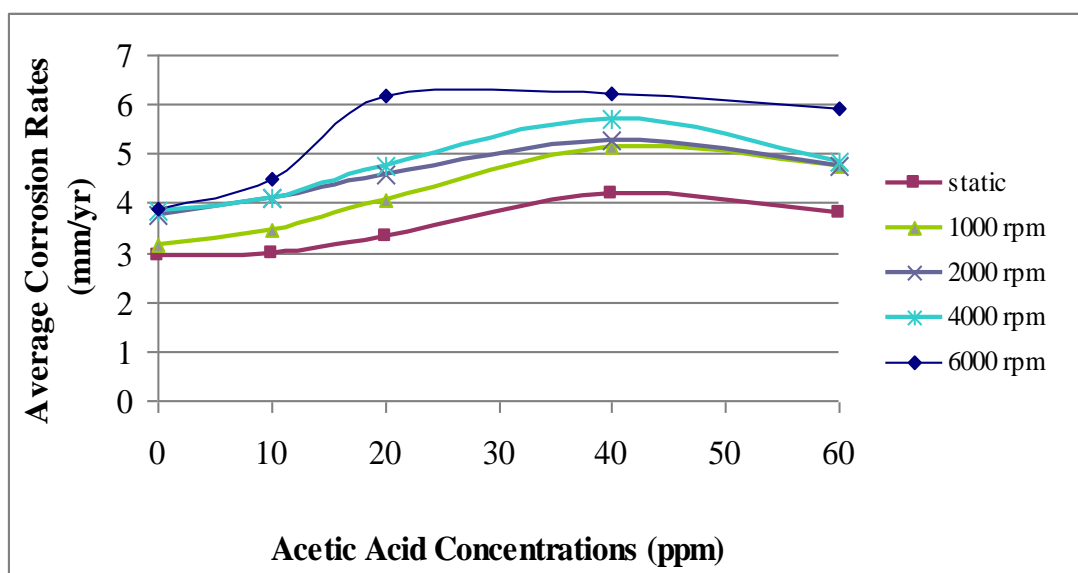


Figure 4.3: Corrosion trend at pH 5 and 60°C.

Generally, corrosion rate trend for both static and turbulent conditions are similar. The corrosion rates increase with addition of HAc up to 40 ppm, and then reduce for 60 ppm HAc. For turbulent conditions, effect of HAc is more pronounced at 40 ppm. The results are summarized in Table 4.5 below.

Table 4.5: Percentage increase in corrosion rates with the increase in HAc concentration at pH 5, 60°C.

Rotation speed (rpm)	Blank solution (mm/yr)	Percentage difference corrosion rates compared to the blank solution			
		10 ppm	20 ppm	40 ppm	60 ppm
1000	3.2	10%	29%	64%	51%
2000	3.77	8%	21%	40%	27%
4000	3.86	6%	24%	47%	25%
6000	3.88	16%	59%	61%	53%

4.1.1.2 Effect of HAc at pH 6

4.1.1.2.1 Temperature 25°C

The corrosion trend at pH 6, 25°C is shown in Figure 4.4. Turbulent conditions have similar trend with static condition which is corrosion rates increase with HAc concentration.

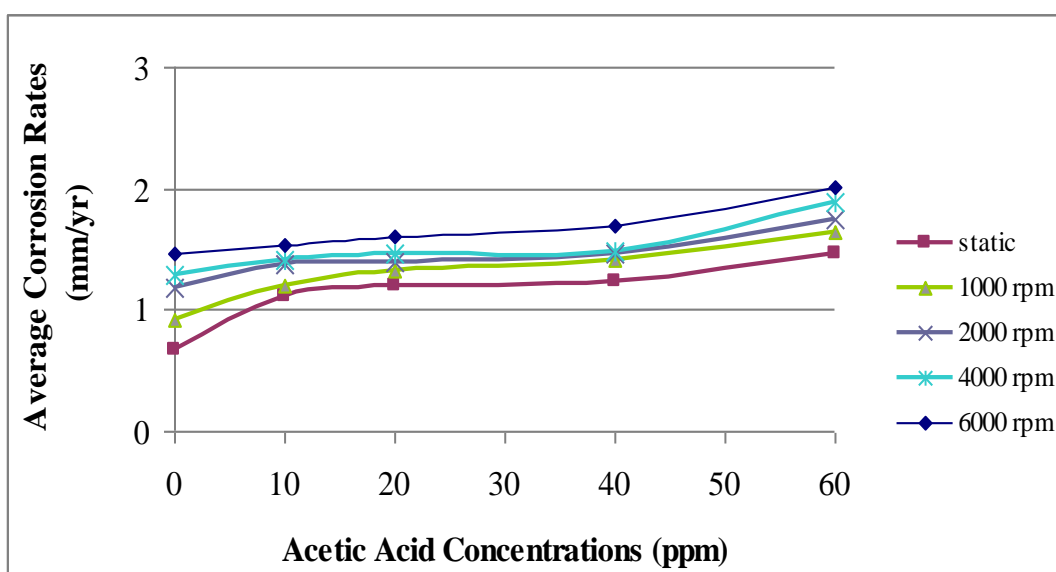


Figure 4.4: Corrosion trend at pH 6 and 25°C.

The apparent effect of HAc is more pronounced at 1000 rpm than the other speeds. It increases up to 80% when added 60 ppm HAc compared to the blank solution. The results are summarized in Table 4.6.

Table 4.6: Percentage increase in corrosion rates with the increase in HAc concentration at pH 6, 25°C.

Rotation speed (rpm)	Blank solution (mm/yr)	Percentage difference corrosion rates compared to the blank solution			
		10 ppm	20 ppm	40 ppm	60 ppm
1000	0.9	32%	45%	55%	80%
2000	1.2	15%	18%	23%	47%
4000	1.3	11%	15%	16%	48%
6000	1.5	5%	10%	16%	38%

4.1.1.2.2 Temperature 40°C

The corrosion trend with the increase addition of HAc at pH 6, 40°C is shown in Figure 4.5. Corrosion rates increase with increasing HAc concentrations for both static and turbulent conditions.

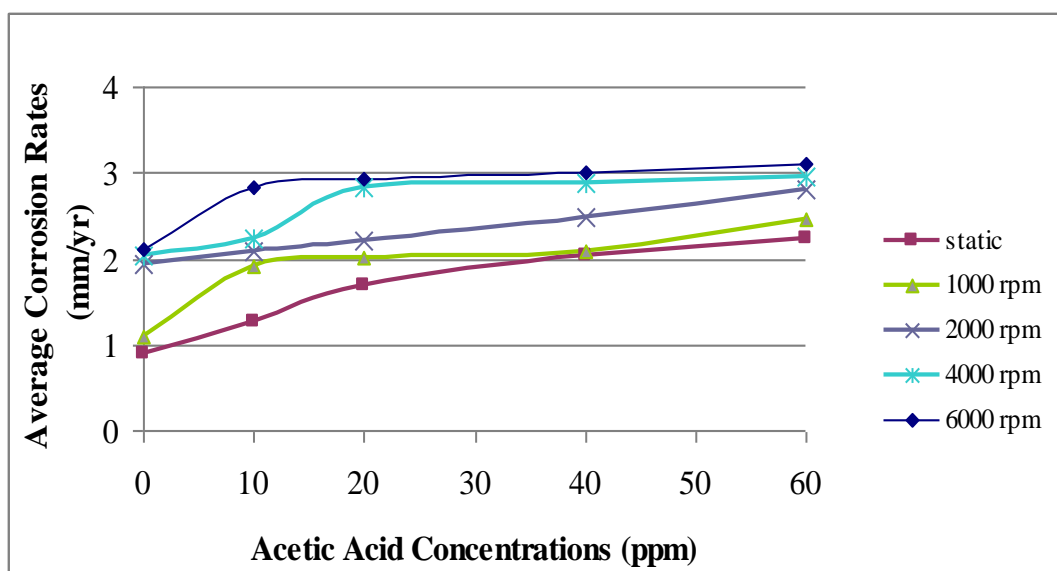


Figure 4.5: Corrosion trend at pH 6 and 40°C.

The effect of HAc is more significant at low speed (1000 rpm) compared to the other speeds. At 1000 rpm, addition of 60 ppm HAc cause increasing corrosion rate until 127% compared to the blank solution. While for other speeds, the increment of corrosion rates is registered around 40%. The results are summarized in Table 4.7 below.

Table 4.7: Percentage increase in corrosion rates with the increase in HAc concentration at pH 6, 40°C.

Rotation speed (rpm)	Blank solution (mm/yr)	Percentage difference corrosion rates compared to the blank solution			
		10 ppm	20 ppm	40 ppm	60 ppm
1000	1.09	75%	84%	92%	127%
2000	1.11	7%	13%	29%	44%
4000	2	10%	39%	42%	45%
6000	2.1	35%	40%	43%	48%

4.1.1.2.3 Temperature 60°C

The effect of different concentrations of HAc on the corrosion rates as obtained by LPR tests at pH 6, 60°C are shown in Figure 4.6 below. In summary, corrosion rates increase with increasing HAc concentrations. This trend is true for both static and dynamic conditions.

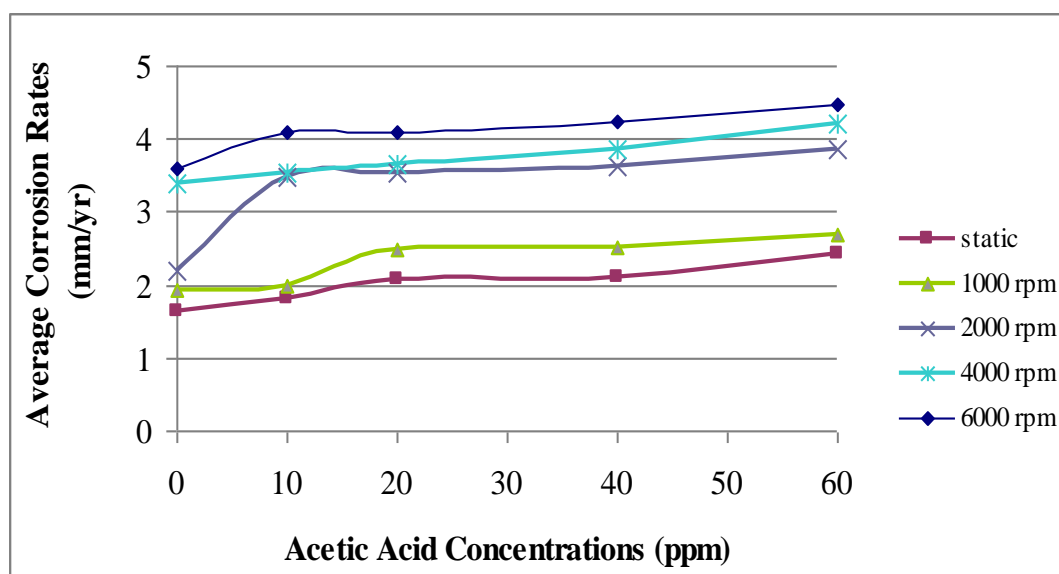


Figure 4.6: Corrosion trend at pH 6 and 60°C.

However at pH 6, 60°C, the apparent effect of HAc occurs at 2000 rpm only. At this speed, the corrosion rate increases until 76% compared to the blank solution. The results are summarized in Table 4.8.

Table 4.8: Percentage increase in corrosion rates with the increase in HAc concentration at pH 6, 60°C.

Rotation speed (rpm)	Blank solution (mm/yr)	Percentage difference corrosion rates compared to the blank solution			
		10 ppm	20 ppm	40 ppm	60 ppm
1000	1.9	2%	28%	30%	39%
2000	2.2	58%	62%	66%	76%
4000	3.4	4%	7%	13%	24%
6000	3.6	13%	14%	18%	24%

Generally, for both pH 5 and 6 at temperature 25°C, 40°C and 60°C, corrosion rate increases with increasing HAc concentrations.

4.1.2 Effect of rotational velocity

Effect of velocity for both pH 5 and pH 6 with various HAc concentrations are shown in Figure 4.7 to Figure 4.12.

4.1.2.1 Effect of rotational velocity at pH 5

4.1.2.1.1 Effect of rotational velocity at pH 5, Temperature 25°C

The effect of rotational velocity on the corrosion rates as obtained by LPR tests at pH 5, 25°C with various HAc concentrations are shown in Figure 4.7 below.

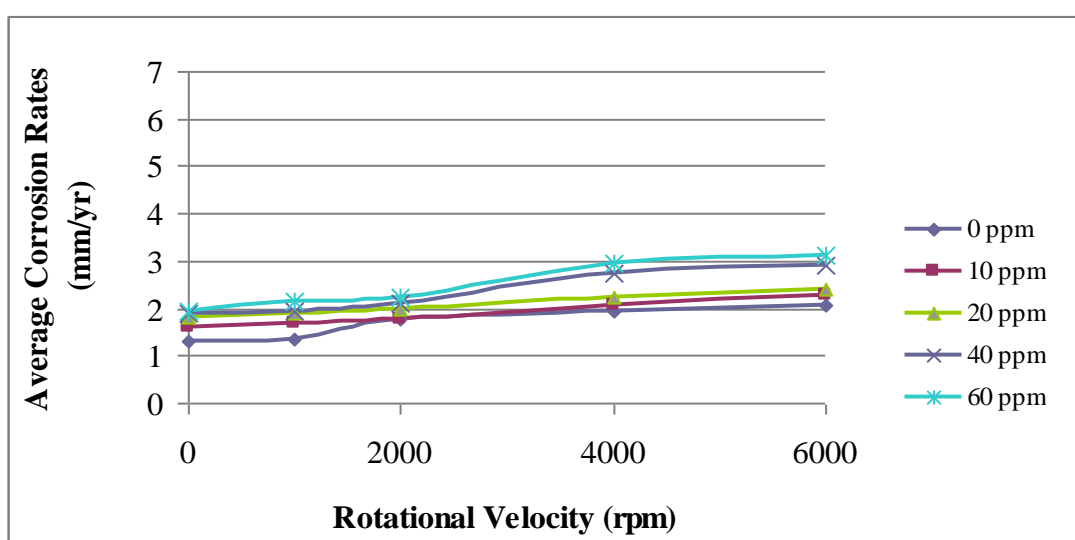


Figure 4.7: Effect of rotational velocity at pH 5, 25°C with different acetic acid concentrations.

In general, corrosion rate at pH 5, 25°C with various HAc concentrations increases with increasing rotational velocity. No further effect of rotational velocity to the corrosion rate is observed at 6000 rpm, where increasing only 10 % as compared to 4000 rpm. The results are shown in Table 4.9 below.

Table 4.9: Percentage increase in corrosion rates with the increase in rotational velocity at pH 5, 25°C.

Acetic acid concentration (ppm)	Corrosion rate at static condition (mm/yr)	Percentage difference corrosion rates compared to the static condition			
		1000 rpm	2000 rpm	4000 rpm	6000 rpm
0	0.7	8 %	38 %	46 %	62 %
10	1.1	6 %	13 %	31 %	44 %
20	1.2	6 %	11 %	22 %	33 %
40	1.2	5 %	11 %	47 %	53 %
60	1.5	16 %	16 %	53 %	63 %

4.1.2.1.2 Effect of rotational velocity at pH 5, Temperature 40°C

The effect of rotational velocity on the corrosion rates as obtained by LPR tests at pH 5, 40°C with various HAc concentrations are shown in Figure 4.8 below.

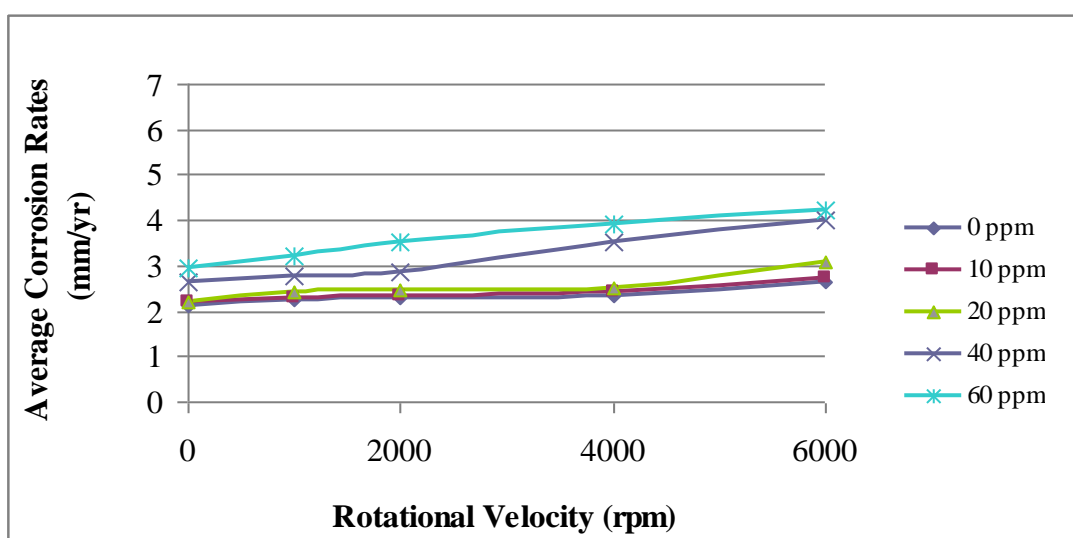


Figure 4.8: Effect of rotational velocity at pH 5, 40°C with different acetic acid concentrations.

It is observed at pH 5, 40°C that corrosion rate increases with increasing rotational velocity, especially at 40 ppm and 60 ppm HAc. An appreciable effect of rotational

velocity to the increment of corrosion rate is seen up to 2000 rpm only. At higher speed, the effect of rotational velocity becomes minimal. As for example, at 6000 rpm, 10 ppm HAc, corrosion rate increases 18% only as compared to 2000 rpm. The results are shown in Table 4.10 below.

Table 4.10: Percentage increase in corrosion rates with the increase in rotational velocity at pH 5, 40°C.

Acetic acid concentration (ppm)	Corrosion rate at static condition (mm/yr)	Percentage difference corrosion rates compared to the static condition			
		1000 rpm	2000 rpm	4000 rpm	6000 rpm
0	0.9	10%	10%	10%	29%
10	1.3	6%	5%	9%	23%
20	1.7	9%	14%	14%	41%
40	2	8%	12%	35%	54%
60	2.2	10%	21%	35%	45%

4.1.2.1.3 Effect of rotational velocity at pH 5, Temperature 60°C

The effect of rotational velocity on the corrosion rates as obtained by LPR tests at pH 5, 60°C with various HAc concentrations are shown in Figure 4.9 below.

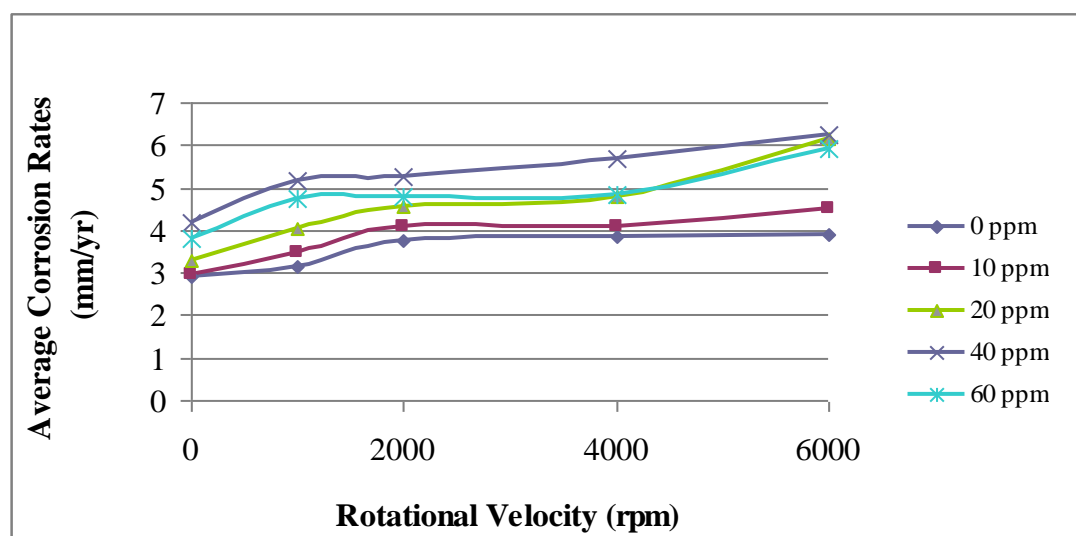


Figure 4.9: Effect of rotational velocity at pH 5, 60°C with different acetic acid concentrations.

In general, rotational velocity has major effect in increasing corrosion rate up to 2000 rpm only. No further effect of rotational velocity to the corrosion rate after 2000 rpm. It is seen approximately an increment of corrosion rate at 6000 rpm from 13% - 43% as compared to 2000 rpm. The results are shown in Table 4.11 below.

Table 4.11: Percentage increase in corrosion rates with the increase in rotational velocity at pH 5, 60°C.

Acetic acid concentration (ppm)	Corrosion rate at static condition (mm/yr)	Percentage difference corrosion rates compared to the static condition			
		1000 rpm	2000 rpm	4000 rpm	6000 rpm
0	1.6	10%	31%	34%	34%
10	1.8	17%	37%	37%	50%
20	2.1	24%	39%	45%	88%
40	2.1	24%	26%	35%	48%
60	2.4	26%	26%	26%	55%

4.1.2.2 Effect of rotational velocity at pH 6

4.1.2.2.1 Effect of rotational velocity at pH 6, Temperature 25°C

The effect of rotational velocity on the corrosion rates as obtained by LPR tests at pH 6, 25°C with various HAc concentrations are shown in Figure 4.10 below.

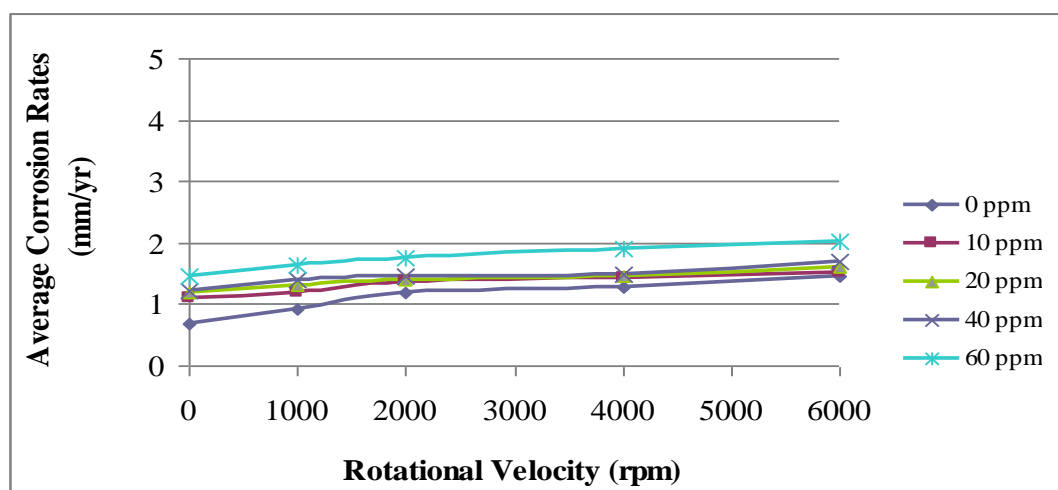


Figure 4.10: Effect of rotational velocity at pH 6, 25°C with different acetic acid concentrations.

In general, rotational velocity has major effect in increasing corrosion rate until 2000 rpm. No significant effect of rotational velocity to the corrosion rate above 2000 rpm. It is seen approximately an increment of corrosion rate at 6000 rpm from 6% - 28% as compared to 2000 rpm. The results are shown in Table 4.12 below.

Table 4.12: Percentage increase in corrosion rates with the increase in rotational velocity at pH 6, 25°C.

Acetic acid concentration (ppm)	Corrosion rate at static condition (mm/yr)	Percentage difference corrosion rates compared to the static condition			
		1000 rpm	2000 rpm	4000 rpm	6000 rpm
0	0.7	29%	71%	86%	114%
10	1.1	9%	27%	27%	36%
20	1.2	8%	17%	25%	33%
40	1.2	17%	25%	25%	42%
60	1.5	7%	20%	27%	33%

4.1.2.2.2 Effect of rotational velocity at pH 6, Temperature 40°C

The corrosion trend with the increase rotational velocity at pH 6, 40°C is shown in Figure 4.11. Corrosion rates increase with increasing rpm for both blank solution (0 ppm HAc) and solution with HAc.

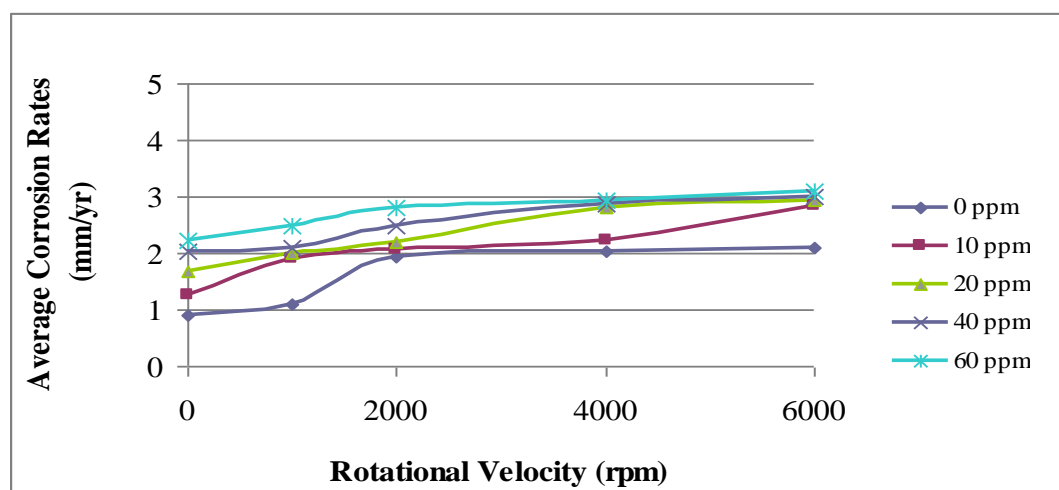


Figure 4.11: Effect of rotational velocity at pH 6, 40°C with different acetic acid concentrations.

In general, a considerable effect of rotational velocity is seen at 2000 rpm. After 2000 rpm, there is no significant effect of rotational velocity in increasing corrosion rate. It is recorded an increment of corrosion rate from 22% - 53% depending on HAc concentration. The results are shown in Table 4.13 below.

Table 4.13: Percentage increase in corrosion rates with the increase in rotational velocity at pH 6, 40°C.

Acetic acid concentration (ppm)	Corrosion rate at static condition (mm/yr)	Percentage difference corrosion rates compared to the static condition			
		1000 rpm	2000 rpm	4000 rpm	6000 rpm
0	0.9	22%	111%	122%	133%
10	1.3	46%	62%	69%	115%
20	1.7	18%	29%	65%	71%
40	2	5%	25%	45%	50%
60	2.2	14%	27%	36%	41%

4.1.2.2.3 Effect of rotational velocity at pH 6, Temperature 60°C

The corrosion trend with the increase rotational velocity at pH 6, 60°C is shown in Figure 4.12. Corrosion rates increase with increasing rpm for both blank solution (0 ppm HAc) and solution with HAc.

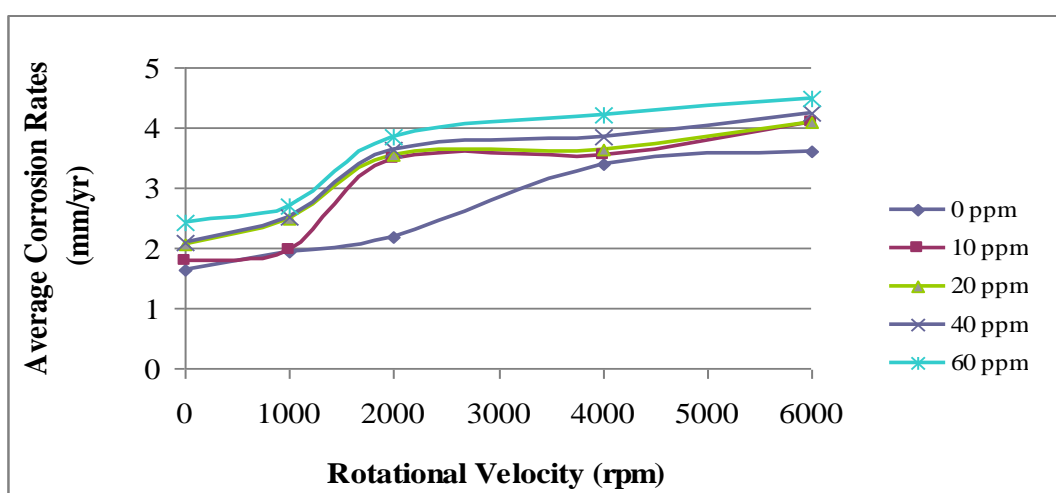


Figure 4.12: Effect of rotational velocity at pH 6, 60°C with different acetic acid concentrations.

In general, corrosion rate at pH 6, 60°C increases with increasing rotational velocity. No major effect of rotational velocity to the increasing of corrosion rate above 2000 rpm for 10 ppm – 60 ppm HAc. The results are shown in Table 4.14 below.

Table 4.14: Percentage increase in corrosion rates with the increase in rotational velocity at pH 6, 60°C.

Acetic acid concentration (ppm)	Corrosion rate at static condition (mm/yr)	Percentage difference corrosion rates compared to the static condition			
		1000 rpm	2000 rpm	4000 rpm	6000 rpm
0	1.6	19%	38%	113%	125%
10	1.8	11%	94%	94%	128%
20	2.1	19%	67%	76%	95%
40	2.1	19%	71%	86%	100%
60	2.4	13%	63%	75%	88%

In most cases, for both pH 5 and pH 6 at temperature 25°C, 40°C and 60°C, corrosion rate increases with increasing rotational velocity. However, it is observed an appreciable effect of rotational velocity up to 2000 rpm only, beyond this not much effect of rotational velocity is observed

4.1.3 Effect of temperature

Effect of temperature on CO_2 corrosion with the presence of various HAc concentrations in turbulent conditions are shown in Figure 4.13 to Figure 4.22.

4.1.3.1 Effect of temperature at pH 5

Effect of temperature on CO_2 corrosion with the presence of various HAc concentrations in turbulent conditions at pH 5 are shown in Figure 4.13 to Figure 4.17.

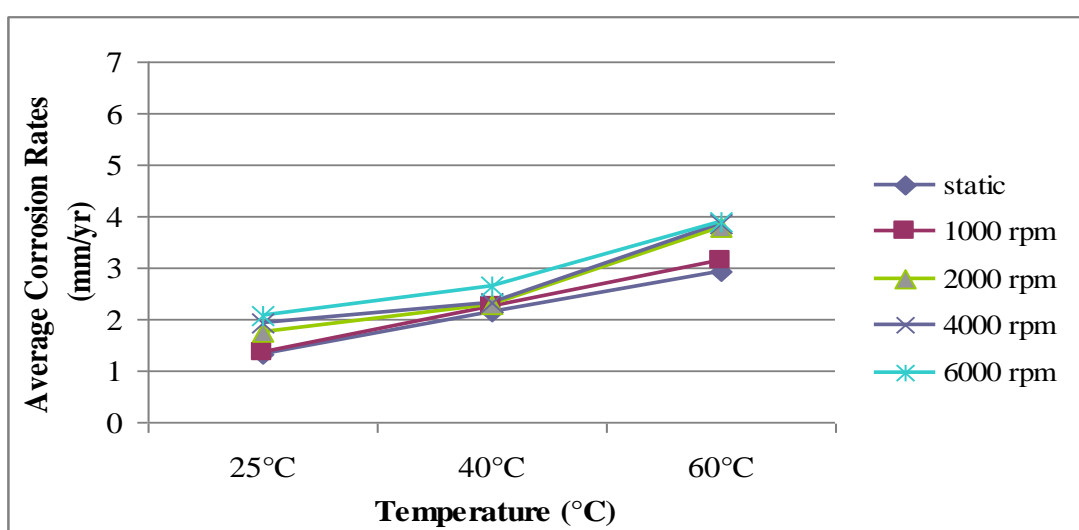


Figure 4.13: Average corrosion rates at different temperature with blank solution.

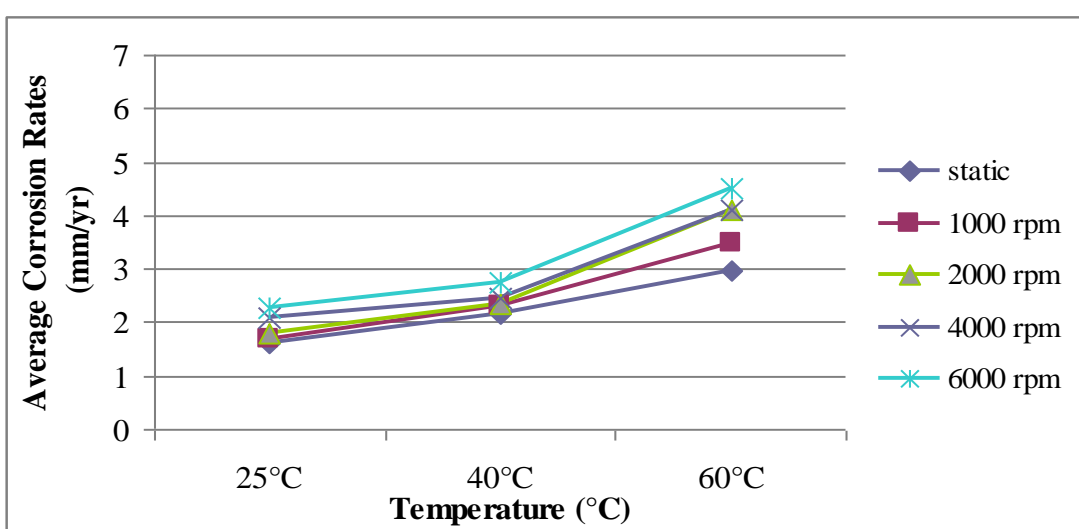


Figure 4.14: Average corrosion rates at different temperature with 10 ppm HAc.

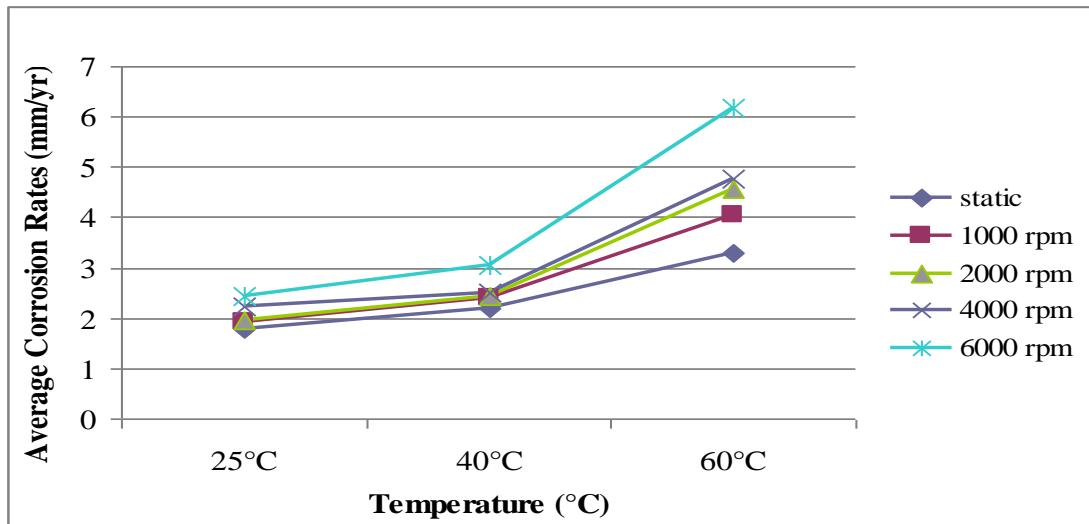


Figure 4.15: Average corrosion rates at different temperature with 20 ppm HAc.

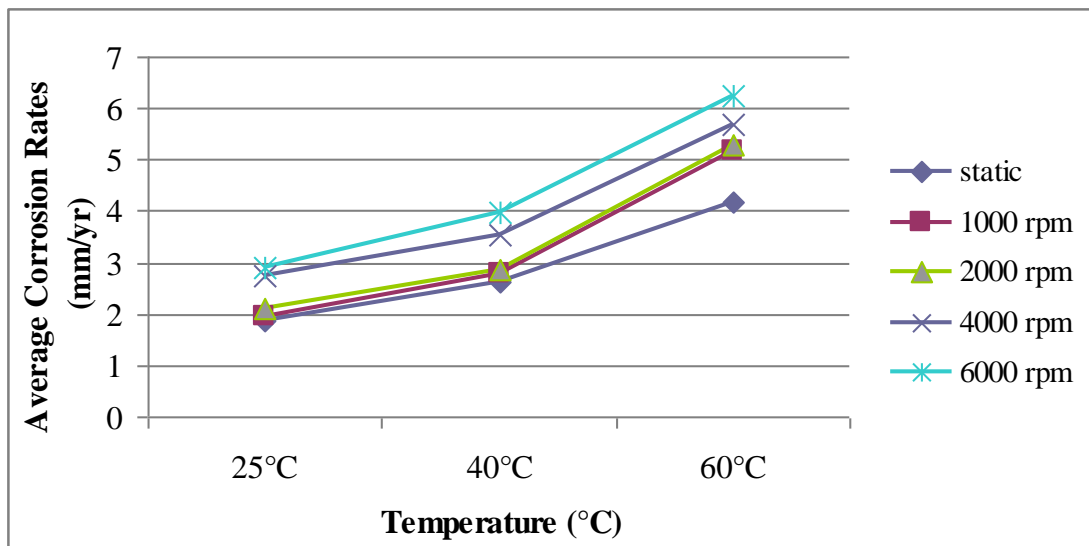


Figure 4.16: Average corrosion rates at different temperature with 40 ppm HAc.

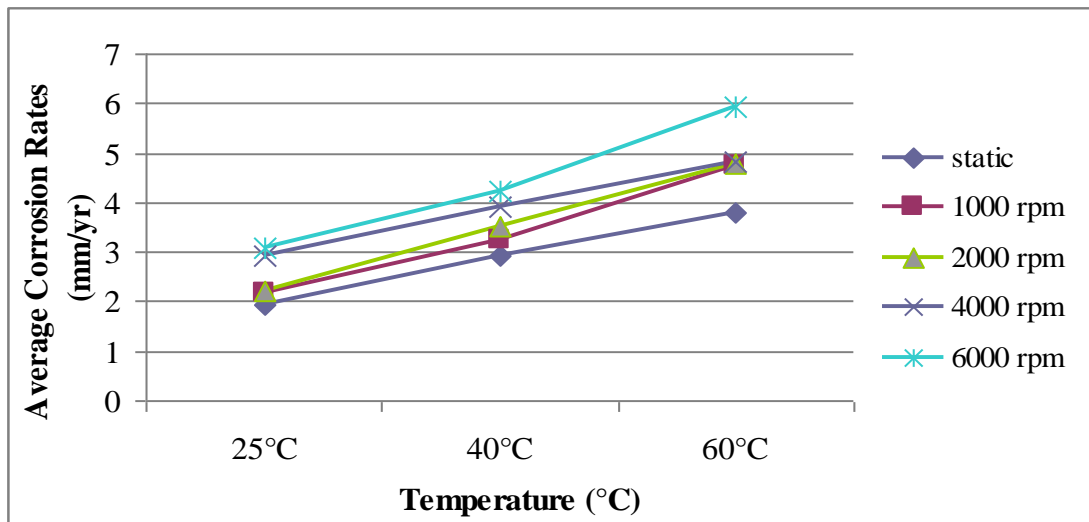


Figure 4.17: Average corrosion rates at different temperature with 60 ppm HAc.

At pH 5, temperature has significant effect in increasing corrosion rate. Depending on HAc concentration and rotational rate, temperature could increase corrosion rate from 14% - 158% as compared to temperature 25°C. The results are shown in Table 4.15 below.

Table 4.15: Percentage increase of corrosion rate at pH 5 with the increasing of temperature as compared to corrosion rate at temperature 25°C.

[HAc]	Temperature (°C)	Percentage increase of corrosion rate as compared to corrosion rate at temperature 25 °C				
		0 rpm	1000 rpm	2000 rpm	4000 rpm	6000 rpm
Blank Solution	40 °C	62%	64%	28%	21%	29%
	60 °C	123%	129%	111%	105%	86%
10 ppm	40 °C	38%	35%	28%	14%	17%
	60 °C	88%	106%	128%	95%	96%
20 ppm	40 °C	22%	26%	25%	14%	29%
	60 °C	83%	116%	130%	118%	158%
40 ppm	40 °C	37%	40%	38%	25%	38%
	60 °C	121%	160%	152%	104%	114%
60 ppm	40 °C	53%	45%	59%	34%	35%
	60 °C	100%	118%	118%	66%	90%

4.1.3.2 Effect of temperature at pH 6

Effect of temperature on CO_2 corrosion with the presence of various HAc concentrations in turbulent conditions at pH 6 are shown in Figure 4.18 to Figure 4.22.

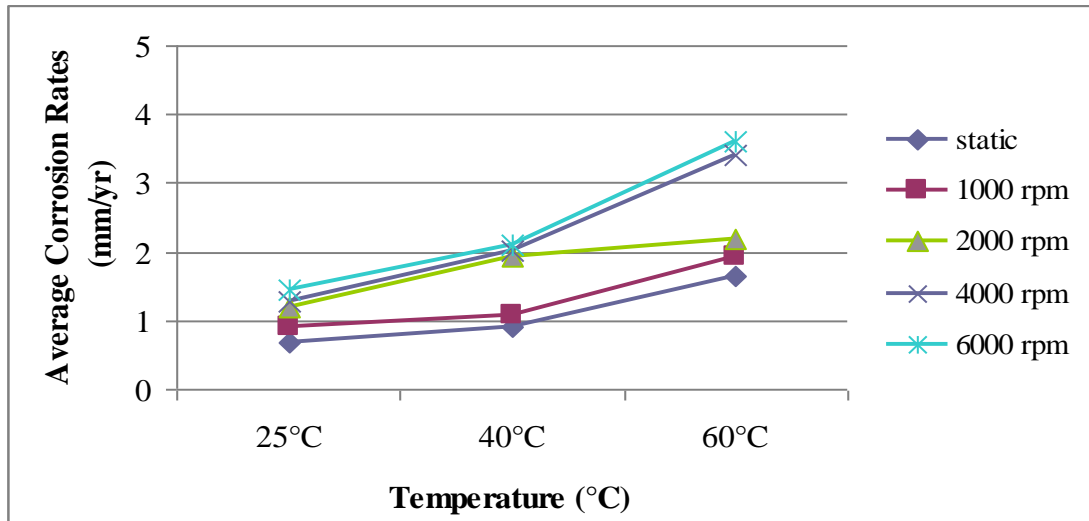


Figure 4.18: Average corrosion rates at different temperature with blank solution.

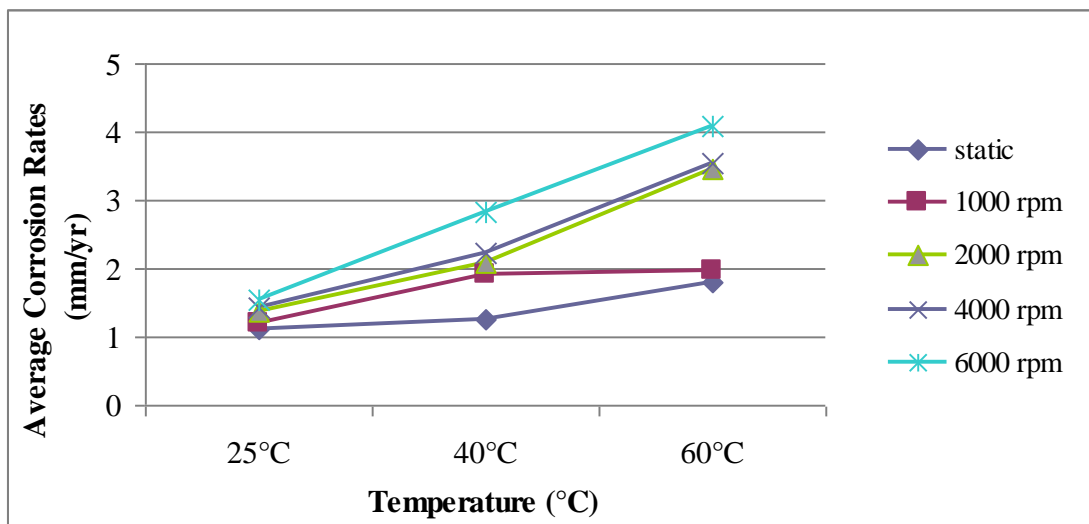


Figure 4.19: Average corrosion rates at different temperature with 10 ppm HAc.

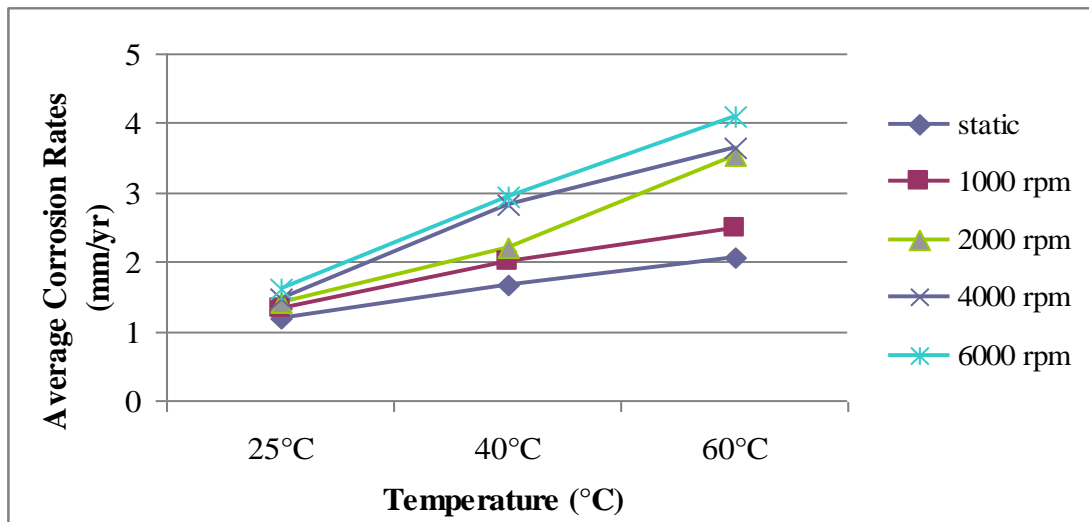


Figure 4.20: Average corrosion rates at different temperature with 20 ppm HAc.

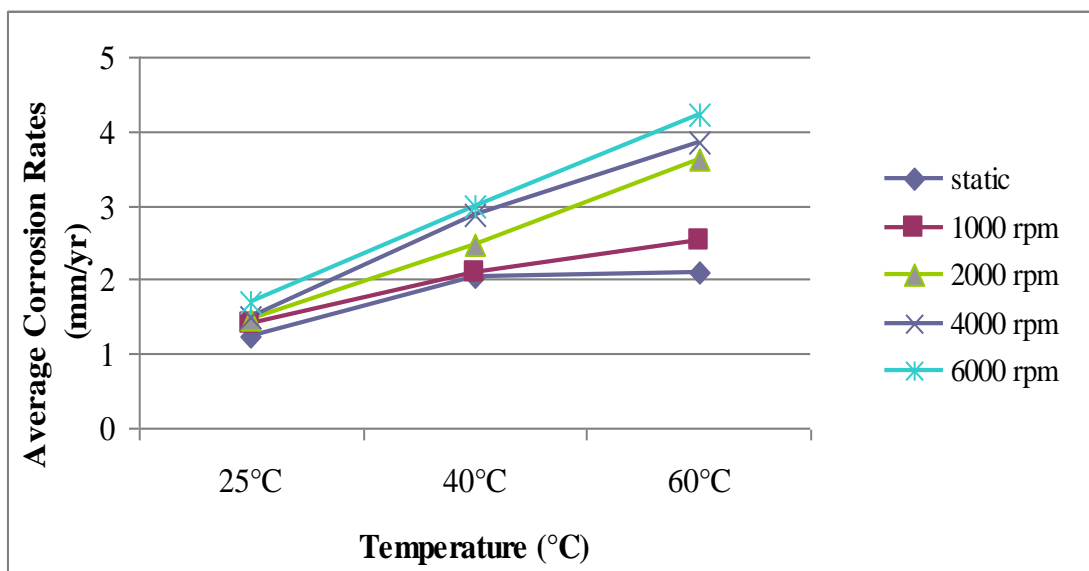


Figure 4.21: Average corrosion rates at different temperature with 40 ppm HAc.

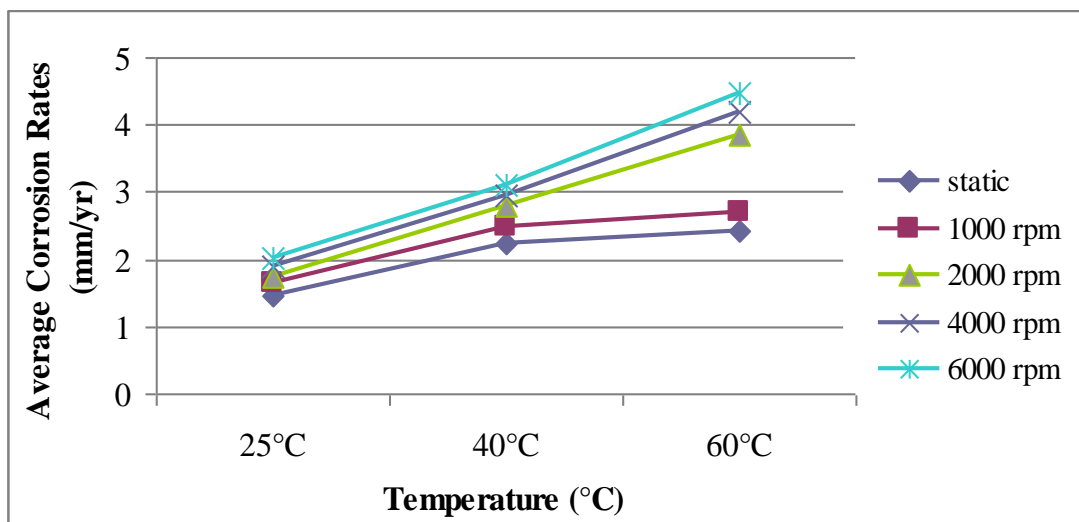


Figure 4.22: Average corrosion rates at different temperature with 60 ppm HAc.

At pH 6, an increasing of corrosion rate due to increasing of temperature is shown in Table 4.16 below. It is seen that temperature has significant effect in increasing corrosion rate. Depending on HAc concentration and rotational rate, temperature could increase corrosion rate from 18% - 156% as compared to temperature 25°C.

Table 4.16: Percentage increase of corrosion rate at pH 6 with the increasing of temperature as compared to corrosion rate at temperature 25°C.

[HAc]	Temperature (°C)	Percentage increase of corrosion rate as compared to corrosion rate at temperature 25 °C				
		0 rpm	1000 rpm	2000 rpm	4000 rpm	6000 rpm
Blank Solution	40 °C	29%	22%	58%	54%	40%
	60 °C	129%	111%	83%	162%	140%
10 ppm	40 °C	18%	58%	50%	57%	87%
	60 °C	64%	67%	150%	150%	173%
20 ppm	40 °C	42%	54%	57%	87%	81%
	60 °C	75%	92%	150%	147%	156%
40 ppm	40 °C	67%	50%	67%	93%	76%
	60 °C	75%	79%	140%	160%	147%
60 ppm	40 °C	47%	56%	56%	58%	55%
	60 °C	60%	69%	117%	121%	125%

It is observed from both pH 5 and 6, corrosion rates increases linearly with increasing temperature up to 60°C. This trend is true for both static and dynamic conditions. A significant effect of temperature to the increment of corrosion rate is observed in this study. Depending on HAc concentration and rotational rate, corrosion rate at pH 5 and 6 could increases from 60 % until 150 % at temperature 60°C as compared to 25°C.

4.2 Potentiodynamic Polarization Test

Potentiodynamic polarisation tests were performed for both cathodic and anodic polarization. The aim of potentiodynamic polarization test is to study the mechanism of CO_2 corrosion with the presence of acetic acid in turbulent conditions.

4.2.1 Cathodic Polarization Tests

Cathodic polarization tests at different HAc concentrations and rotation rates are carried out at temperature 25°C and 60°C .

4.2.1.1 Cathodic Polarization Tests at 25°C .

Cathodic polarization tests of the mild steel in blank CO_2 solutions and in the presence of various HAc concentrations are presented in Figure 4.23 to Figure 4.29.

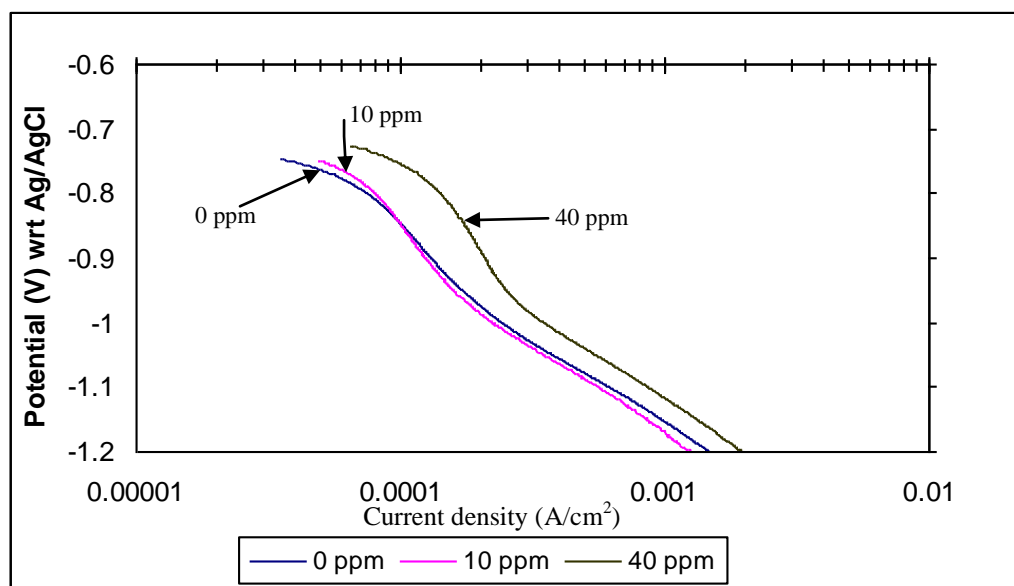


Figure 4.23: Cathodic polarization curves for different HAc concentrations at pH 5, 25°C and 1000 rpm.

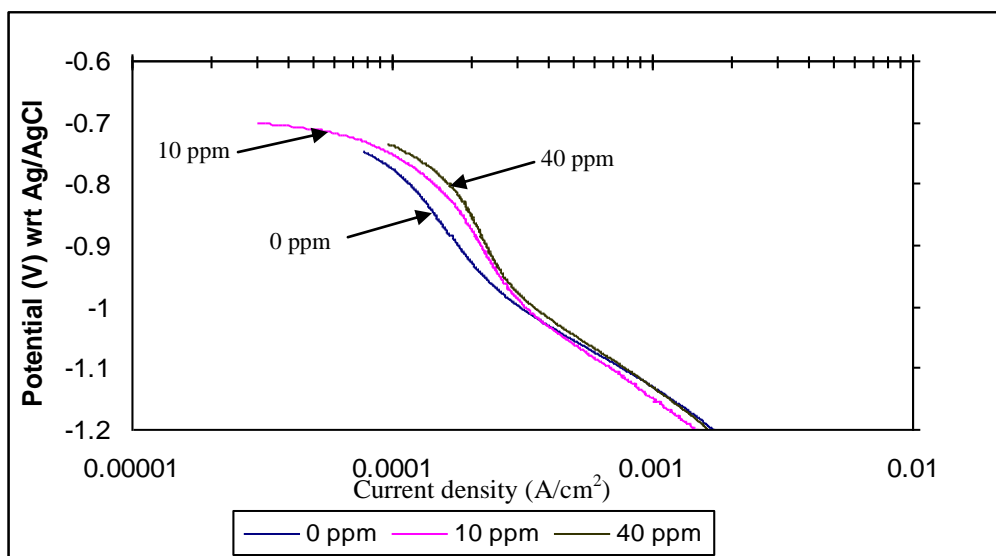


Figure 4.24: Cathodic polarization curves for different HAc concentrations at pH 5, 25°C and 2000 rpm.

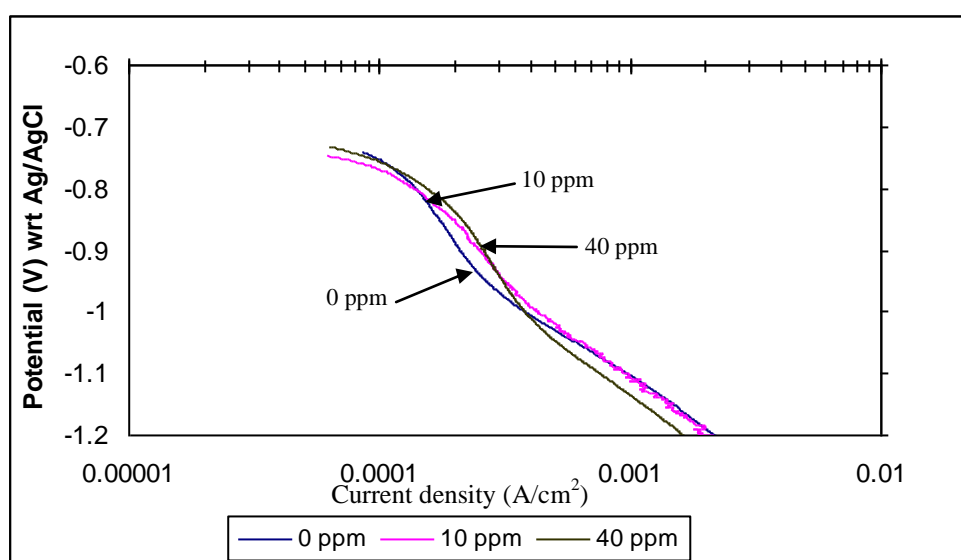


Figure 4.25: Cathodic polarization curves for different HAc concentrations at pH 5, 25°C and 4000 rpm.

At 25°C, cathodic polarization curves demonstrated of mixed cathodic process of diffusion and activation controlled occurring on the surface of electrode. Furthermore, it is observed that limiting current (i_{lim}) increases with increasing HAc concentrations. However, the increment of (i_{lim}) is not significant since there is only few HAc present in the solutions.

4.2.1.2 Cathodic Polarization Tests at 60°C.

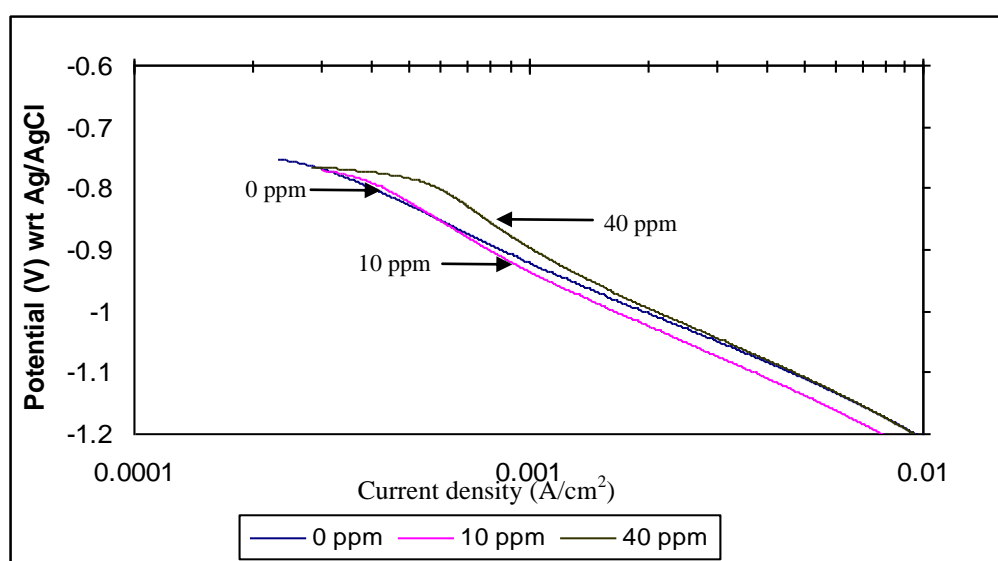


Figure 4.26: Cathodic polarization curves for different HAc concentrations at pH 5, 60°C and 1000 rpm.

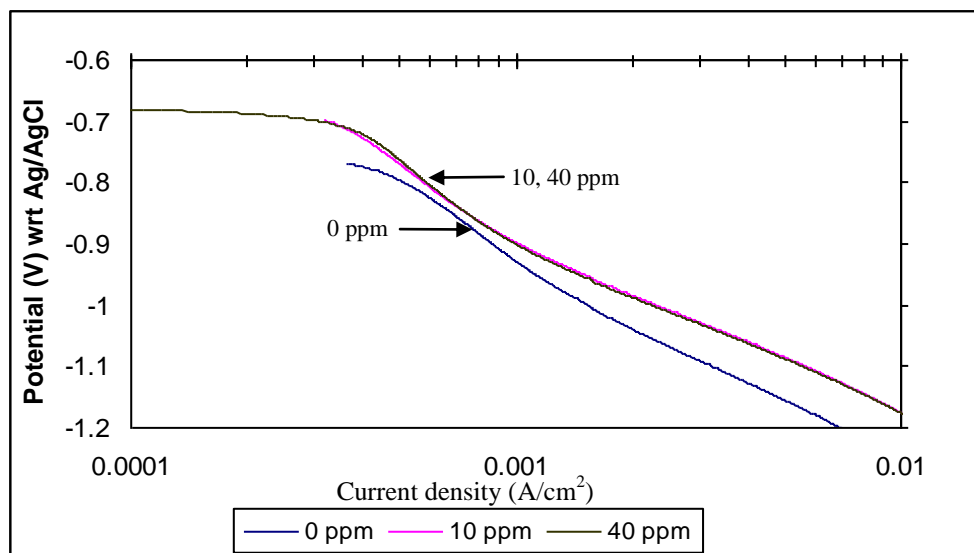


Figure 4.27: Cathodic polarization curves for different HAc concentrations at pH 5, 60°C and 2000 rpm.

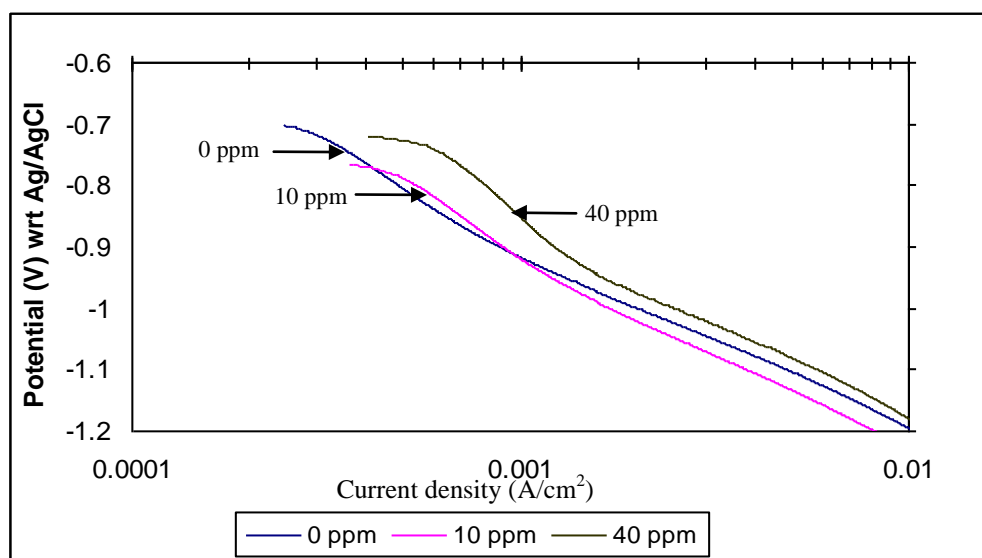


Figure 4.28: Cathodic polarization curves for different HAc concentrations at pH 5, 60°C and 4000 rpm.

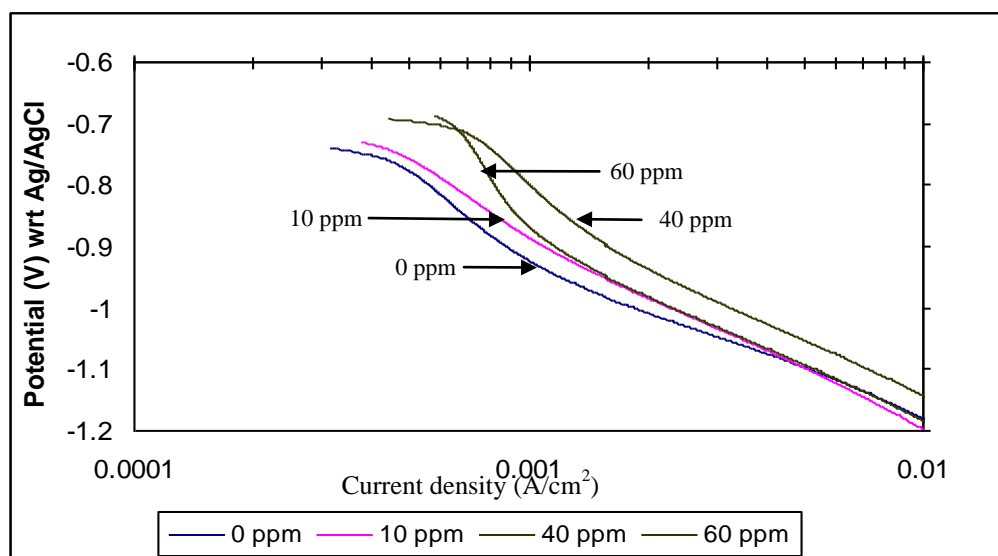


Figure 4.29: Cathodic polarization curves for different HAc concentrations at pH 5, 60°C and 6000 rpm.

It is observed with the presence of acetic acid up to 60 ppm at temperature 60°C, the cathodic polarization curves do not show a well defined limiting current density (i_{lim}) which suggests a mixed cathodic process of diffusion and activation controlled occurring on the surface of electrode. However, cathodic limiting current (i_{lim}) increases with increasing HAc concentrations

4.2.1.3 Flow Effect in CO₂ Corrosion and with the Presence of HAc

Cathodic polarization tests of the mild steel in blank CO₂ solutions and in the presence of various HAc concentrations with different rotation speed are presented in Figure 4.30 to Figure 4.35.

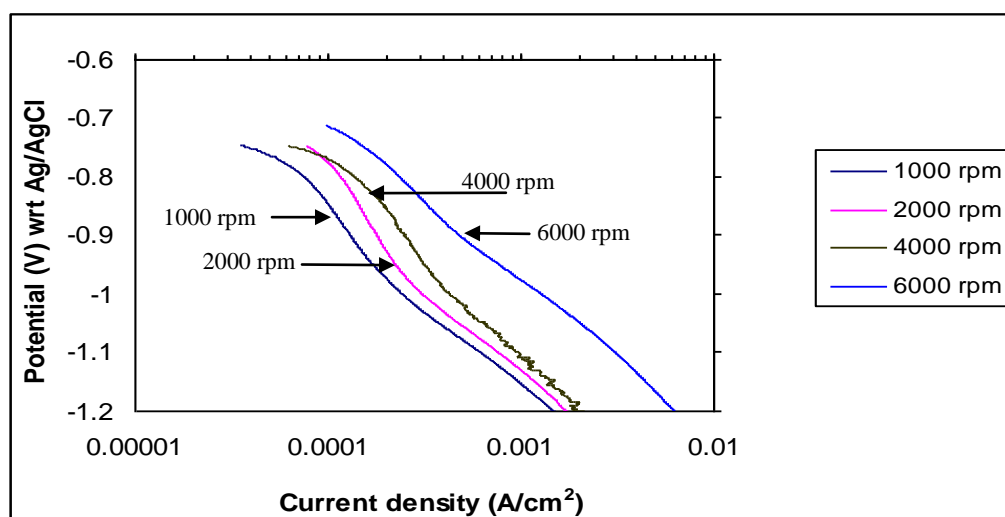


Figure 4.30: Cathodic polarization test at pH 5, 25°C, blank solutions (0 ppm HAc) with various rotation speeds.

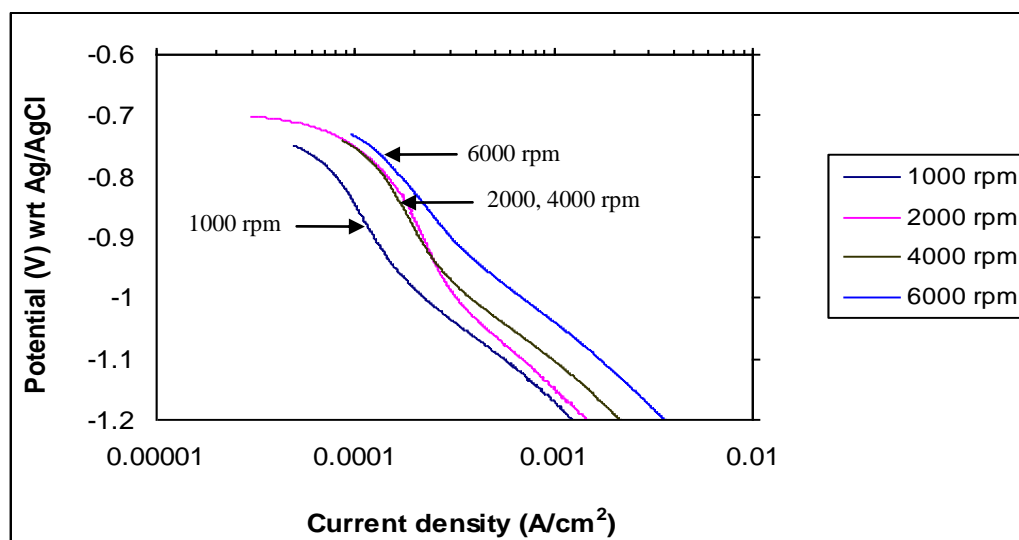


Figure 4.31: Cathodic polarization test at pH 5, 25°C, 10 ppm HAc with various rotation speeds.

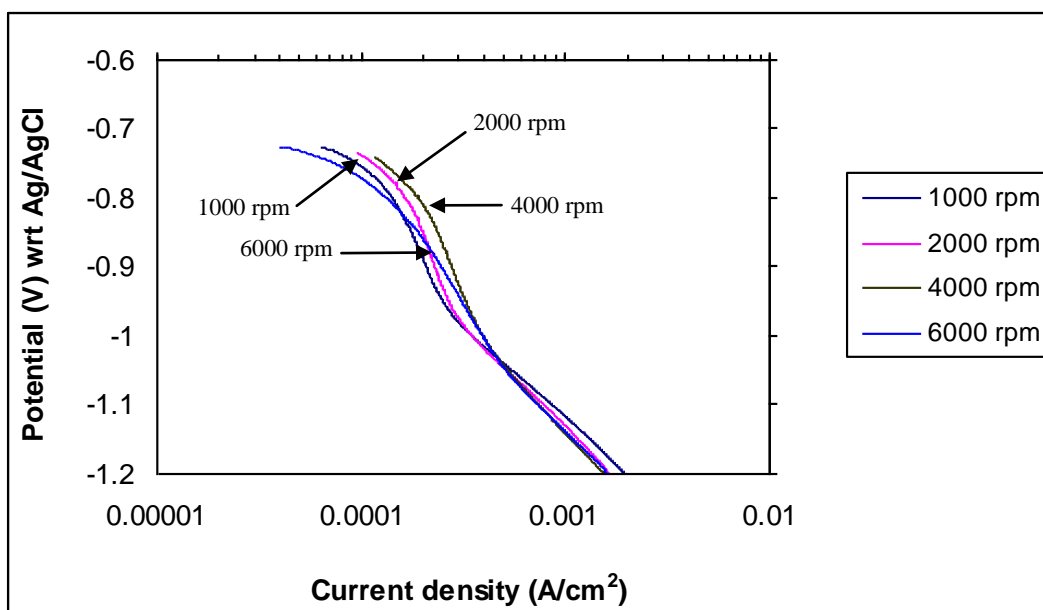


Figure 4.32: Cathodic polarization test at pH 5, 25°C, 40 ppm HAc with various rotation speeds.

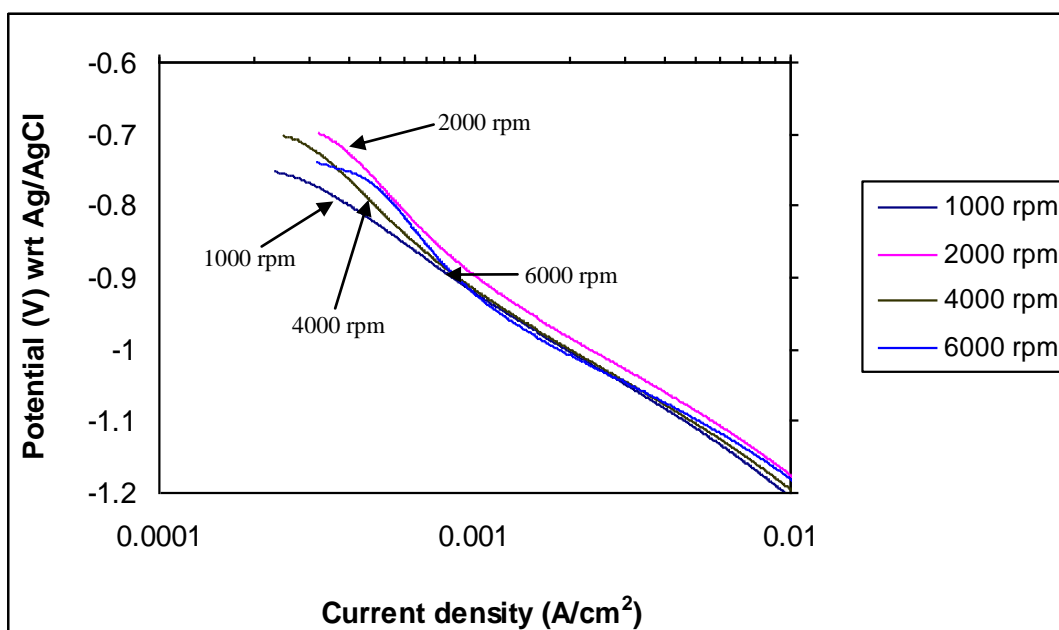


Figure 4.33: Cathodic polarization test at pH 6, 25°C, blank solutions (0 ppm HAc) with various rotation speeds.

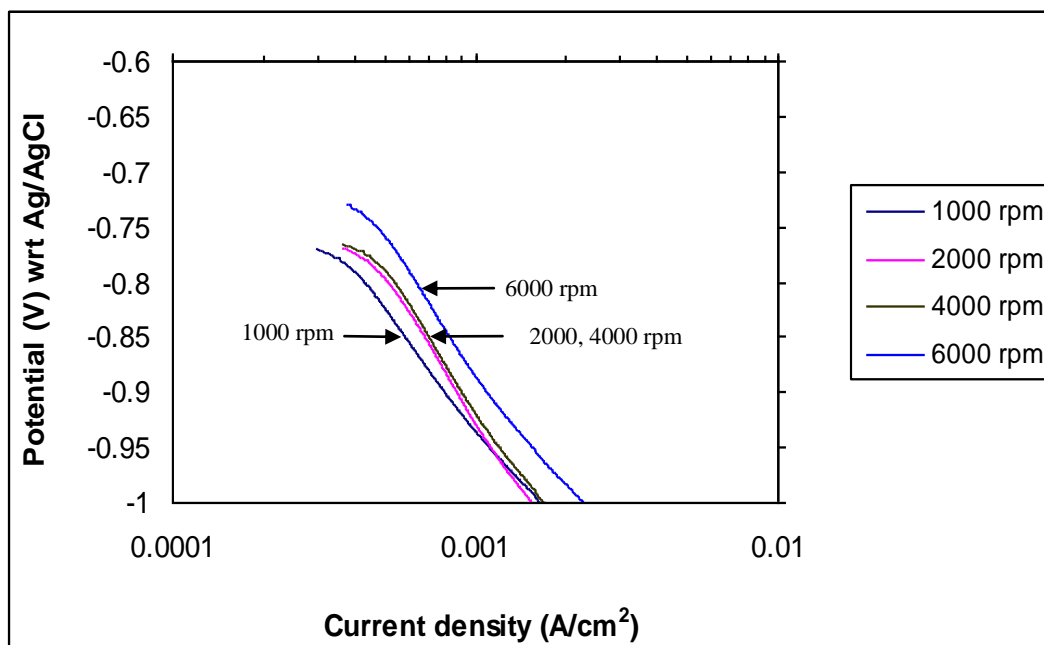


Figure 4.34: Cathodic polarization test at pH 6, 25°C, 10 ppm HAc with various rotation speeds.

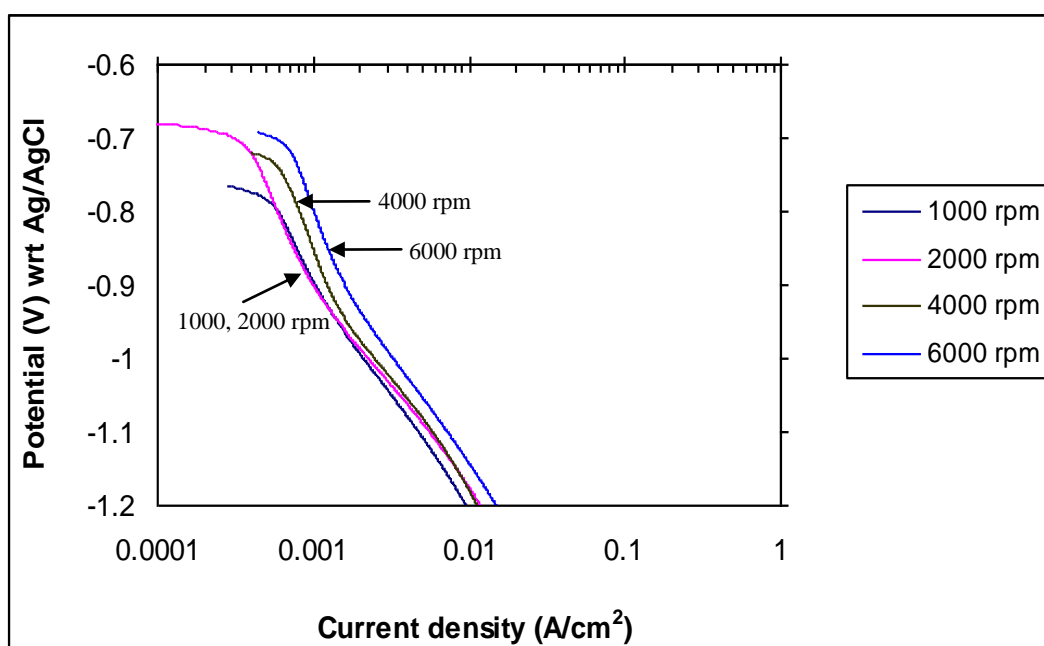


Figure 4.35: Cathodic polarization test at pH 6, 25°C, 40 ppm HAc with various rotation speeds.

It is observed that cathodic limiting current density (i_{lim}) of CO_2 corrosion with the presence of HAc increases with velocity which indicates mass transfer effect in the process. However, cathodic limiting current density (i_{lim}) is also influenced by activation control (chemical reaction). Thus, the behavior of cathodic limiting current density is discussed below in terms of chemical reaction and diffusion process.

4.2.2 Cathodic Polarization Behavior

Cathodic limiting current density (i_{lim}) in turbulent flow conditions of CO_2 corrosion with the presence of HAc species could have contributions from two components, as presented below. This approach follows the findings of Rothman [61], Mendoza [62] and later by Mokhtar [10].

- i) Flow-independent limiting current component or ‘chemical reaction’ limiting current.
- ii) Flow-dependent diffusion of main electro-active species, such as H^+ ions, H_2CO_3 and HAc species.

4.2.2.1 Flow-independent Limiting Current Component or ‘Chemical Reaction’ Limiting Current

By following Eisenberg’s expression, a linear relationship exists between the limiting current densities (i_{lim}) and the rotation rate to power of 0.7. Figure 4.36 to Figure 4.37 show that measured i_{lim} is affected by the rotation rate of the electrode in a linear trend as predicted.

The main point of the plot is the intercept is not zero that indicates a flow independent contribution to the total measured cathodic limiting current density. Thus as in CO_2 corrosion, there seem to be flow-independent and flow dependent components.

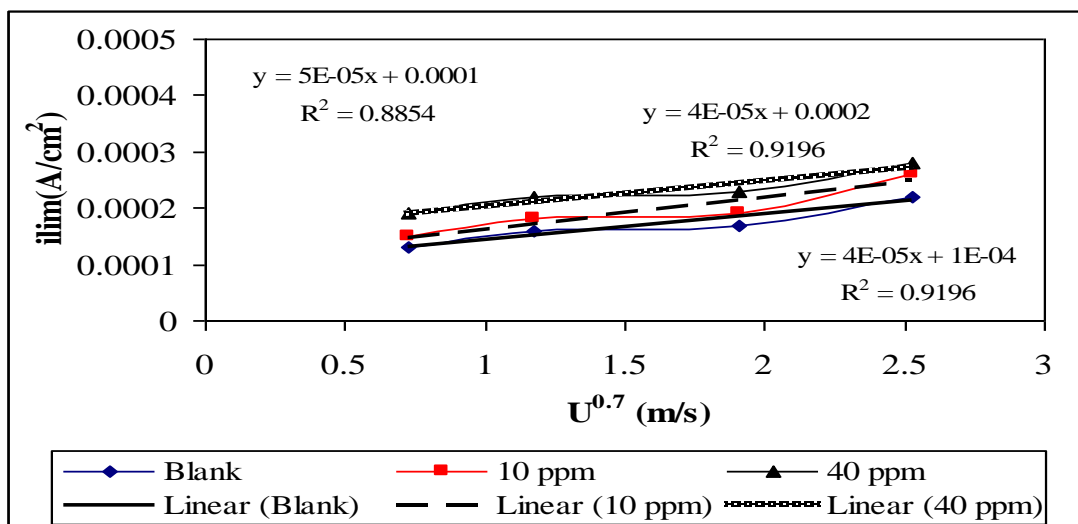


Figure 4.36: Limiting current densities (i_{lim}) as a function of the peripheral velocity (U) to the power of 0.7, 25 °C, pH 5.

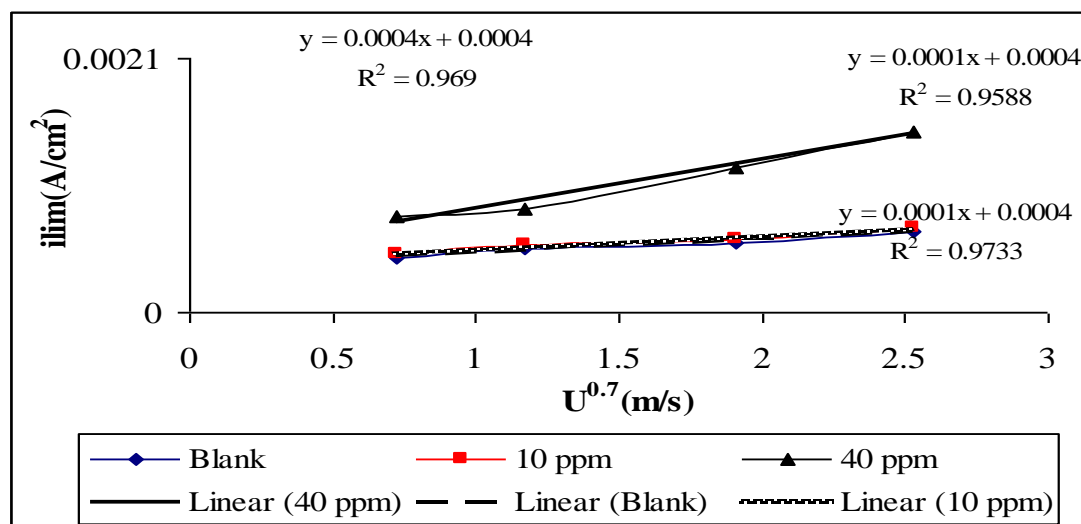


Figure 4.37: Limiting current densities (i_{lim}) as a function of the peripheral velocity (U) to the power of 0.7, 60 °C, pH 5.

The plots based on Eisenberg's correlation in Figure 4.36 to Figure 4.37 reveal that the intercepts are not zero and that indicates a flow independent contribution to the measured cathodic limiting current density. This could be either due to slow hydration of carbonic acid or chemical reaction of HAc.

Since the reaction constant for HAc is fast, in the order of 10^6 s^{-1} , the flow-independent limiting current observed is not due to the slow chemical reaction of HAc dissociation. This suggests it is due to slow hydration of carbonic acid as observed in pure CO_2 corrosion. The limiting current due to slow hydration of carbonic acid can be calculated from the following expression:

$$i_{\text{lim}(\text{H}_2\text{CO}_3)} = FC_{b\text{H}_2\text{CO}_3} \sqrt{(D_{\text{H}_2\text{CO}_3} K_{-1})} \quad (4.1)$$

The intercept value is approximately 0.0001 A/cm^2 at 25°C and 0.0004 A/cm^2 at 60°C and correlates well with the calculated value as shown in Table 4.17 below.

Table 4.17: Intercept values at 25°C and 60°C of the chemical reaction limiting-current calculated versus experimental values.

Test Condition	Limiting Current Density at Intercept (A/cm^2)	
	25°C	60°C
Blank (Calculation)	0.00012	0.0004
Blank (Experiment)	0.0001	0.0004
10 ppm HAc	0.0001	0.0004
40 ppm HAc	0.0002	0.0004

Since HAc does not contribute to the chemical reaction limiting current, we can suggest that the distinct limiting current observed with 10-40 ppm at 25°C and 60°C is due to mass transfer or diffusion of acetic species and other species present in the solution.

4.2.2.2 Flow-dependent Limiting Current Density

The mass transfer limiting current density arising from the presence of acetic acid can be calculated from the following expression.

$$i_{im} = Fk_m [HAc]_b \quad (4.2)$$

Where k_m is the HAc mass transfer coefficient in m/s and $[HAc]_b$ is the bulk concentration of HAc.

The mass transfer coefficient, k_m , is obtained from the expression for the rotating cylinder correlation [52]:

$$Sh = \frac{k_m d}{D} = 0.0791 Re^{0.7} Sc^{0.356} = 0.079 \left(\frac{ud}{\nu} \right)^{0.7} \left(\frac{\nu}{D} \right)^{0.7} \quad (4.3)$$

Where d is the diameter of the electrode in m, D is the hydrogen diffusion coefficient in m²/s, Re is the Reynolds number, Sh is the Sherwood number and Sc is the Schmidt number.

The temperature dependence of the diffusion coefficient is given by:

$$D = D_{ref} \left(\frac{T}{T_{ref}} \right) \left(\frac{\mu_{ref}}{\mu} \right) \quad (4.4)$$

Where D_{ref} is the diffusion coefficient at a reference temperature T_{ref} , μ is the viscosity in kg/(ms) and μ_{ref} is the viscosity at a reference temperature. At 20°C, the μ_{ref} of water is 1.002×10^{-3} kg/(ms) and the D_{ref} of hydrogen ion is 9.31×10^{-9} m²/s [63].

The density of water in kg/m³ is found from:

$$\rho = 1152.3 - 0.5116T, \text{ where } T \text{ is temperature in } ^\circ\text{K}; \quad (4.5)$$

And the water viscosity is given by

$$\mu = \mu_{ref} 10^{\frac{1.327(2-t) - 0.00105(20-t)^2}{t+105}}, \quad t \text{ is temperature in } ^\circ\text{C}. \quad (4.6)$$

Similarly, the limiting current densities due to the diffusion of H^+ ions and H_2CO_3 molecules can be calculated by the expression proposed by Eisenberg et al.

4.2.2.2.1 Limiting Current due to Hydrogen Ion (H^+) and Carbonic Acid (H_2CO_3) Species

Based on the experimental results of blank solution at both 25°C and 60°C , the contribution of limiting current due to reduction of hydrogen ions (H^+) and carbonic acid (H_2CO_3) species is determined by subtracting the chemical reaction limiting current at each rotation rate. The experimental data and calculated values are compared as shown in the Figure 4.38 to Figure 4.39.

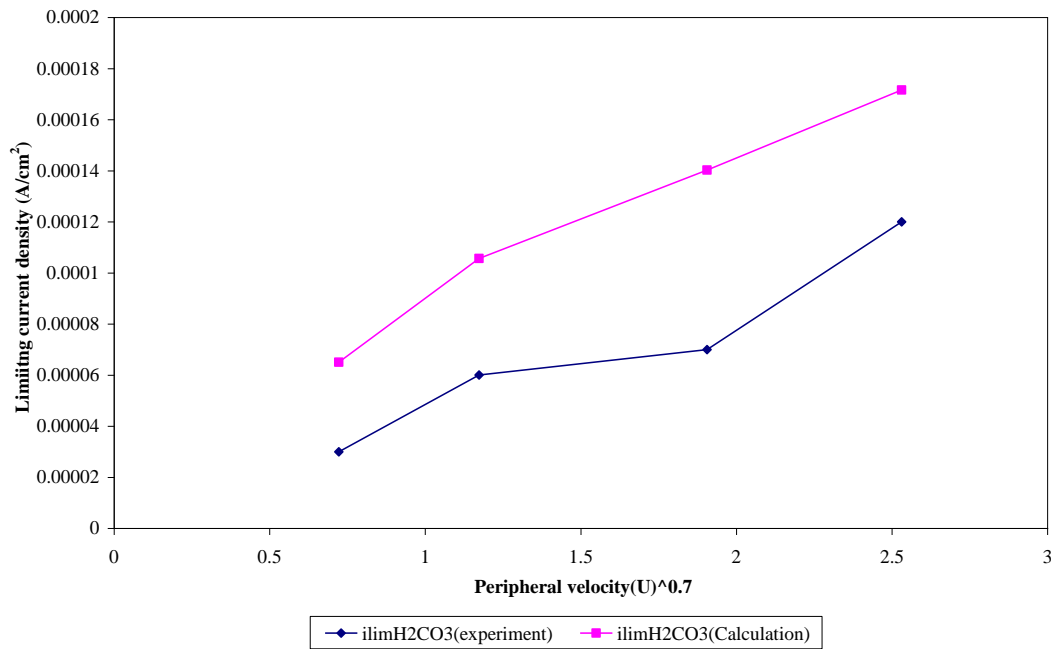


Figure 4.38: Comparison of the limiting current due to H^+ and H_2CO_3 species at 25°C .

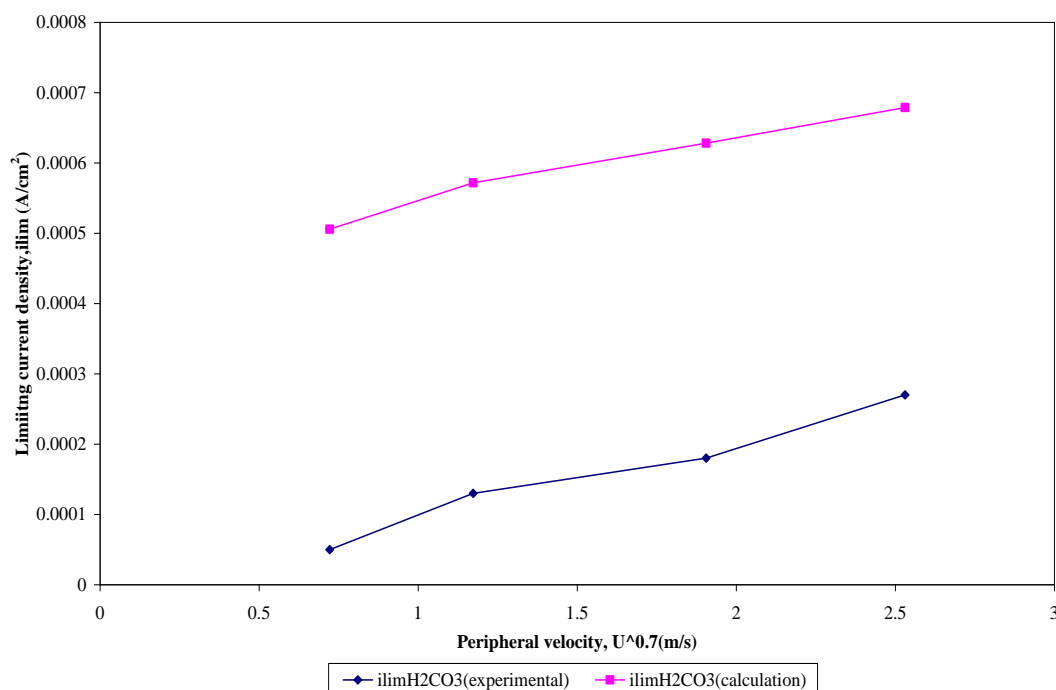


Figure 4.39: Comparison of the limiting current due to H^+ and H_2CO_3 species at 60°C.

4.2.2.2.2 Limiting Current Density due to Acetic Acid

The limiting current density due to acetic acid (HAc) is calculated by subtracting the contribution of limiting current density from other species of the blank solution. The calculated values and experimental data of the i_{lim} due to HAc species are presented in the Figure 4.40 to Figure 4.43. The calculated limiting current increases with the peripheral velocity, while the experimental limiting current increases at 10 ppm, 25°C and 40 ppm 60°C only.

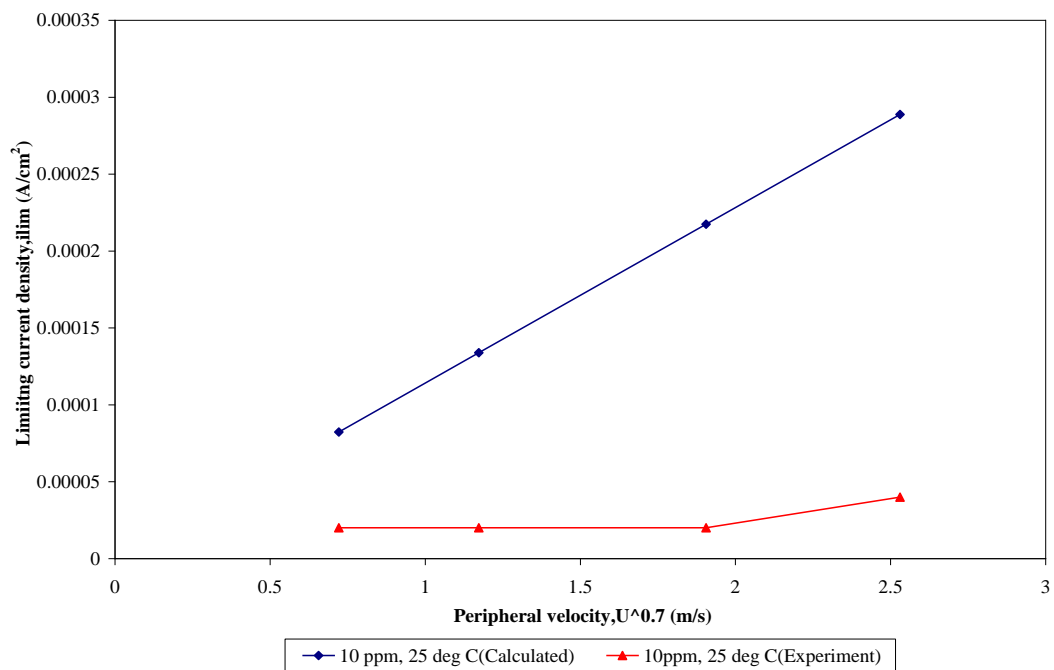


Figure 4.40: Calculated limiting current density due to 10 ppm HAc vs experimental i_{lim} at 25°C.

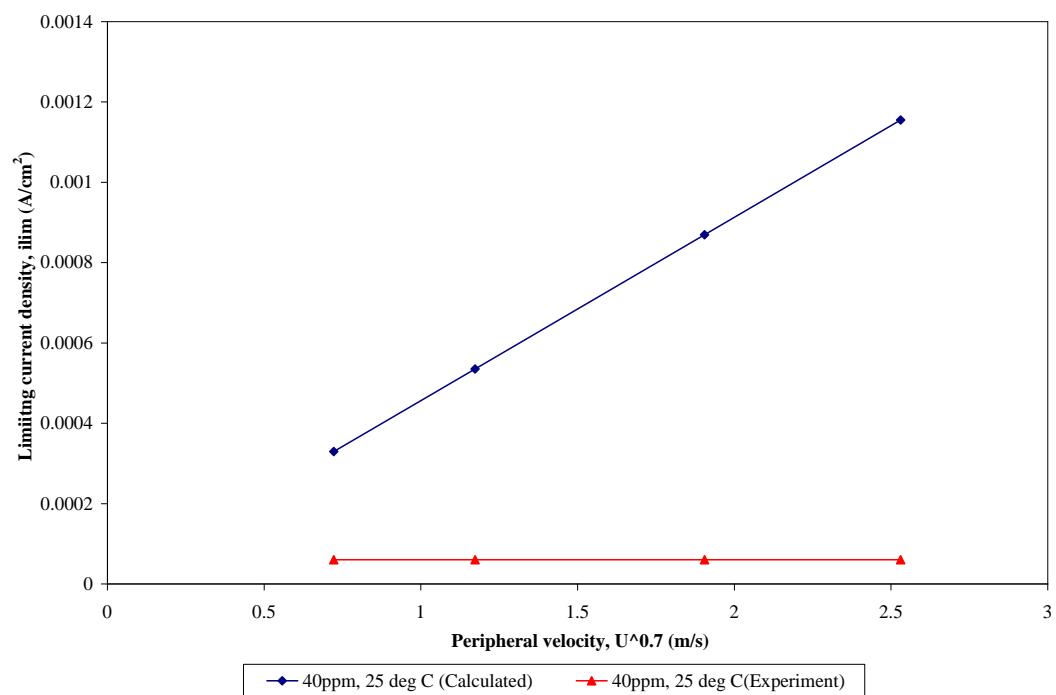


Figure 4.41: Calculated limiting current density due to 40 ppm HAc vs experimental i_{lim} at 25°C.

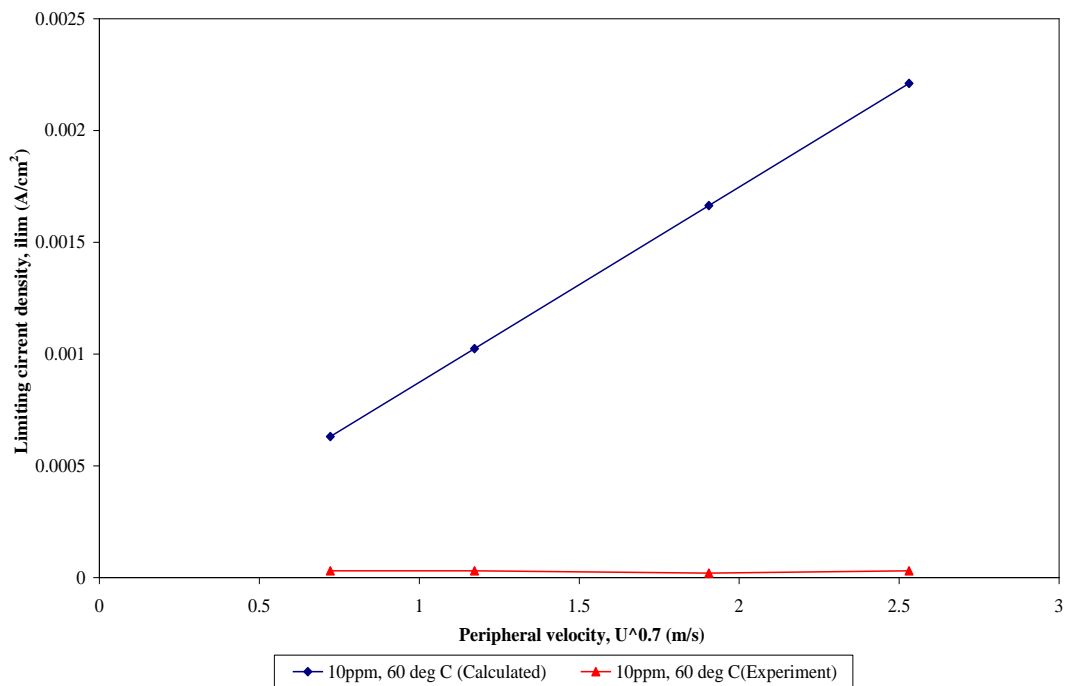


Figure 4.42: Calculated limiting current density due to 10 ppm HAc vs experimental i_{lim} at 60°C.

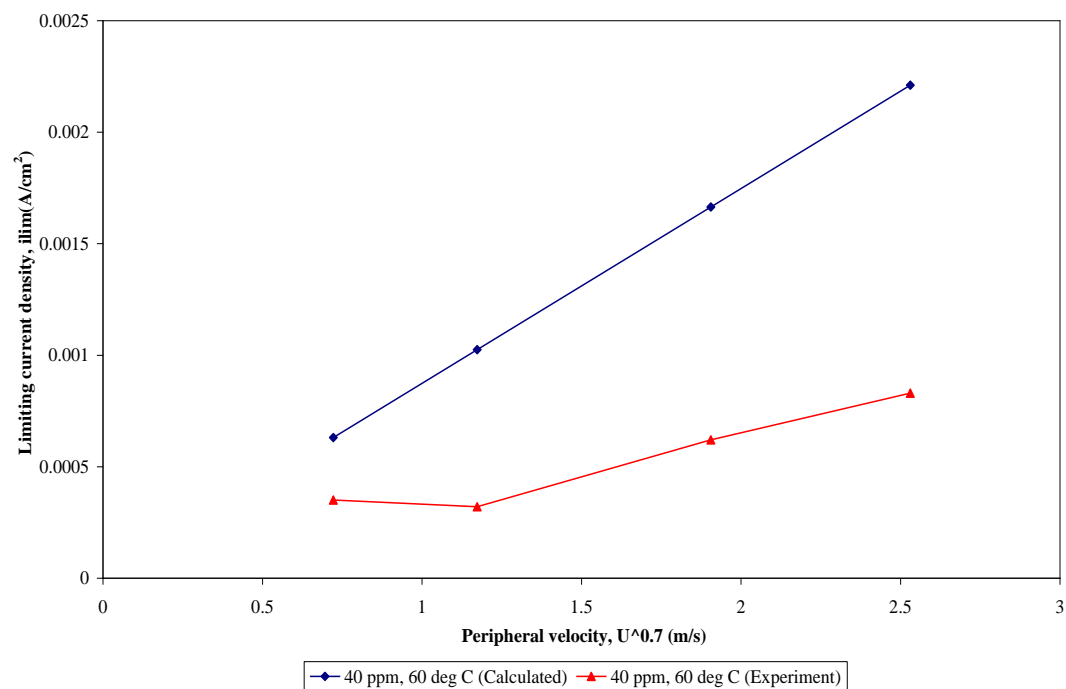


Figure 4.43: Calculated limiting current density due to 40 ppm HAc vs experimental i_{lim} at 60°C.

It is evident that the calculated limiting currents are quite similar in magnitude to the experimental values. The limiting currents calculated would be in better agreement with the experimental values if total limiting currents were taken into account. The total calculated i_{lim} comes from the contribution of CO_2 corrosion and due to the presence of HAc species. The results are shown in Figure 4.44 to Figure 4.47 below.

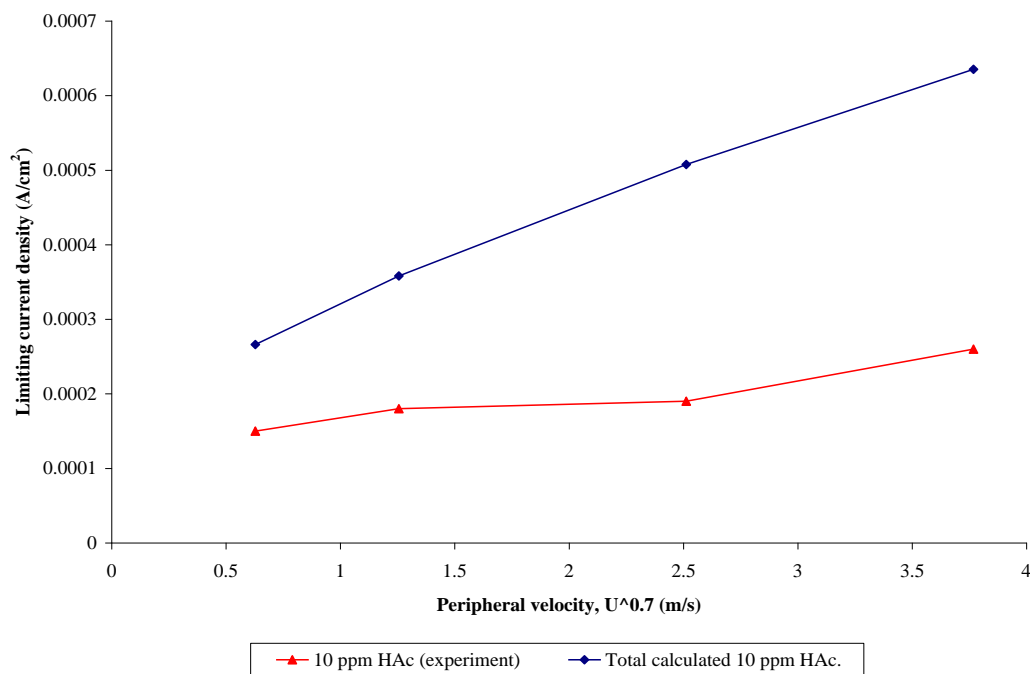


Figure 4.44: Comparing calculated total limiting current to experimental i_{lim} , 10 ppm HAc, 25°C.

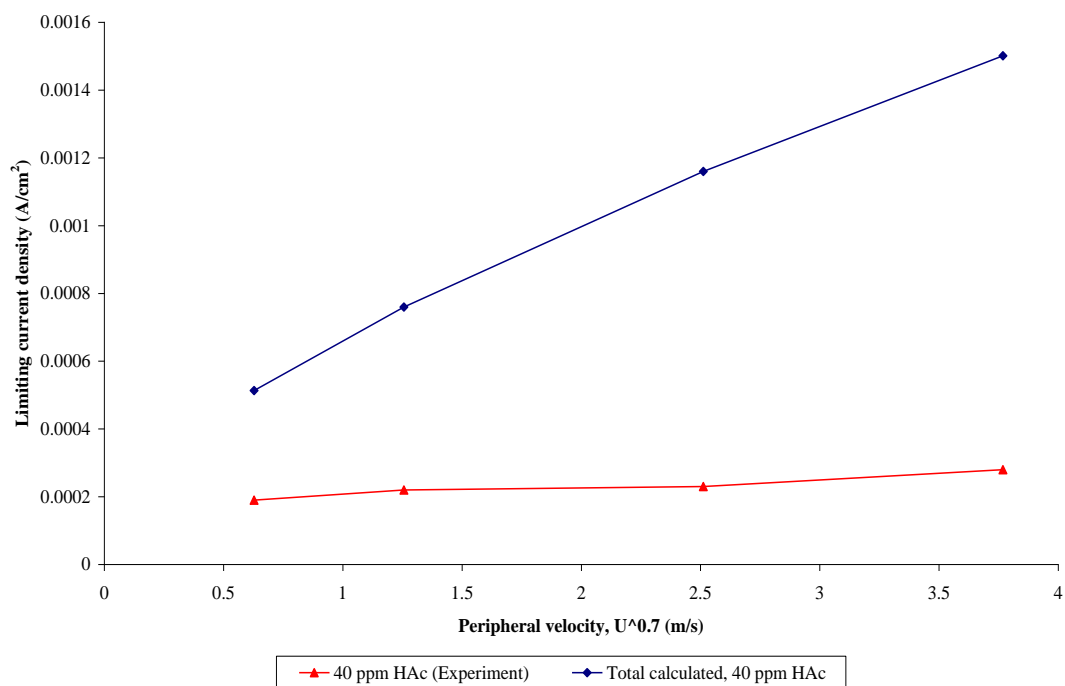


Figure 4.45: Comparing calculated total limiting current to experimental i_{lim} , 40 ppm HAc, 25°C.

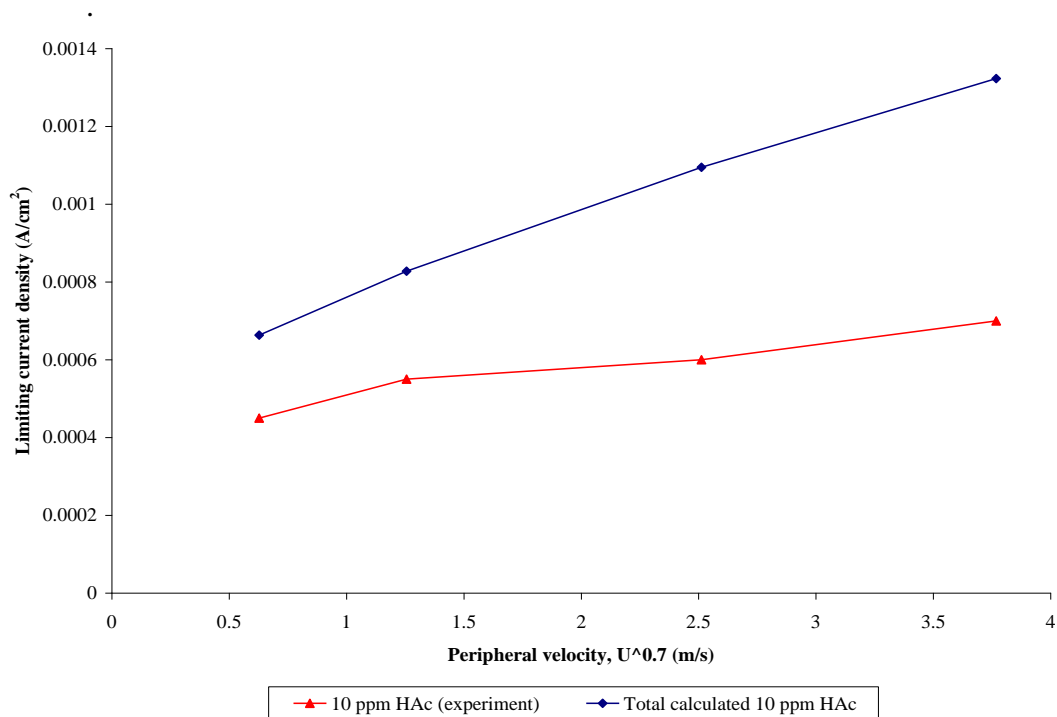


Figure 4.46: Comparing calculated total limiting current to experimental i_{lim} , 10 ppm HAc, 60°C.

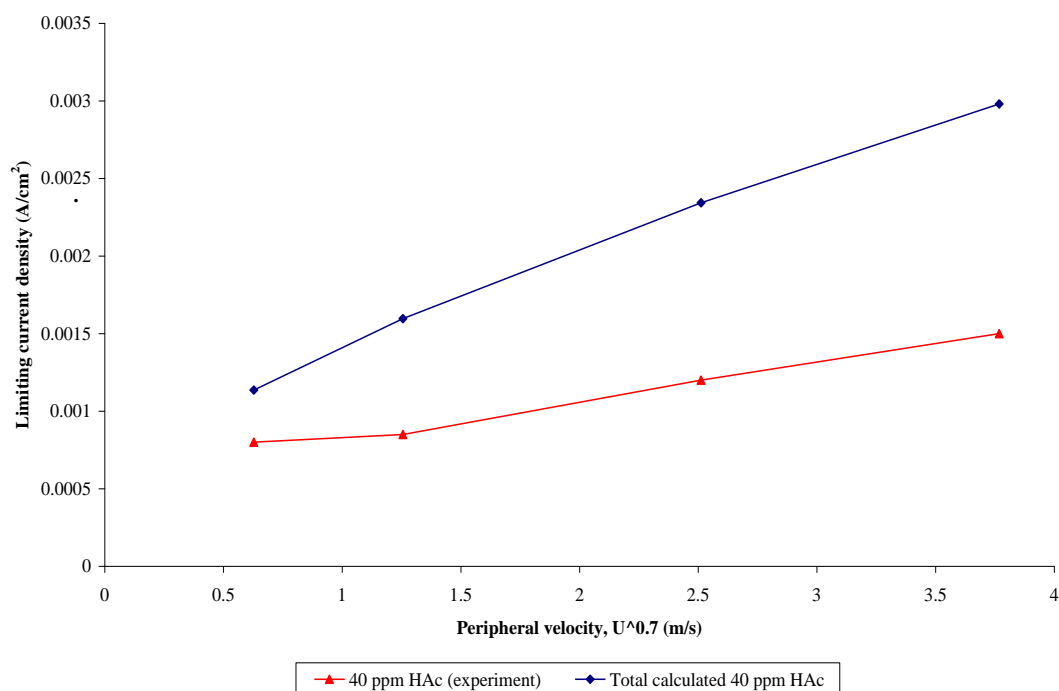


Figure 4.47: Comparing calculated total limiting current to experimental i_{lim} , 40 ppm HAc, 60°C.

4.2.2.2.3 The Effect of HAc Concentration on Limiting Current (i_{lim})

In both cases at 25°C and 60°C, most of the cathodic limiting current densities increase with the increase in HAc concentration, except at pH 5, 60°C. At this condition, corrosion rates decrease when added by 60 ppm HAc as compared to 40 ppm HAc. This fact is due to decline of cathodic reaction as shown in Figure 4.48.

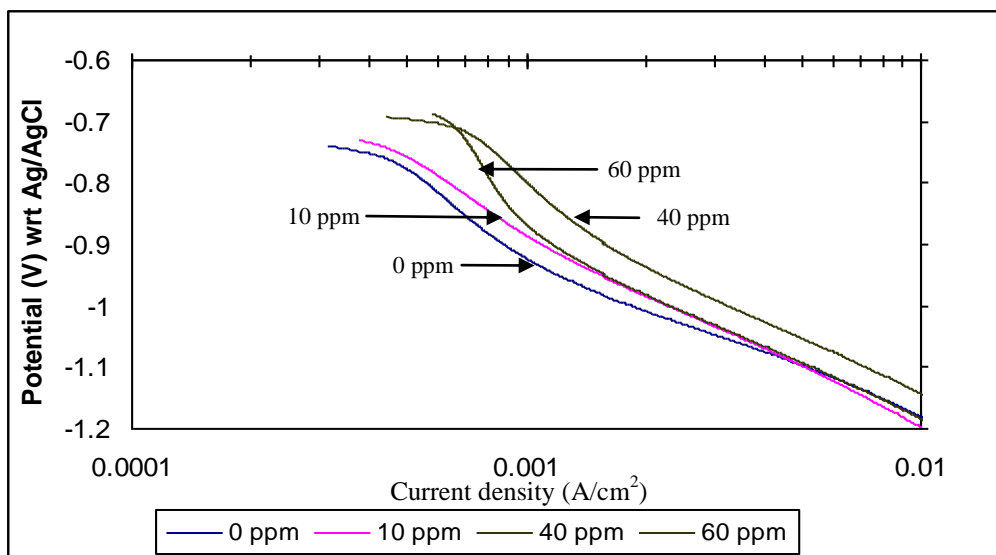


Figure 4.48: Cathodic polarization tests at pH 5, 60°C, 4000 rpm with various HAc concentrations.

However, the increase of corrosion rate can be attributed to the presence of more availability of acetic acid species to be transported and reduced on the surface. The increase in i_{lim} with concentration is shown in Table 4.18 below for both 25°C and 60°C.

Table 4.18: Experimental and calculated limiting current densities.

HAc Concentration	Limiting Current Density, i_{lim} (A/cm ²)			
	25°C		60°C	
	Experimental	Calculation	Experimental	Calculation
10 ppm	0.00015	0.000082	0.00048	0.00016
40 ppm	0.00019	0.00033	0.00056	0.00063

4.2.3 Anodic Polarization Tests

The anodic polarization sweeps were done at pH 5, 60°C, 40 ppm HAc with various rotation speeds. Furthermore, anodic polarization sweeps were done at pH 5, 60°C, 4000 rpm with various HAc concentrations. The results are shown in Figure 4.49 to Figure 4.50.

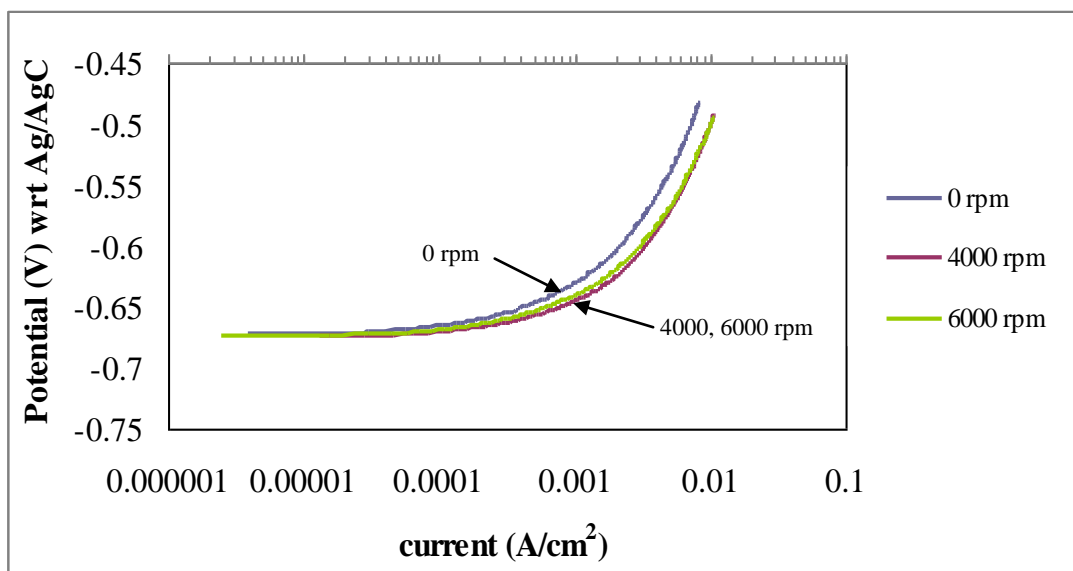


Figure 4.49: Flow effect on anodic sweeps at pH 5, 60°C, 40 ppm HAc.

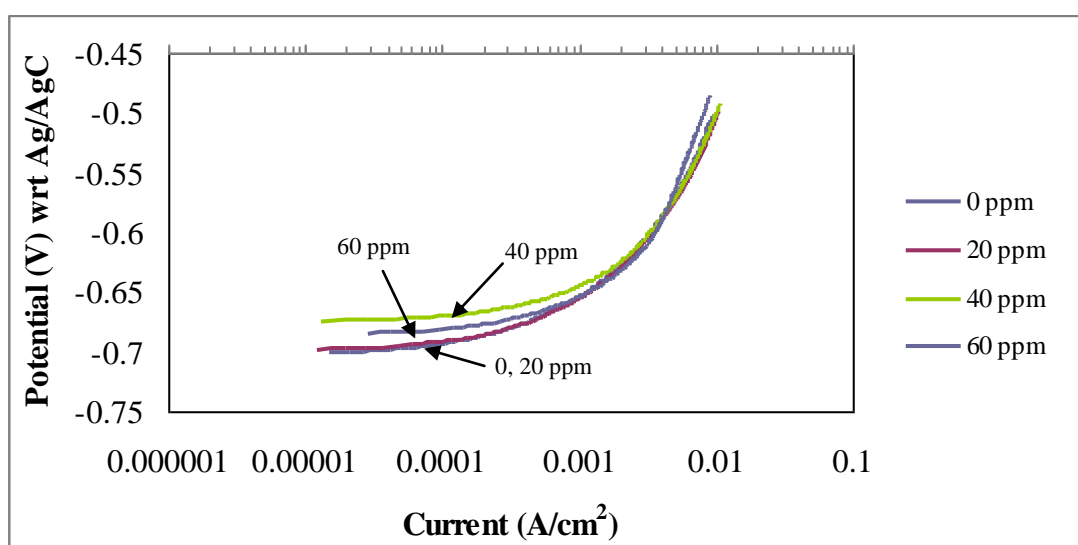


Figure 4.50: The effect of HAc concentrations on the anodic sweeps in bubbling CO_2 solutions at 4000 rpm, pH 5 and 60°C.

Anodic polarization tests illustrated that there is no change in anodic mechanism of CO₂ corrosion with HAc in turbulent conditions. These results have good agreement with study that have been done by George and Mokhtar [5,10].

4.2.4 Corrosion Rate Behavior based on LPR Tests.

It is examined that there is no significant increase of corrosion rate for both pH 5 and 6 when concentration of HAc below 40 ppm. It increases approximately 20 % as compared to the blank solution. An addition of HAc 40 ppm is required to give a significant effect in corrosion rate, whereby a maximum 68 % at pH 5 and 120 % at pH 6 depending on temperatures.

It is also investigated that corrosion rate rises at higher temperature. This is due to acceleration of cathodic reaction when temperature increases. The increase of cathodic reaction in CO₂ corrosion is due to the HAc contribution to hydrogen ions through possibly dissociation and reduction. It is worthy note that below the inhibitive level, the higher the concentration of acetic present, the higher is the hydrogen ions produced.

At higher temperature, the diffusion coefficient of HAc is higher which result in more species availability, approximately a twofold increase of corrosion rate with 60 ppm HAc at 25°C than at 60°C. At room temperature, the value of diffusion coefficient of HAc is $1.24 \times 10^{-9} \text{ m}^2/\text{s}$ whereas at 60°C the value is $2.3 \times 10^{-9} \text{ m}^2/\text{s}$, which is 85 % higher.

Furthermore, LPR tests show that corrosion rate increases with increasing rotational velocity. It is observed a major effect of rotational velocity up to 2000 rpm. No further effect of rotational velocity above 2000 rpm. For not fully developed protective film surface, the effect of rotational velocity is related to the transport of species towards and away from the metal surface. This is related with cathodic limiting current (i_{lim}) which increases with increasing velocity.

The comparison of the measured limiting current density (i_{lim}) and corrosion current density (i_{corr}) with the peripheral velocity is shown in Figure 4.51 to Figure 4.56. As observed in previous data, i_{lim} increases with the velocity indicating the effect of diffusion in the reduction process. However, the corrosion current density (i_{corr}) only varies a little with the velocity. In general we can conclude that i_{corr} values are practically lower than the i_{lim} and independent of the peripheral velocity. Thus with the presence of the HAc species, the overall corrosion process taking place on the surface of electrode is mainly controlled by a charge transfer process.

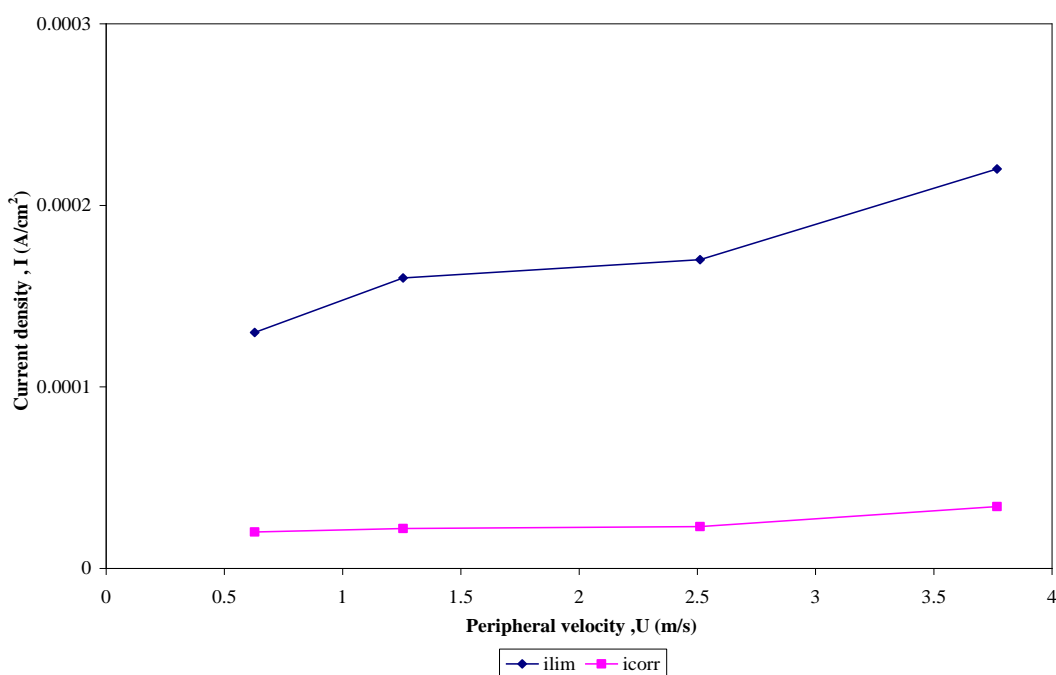


Figure 4.51: Comparison of the measured limiting current density (i_{lim}) with the corrosion current density (i_{corr}) at different peripheral velocity, pH 5, blank, 25°C.

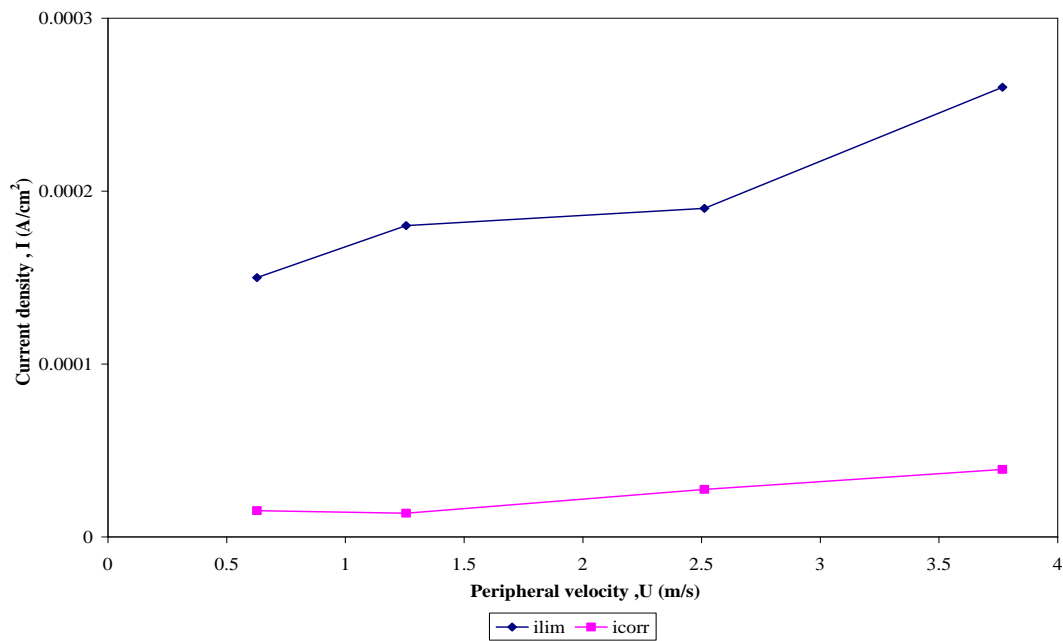


Figure 4.52: Comparison of the measured limiting current density (i_{lim}) with the corrosion current density (i_{corr}) at different peripheral velocity, pH 5, 10 ppm HAc, 25°C.

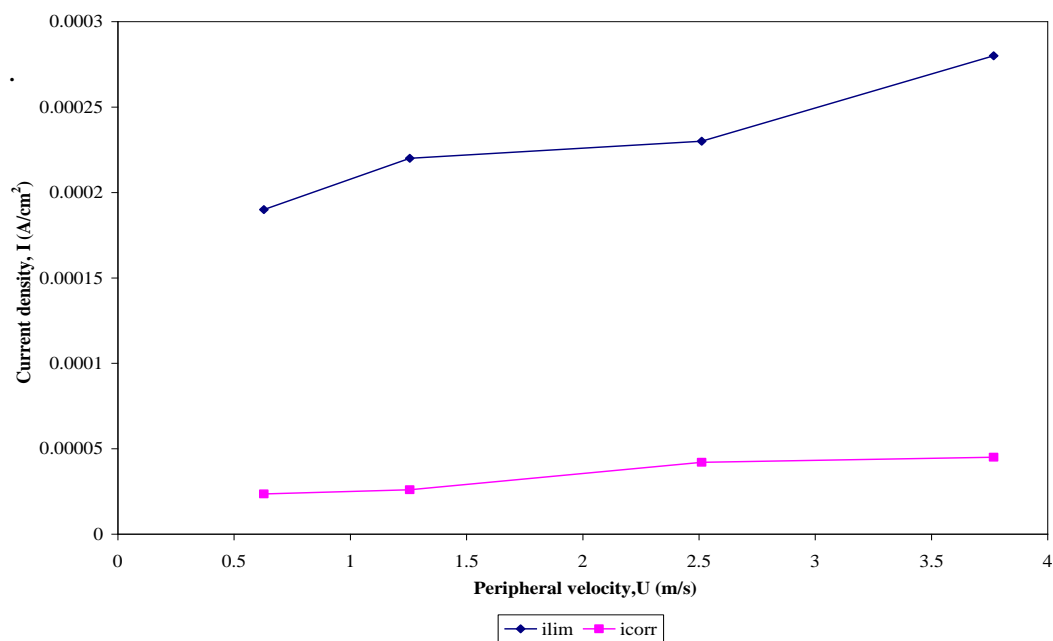


Figure 4.53: Comparison of the measured limiting current density (i_{lim}) with the corrosion current density (i_{corr}) at different peripheral velocity, pH 5, 40 ppm HAc, 25°C.

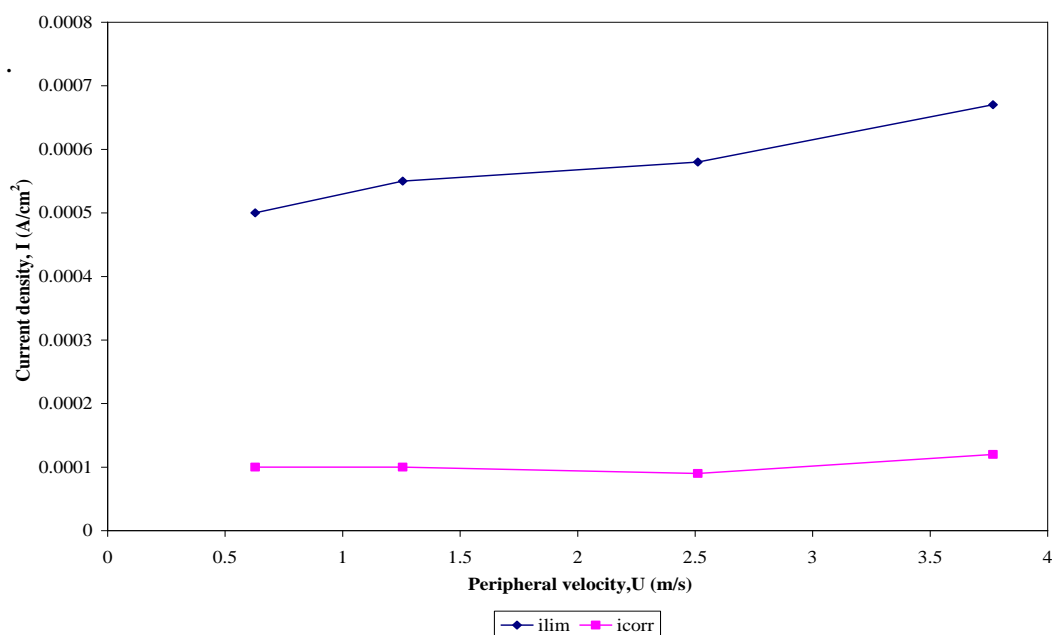


Figure 4.54: Comparison of the measured limiting current density (i_{lim}) with the corrosion current density (i_{corr}) at different peripheral velocity, pH 5, blank, 60°C.

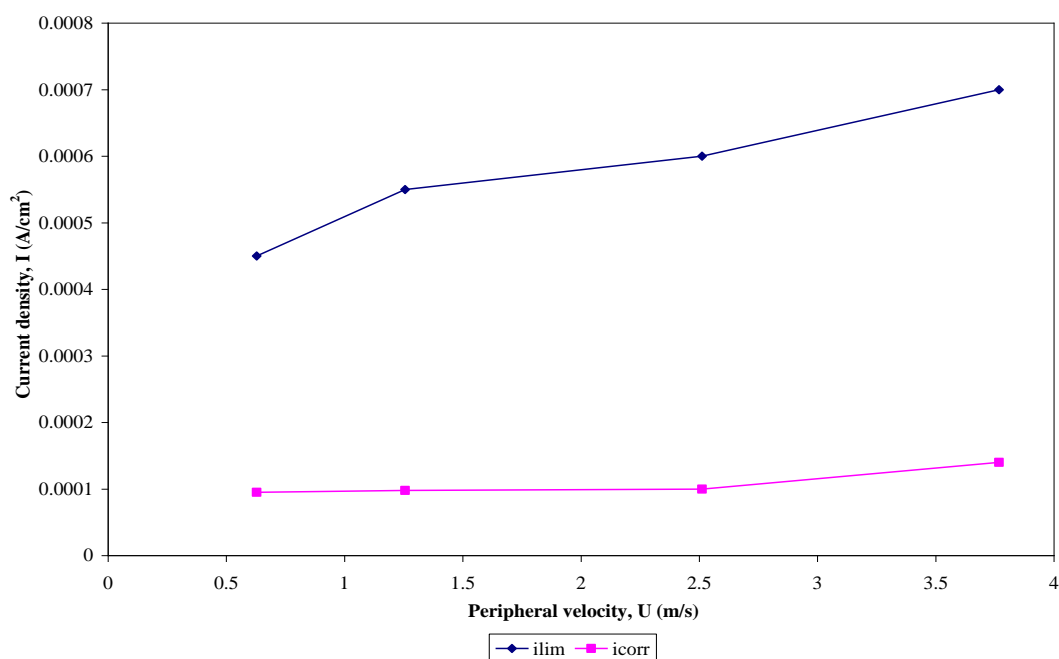


Figure 4.55: Comparison of the measured limiting current density (i_{lim}) with the corrosion current density (i_{corr}) at different peripheral velocity, pH 5, 10 ppm HAC, 60°C.

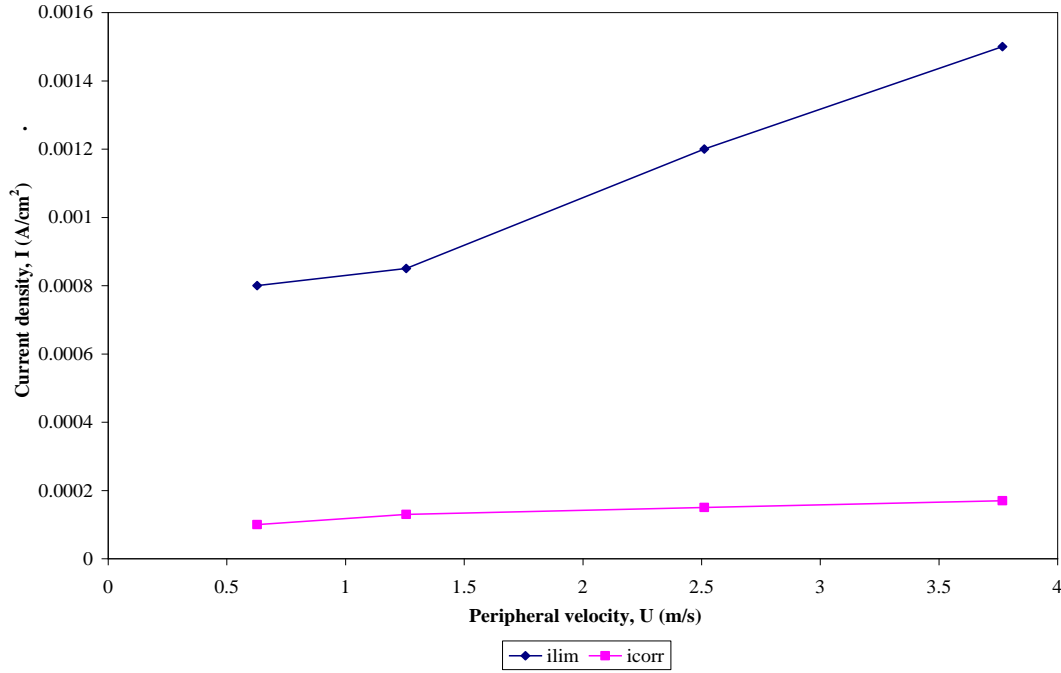


Figure 4.56: Comparison of the measured limiting current density (i_{lim}) with the corrosion current density (i_{corr}) at different peripheral velocity, pH 5, 40 ppm HAc, 60°C.

4.3 Comparison between Experimental Corrosion Rates and Open Available Predictive Models

The results from the RCE experiment are compared to the open available predictive models, namely: DWM 95, Cassandra 93/95 and NORSOK models. These open available predictive models, do not consider the effect of HAc in the analysis. DWM 95 and Cassandra 93/95 take velocity as input whereas NORSOK takes wall shear stress as input. The comparisons are shown in Figure 4.57 to Figure 4.62.

4.3.1 Comparison at pH 5

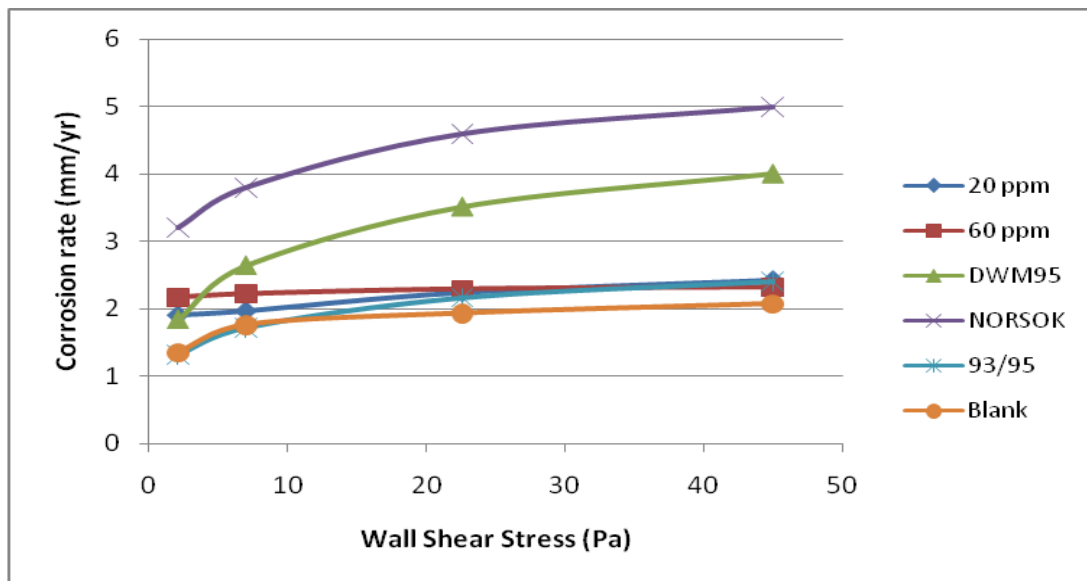


Figure 4.57: Comparison between experimental corrosion rates and predictive models at 25°C.

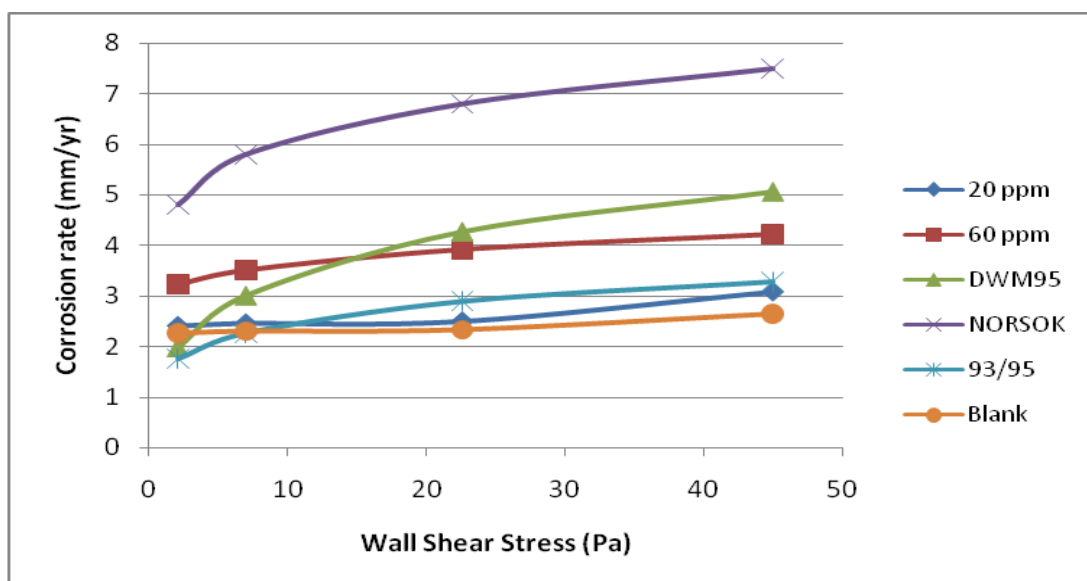


Figure 4.58: Comparison between experimental corrosion rates and predictive models at 40°C.

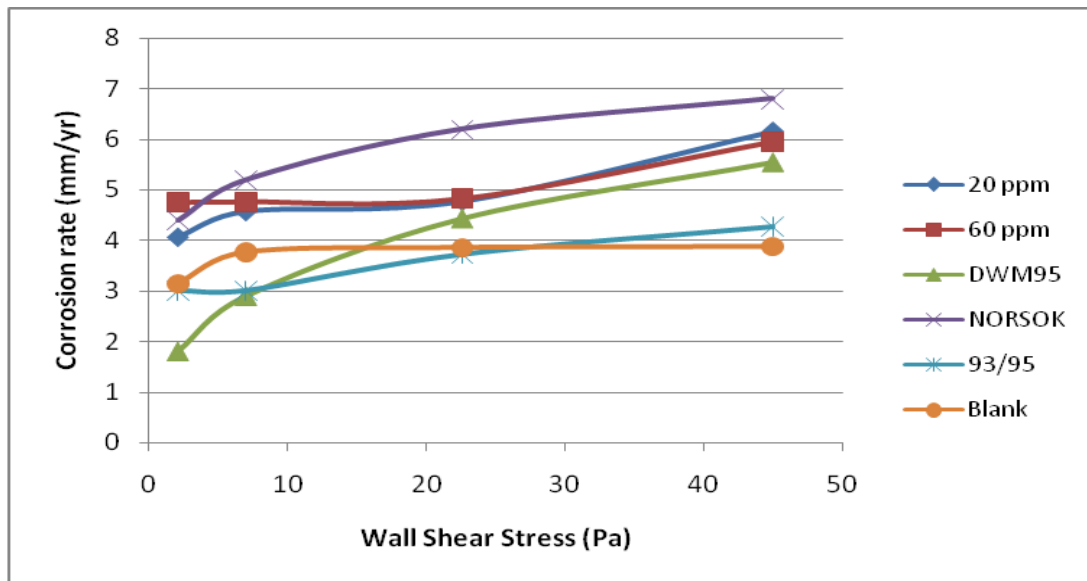


Figure 4.59: Comparison between experimental corrosion rates and predictive models at 60°C.

4.3.2 Comparison at pH 6

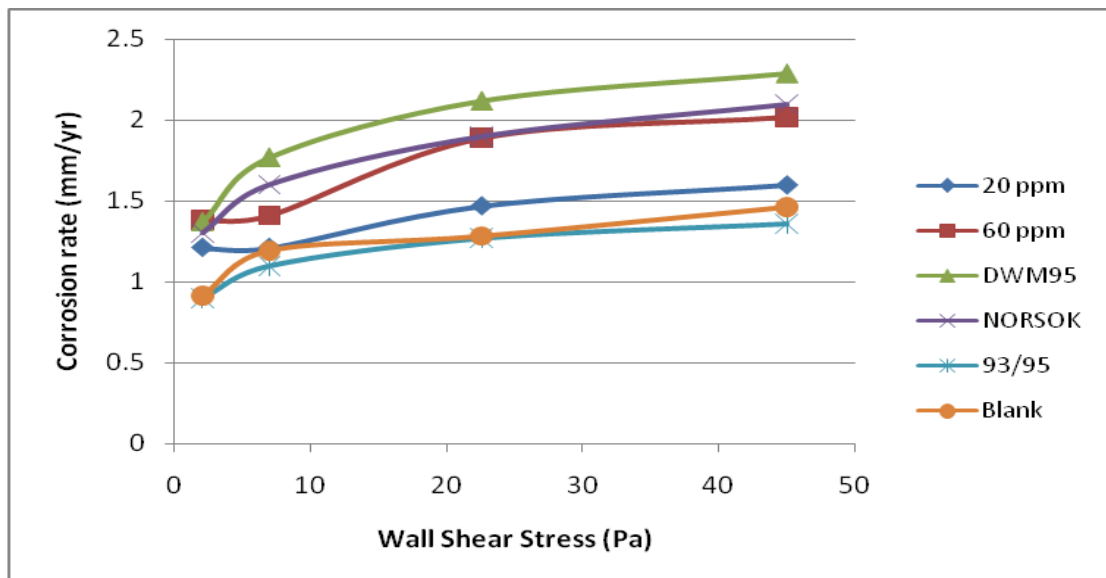


Figure 4.60: Comparison between experimental corrosion rates and predictive models at 25°C.

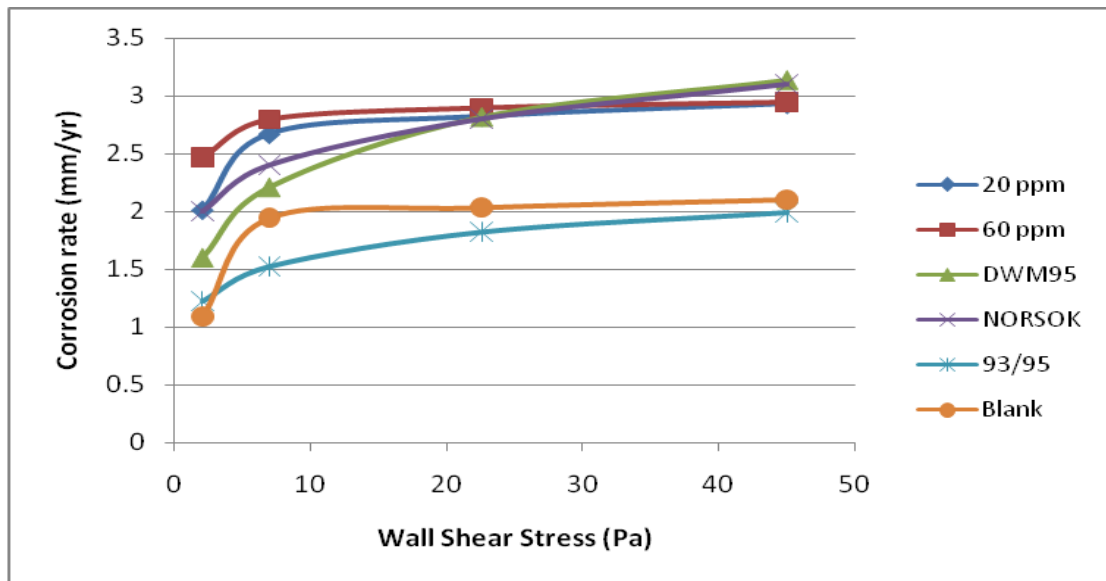


Figure 4.61: Comparison between experimental corrosion rates and predictive models at 40°C.

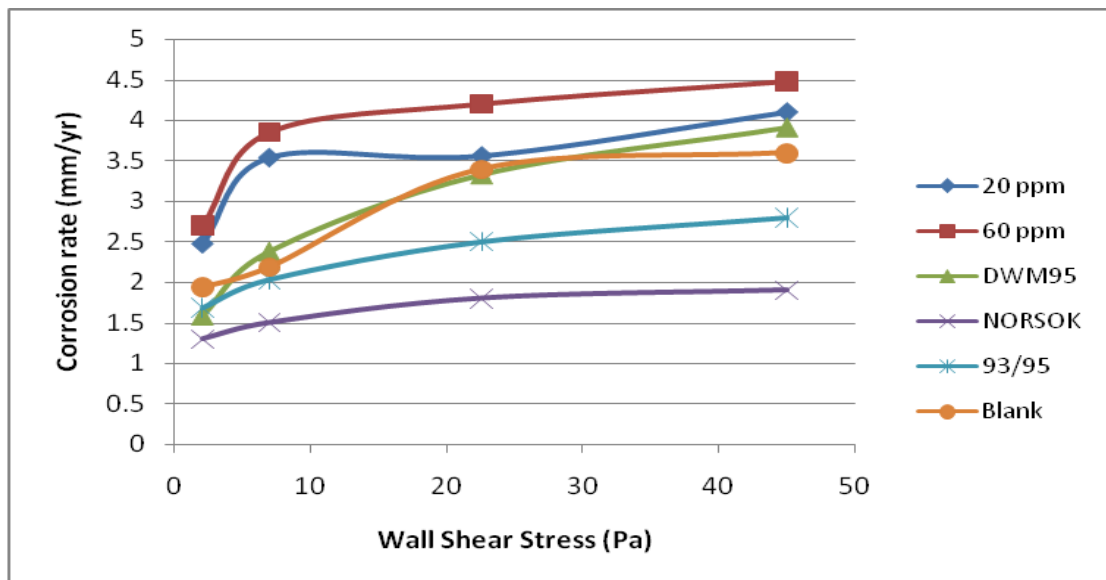


Figure 4.62: Comparison between experimental corrosion rates and predictive models at 60°C.

Based on the comparison results, it is observed that NORSOK, DWM 95 and Cassandra 93/95 models show similar behavior with experimental results. However, Cassandra 93/95 shows well correlation with blank experimental model than other models. Thus, Cassandra 93/95 model is preferable to be used in predict blank corrosion rate under turbulent flow conditions.

CHAPTER FIVE

CO₂ CORROSION PREDICTION WITH THE PRESENCE OF LOW CONCENTRATION OF HAc AT TURBULENT FLOW CONDITIONS

A corrosion prediction equation is developed based on the experimental results of the RCE flow-simulated tests conducted at pH 5, temperature 25°C, 40°C, and 60°C with various HAc concentrations and rotational rates. The RCE tests represent the turbulent-flow conditions. The prediction equation then validated against the predicted results from MULTICORP Version 4 software which consider the effect of HAc in the analysis.

5.1 Empirical Prediction Equation

5.1.1 RCE Tests at 25°C

The relationship between corrosion rate and HAc concentration is plotted at different rotation rates as shown in Figure 5.1 below. This relationship is plotted in Figure 5.2.

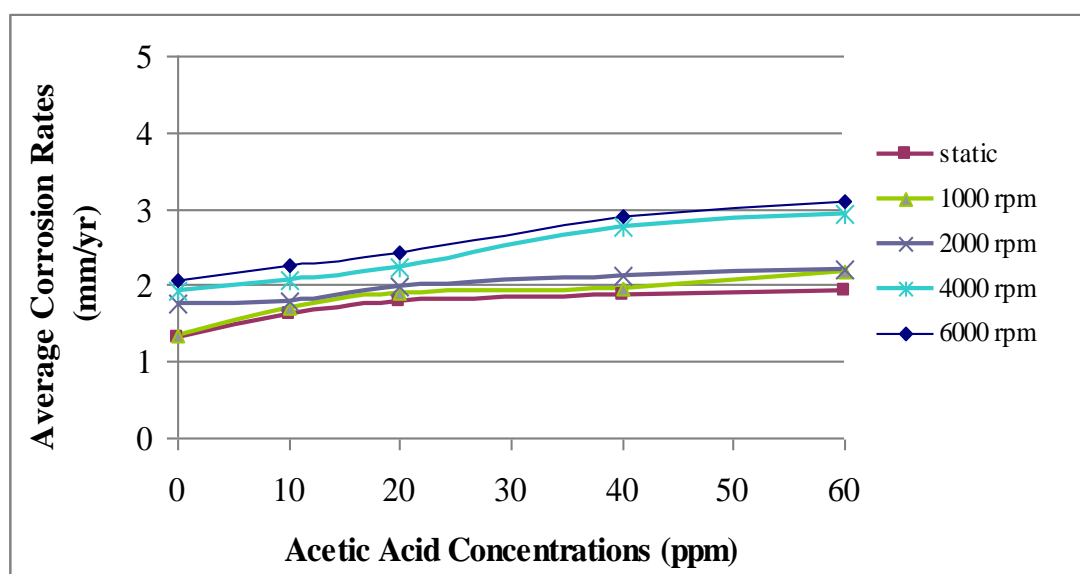


Figure 5.1: RCE tests at 25°C.

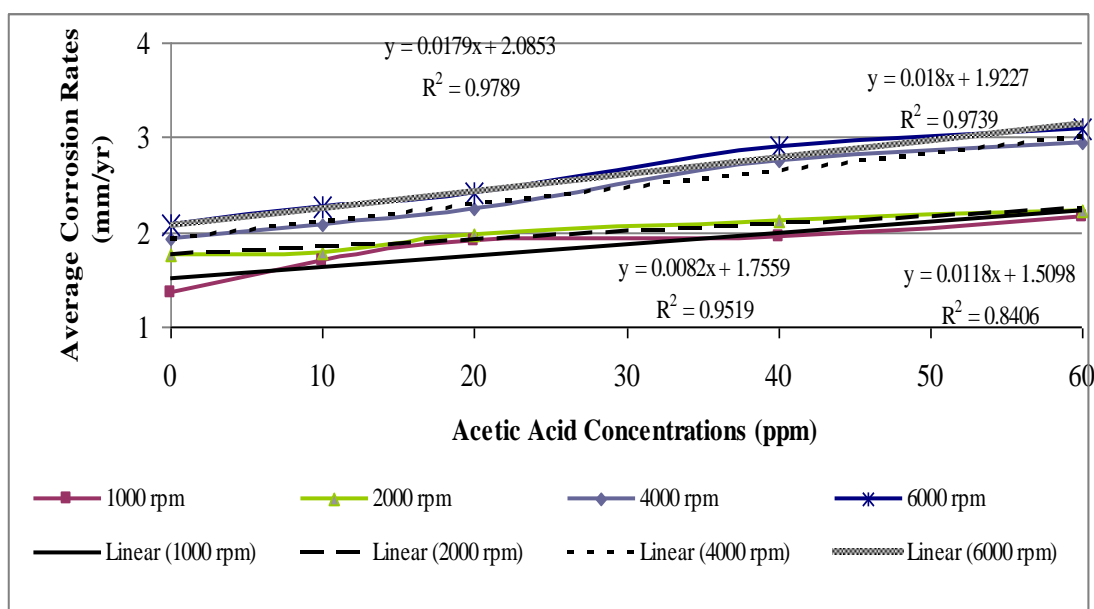


Figure 5.2: Prediction based on RCE tests at 25°C.

Corrosion rates vary linearly with the concentration of the added HAc. In general, this linear relationship can be represented by best-fit equations. The best-fit equations, as shown in the Figure 5.2, reveal a good correlation and suggest a good linear relationship between corrosion rate and the HAc. This relationship can be expressed as:

$$\text{Corrosion Rate (CR)} = \text{Corrosion rate of blank solution (CRb)} + \text{Constant} \times [\text{HAc}]$$

Where, [HAc] = concentration of acetic acid (ppm).

Thus, the corrosion rate of mild steel in CO₂ containing solution with the presence of HAc can be predicted by adding the contribution of the HAc to the blank corrosion rate.

The constant in the equation, which is the slope of the curve, varies with rotation rate and could be approximated by plotting the slopes against temperatures as shown in Figure 5.3.

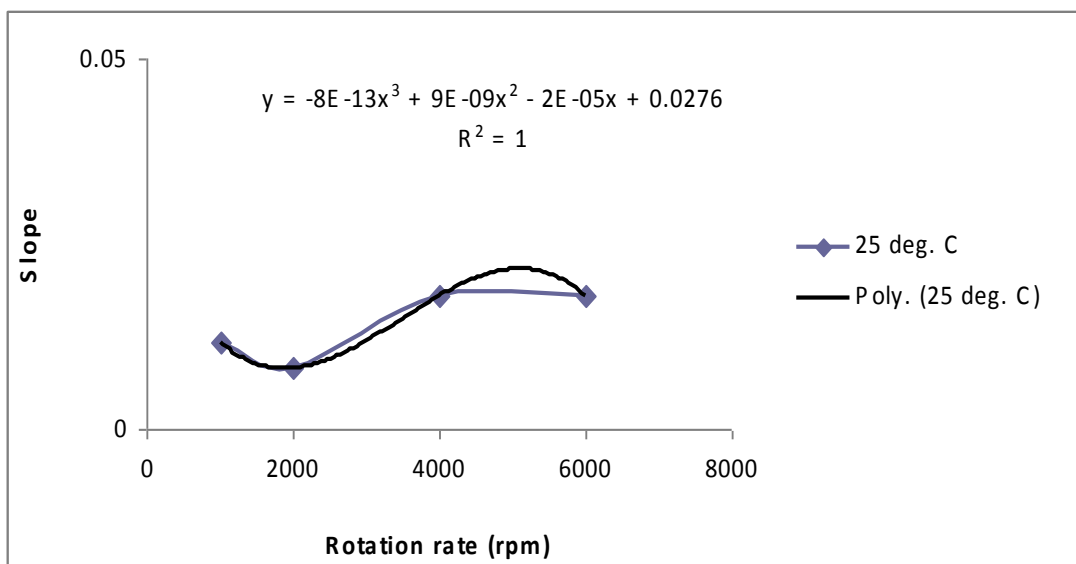


Figure 5.3: The variation of slopes with the rotation rate.

Thus, the corrosion rate prediction at 25°C can be expressed as:

$$\mathbf{CR = CRb + (-8E-13(R^3)+9E-09(R^2)-2E-05(R) + 0.0276) \times [HAc];} \quad (5.1)$$

Where CRb = Corrosion rate of blank solution, R = Rotation rate in rpm, [HAc] = concentration of acetic acid (ppm)

5.1.2 RCE Tests at 40°C

Similarly at 25°C, the relationship between corrosion rate and HAc concentration is plotted at different rotation rates as shown in Figure 5.4. The linear relationship is plotted in Figure 5.5.

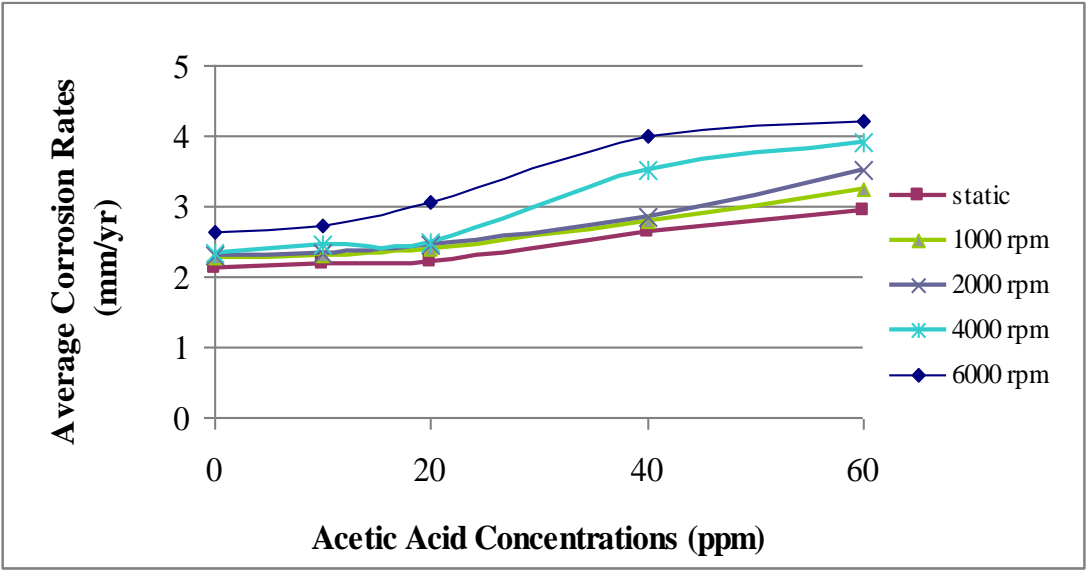


Figure 5.4: Relationship between corrosion rate and HAC concentration as plotted at different rotation rates at 40°C.

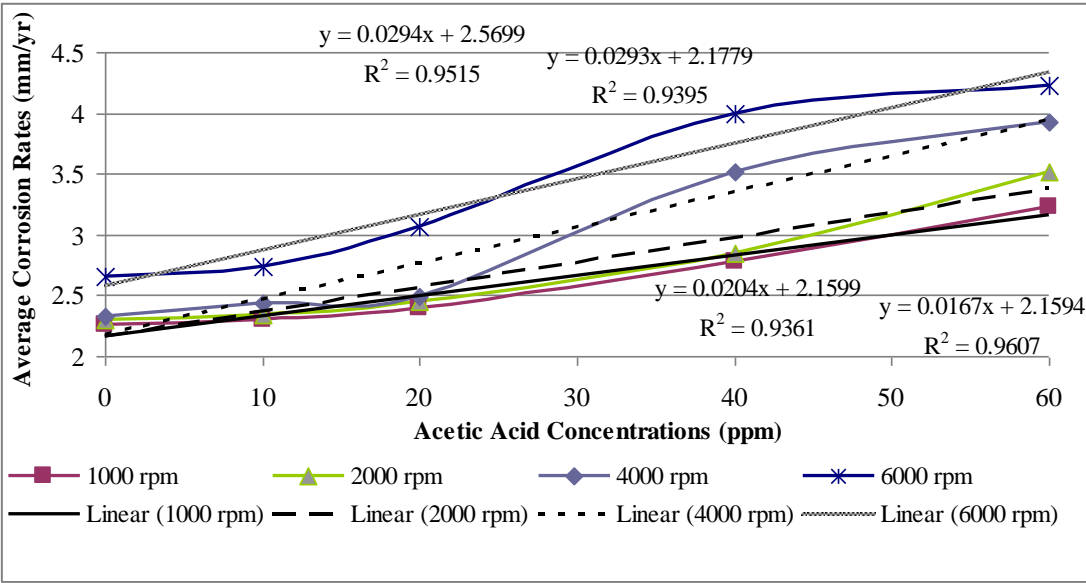


Figure 5.5: Best-fit equations for relationship between corrosion rate and HAC concentration as plotted at different rotation rates at 40°C.

The change of the slope with the rotation rate is plotted below.

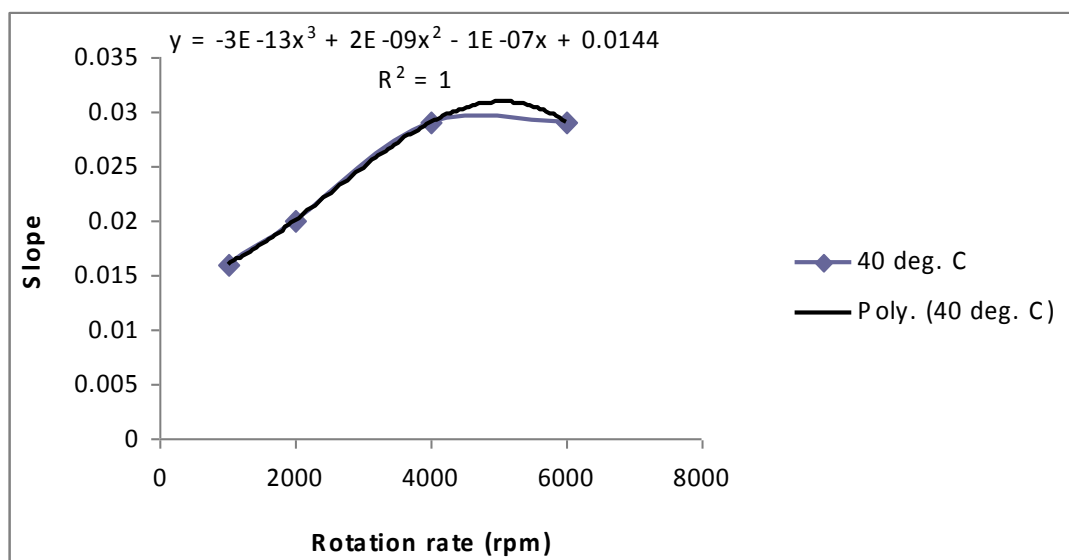


Figure 5.6: The variation of slopes with rotation rate.

Thus the corrosion rate prediction at 40°C can be expressed as:

$$\text{CR} = \text{CRb} + (-3\text{E}-13(\text{R}^3) + 2\text{E}-09(\text{R}^2) - 1\text{E}-07(\text{R}) + 0.0144) \times [\text{HAc}]; \quad (5.2)$$

Where CRb = Corrosion rate of blank solution, R = Rotation rate in rpm, [HAc] = concentration of acetic acid (ppm).

5.1.3 RCE Tests at 60°C

Similarly at 25 and 40°C, the relationship between corrosion rate and HAC concentration is plotted at different rotation rates as shown in Figure 5.7. The linear relationship is observed below 40 ppm, which is the inhibitive threshold of HAC concentration. This relationship is plotted in Figure 5.8.

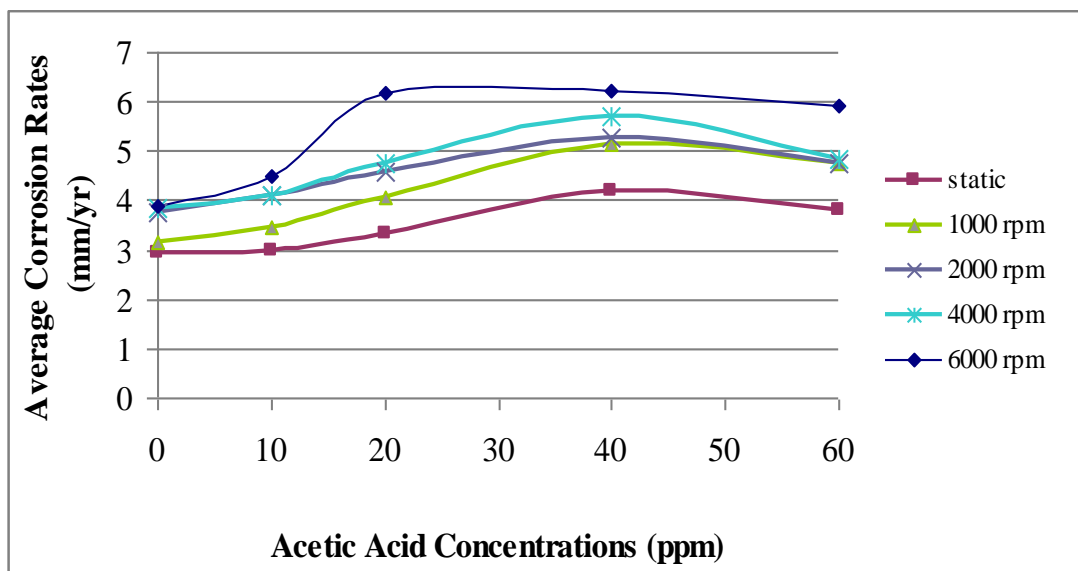


Figure 5.7: Relationship between corrosion rate and HAc concentration as plotted at different rotation rates at 60°C.

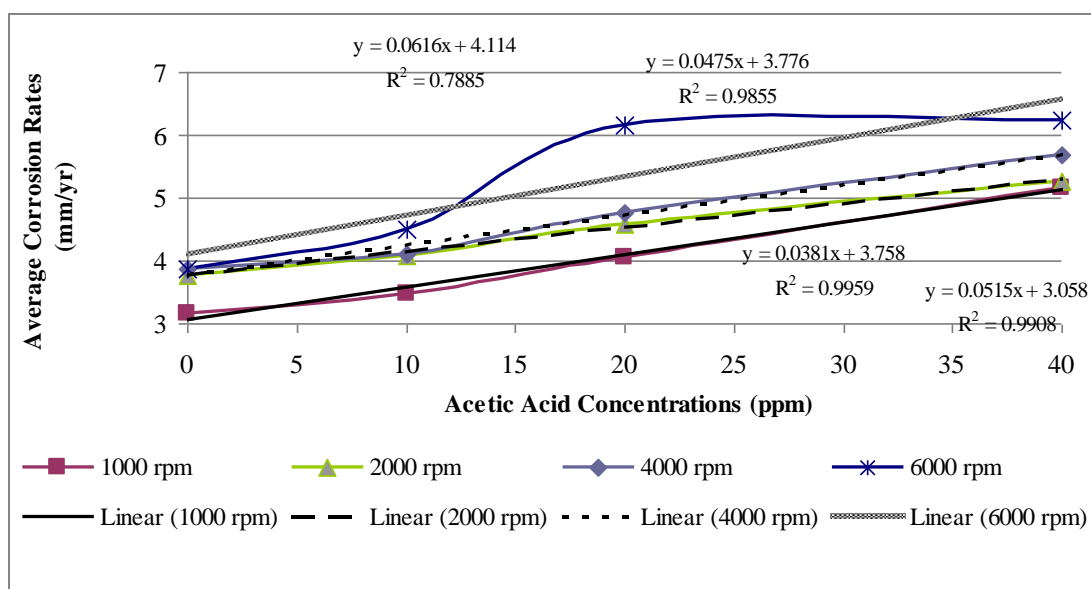


Figure 5.8: Best-fit equations for relationship between corrosion rate and HAc concentration as plotted at different rotation rates at 60°C.

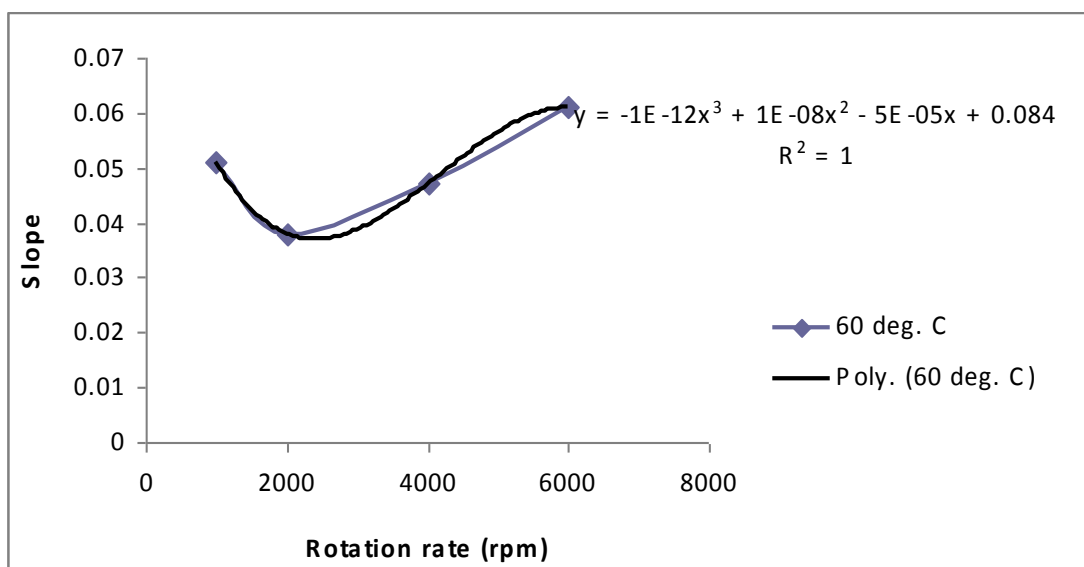


Figure 5.9: The variation of slopes with rotation rate.

Thus the corrosion rate prediction at 60°C can be expressed as:

$$\mathbf{CR = CRb + (-1E-12(R^3)+1E-08(R^2)-5E-05(R) + 0.084)x [HAc];} \quad (5.3)$$

Where CRb = Corrosion rate of blank solution, R = Rotation rate in rpm, [HAc] = concentration of acetic acid (ppm).

In order to include the effect of temperature in the prediction equation, the variation of the constants with the temperature at 25°C, 40°C and 60°C is plotted for each rotation rate and this is presented in Figure 5.10.

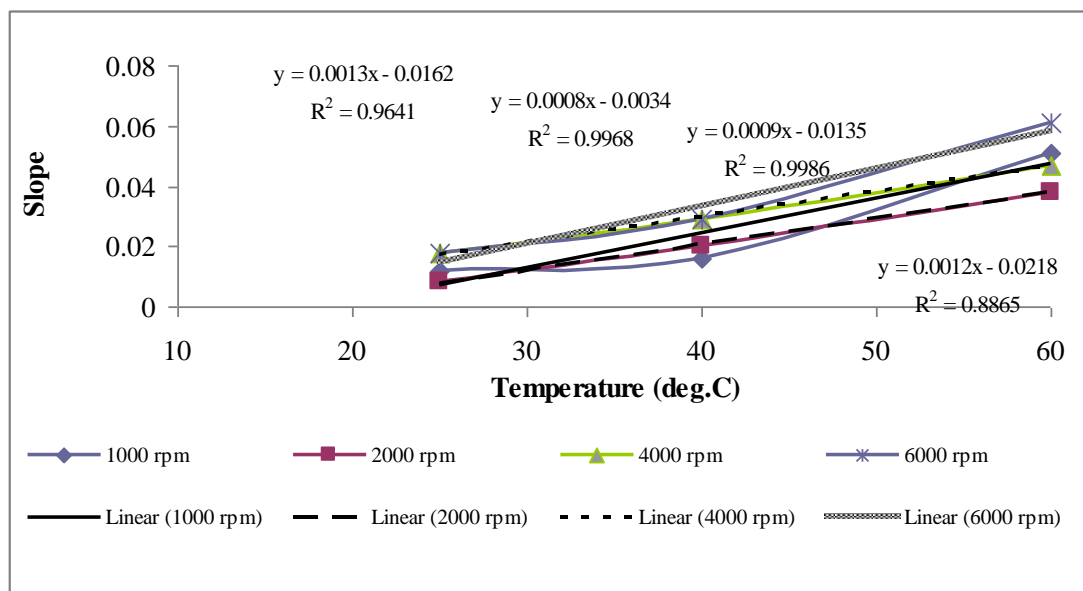


Figure 5.10: The variation of the constant with the temperature.

We observe that the corrosion rates are affected by the increase in rotation rate at temperature 25°C, 40°C and 60°C. The prediction equation can be expressed as

$$CR = CRb + (0.00105(T) - 0.01) \times [HAc]; \quad (5.4)$$

Where CRb = Corrosion rate of blank solution, R = Rotation rate in rpm, [HAc] = concentration of acetic acid (ppm).

5.2 Comparison of Prediction Equation and Commercial Prediction Model.

The comparison of the predicted corrosion rates based on the above prediction equation (using Cassandra (DWM 93/95) as the CRb) and commercial model are shown in Figure 5.11 to Figure 5.16. The comparisons are done at different conditions of pH 5 and 6 at temperature 25°C, 40°C and 60°C with various HAc concentrations and rotational rate. The prediction equation, derived from the RCE tests at pH 5 is taken as below.

$$\text{CR} = \text{Cassandra (DWM 93/95)} + (0.00105(T) - 0.01) \times [\text{HAc}]; \quad (5.5)$$

A well known commercial model, namely Multicorp version 4, is used to validate the above prediction equation in this study. Multicorp version 4 is built by Institute for Corrosion and Multiphase Technology, Ohio University based on mechanistic model that consider almost all aspects related to CO₂ corrosion of mild steel such as acetic acid and velocity effect.

5.2.1 Comparison at pH 5

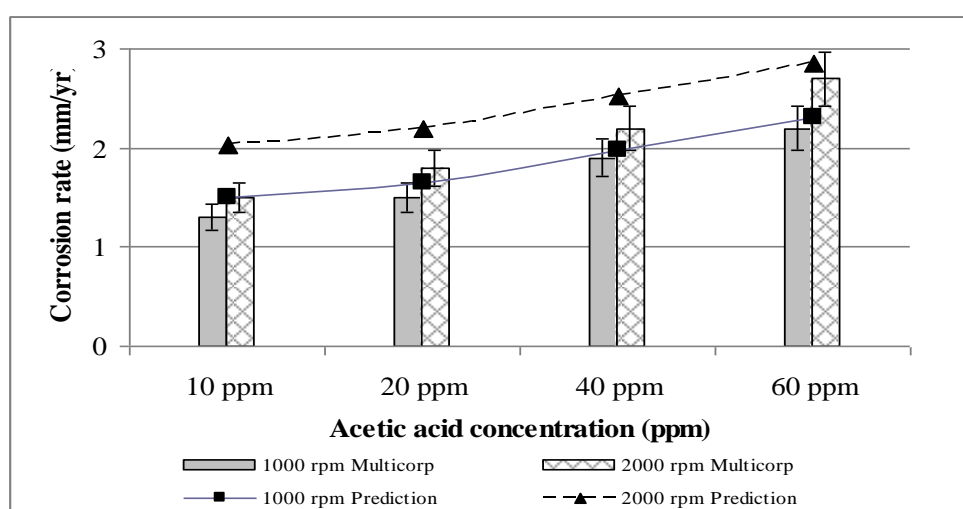


Figure 5.11: Comparison of prediction equation with experimental data at pH 5, 25°C, 1 bar CO₂. Error bars represent 10 % variant of predicted corrosion rate compared to Multicorp version 4 model.

At 25°C, the prediction equation has good agreement with the Multicorp model in 10 – 60 ppm HAc for 1000 and 2000 rpm. It is recorded approximately 15% of variant from prediction equation as compared to the Multicorp model.

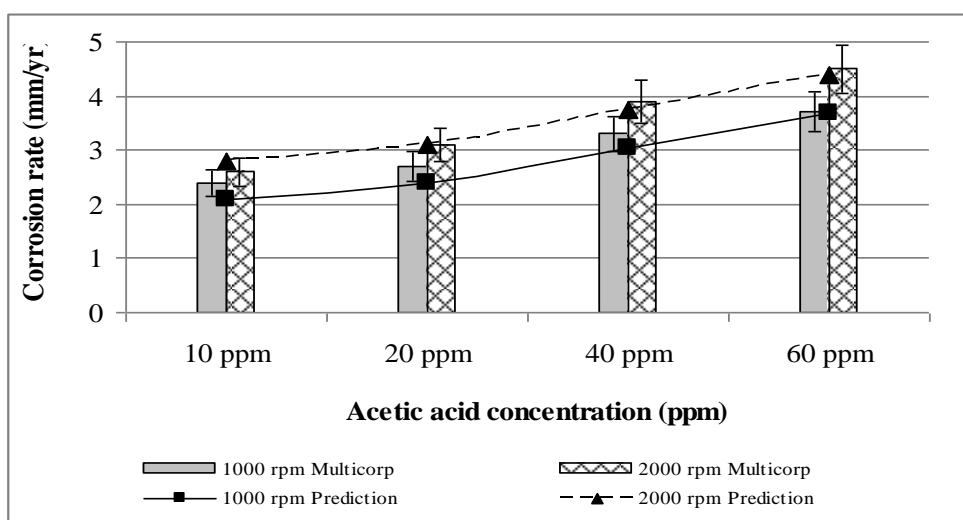


Figure 5.12: Comparison of prediction equation with experimental data at pH 5, 40°C, 1 bar CO₂. Error bars represent 10 % variant of predicted corrosion rate compared to Multicorp version 4 model.

At 40°C, the prediction equation has good agreement with the Multicorp model in all cases. It is recorded approximately 10% of variant from prediction equation as compared to the Multicorp model.

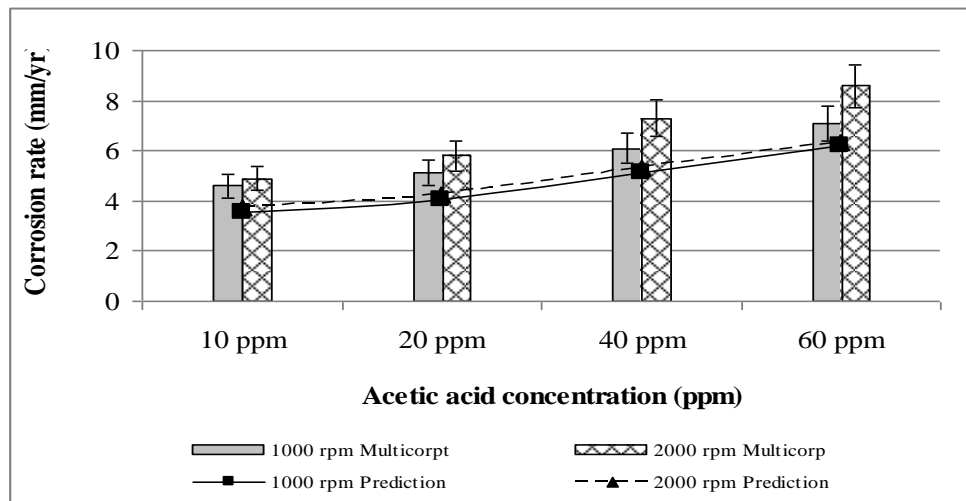


Figure 5.13: Comparison of prediction equation with experimental data at pH 5, 60°C, 1 bar CO₂. Error bars represent 10 % variant of predicted corrosion rate compared to Multicorp version 4 model.

At 60°C, prediction equation predicts lower corrosion rate approximately 20 % almost for all conditions.

5.2.2 Comparison at pH 6

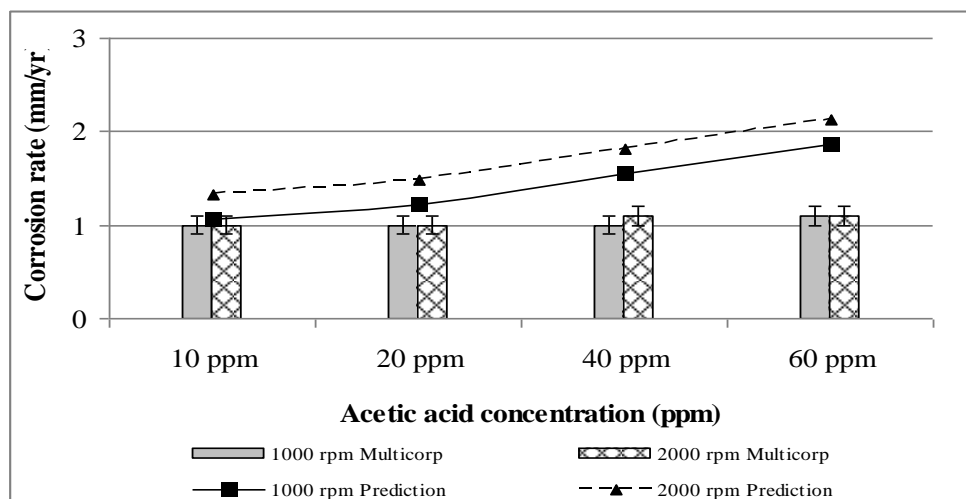


Figure 5.14: Comparison of prediction equation with experimental data at pH 6, 25°C, 1 bar CO₂. Error bars represent 10 % variant of predicted corrosion rate compared to Multicorp version 4 model.

At 25°C, the prediction equation predicts well at 1000 rpm with the presence of 10 ppm HAc. For other conditions, it predicts conservatively at all HAc concentrations.

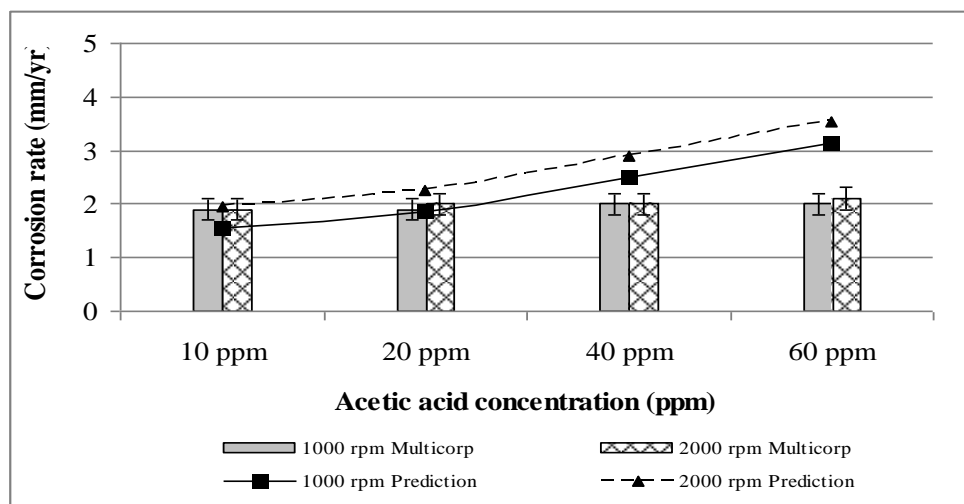


Figure 5.15: Comparison of prediction equation with experimental data at pH 6, 40°C, 1 bar CO₂. Error bars represent 10 % variant of predicted corrosion rate compared to Multicorp version 4 model.

At 40°C, the prediction equation predicts well for 1000 and 2000 rpm at 10 ppm and 20 ppm HAc. Over prediction, around 25%, is observed at 40 and 60 ppm HAc.

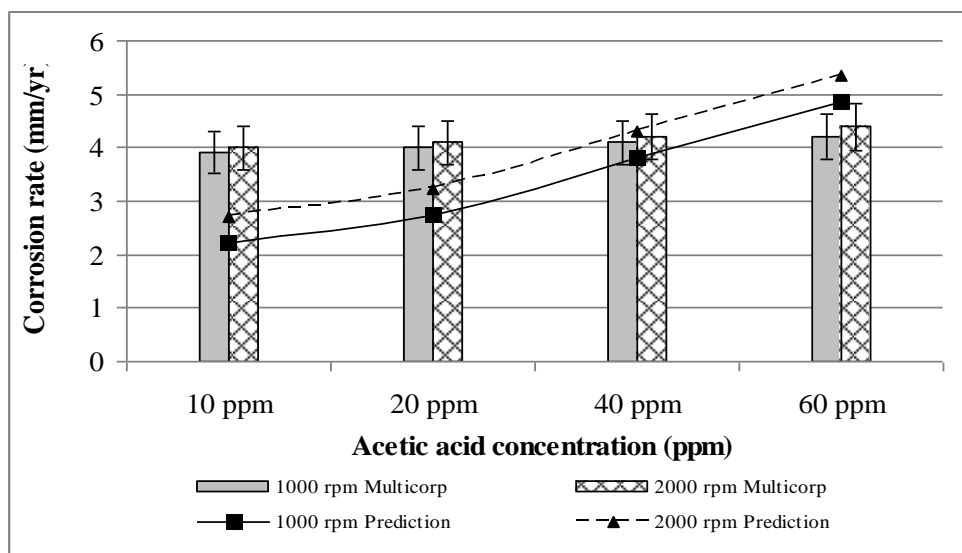


Figure 5.16: Comparison of prediction equation with experimental data at pH 6, 60°C, 1 bar CO₂. Error bars represent 10 % variant of predicted corrosion rate compared to Multicorp version 4 model.

At 60°C, the prediction equation has good agreement with Multicorp model in 40 ppm HAc for all rotation rates. At 10 ppm and 20 ppm HAc, the prediction equation calculate lower corrosion rate than Multicorp model approximately 20 %, while at 60 ppm, it predicts conservatively for all rotation rates.

In general, validation of prediction equation and Multicorp version 4 model show good agreement results. It is observed approximately 20 % the differences predicted corrosion rate between prediction equation and Multicorp version 4 model.

CHAPTER SIX

CONCLUSION

6.1 Conclusions

Based on LPR results, low concentration of HAc below 40 ppm does not contribute much to corrosion rates. An appreciable increase in corrosion rate is observed for HAc concentration more than 40 ppm, whereby a maximum increase of 68 % at pH 5 and 120 % at pH 6 depending on temperatures. The increase in corrosion rate is due to the change in cathodic reaction as shown by the potentiodynamic polarization sweeps. As reported by Crolet [31], HAc increases corrosion rate by extra cathodic reaction which results from dissociation of acetic acid and direct reduction of undissociated HAc molecules. It was also observed that there were no changes on anodic mechanism with the presence of HAc.

LPR tests also showed an increase of corrosion rate at higher temperature. This is due to acceleration of anodic and cathodic reaction when temperature increases, also this is related with availability of HAc species which is much more at higher temperature.

The corrosion rate is also influenced by the flow below 2000 rpm due to mixed cathodic reactions of mass transfer and charge transfer process. However, above 2000 rpm, the cathodic reactions is charge transfer process. It is indicated by corrosion current (i_{corr}) value lower than limiting current (i_{lim}) and do not depend on velocity.

Simulation results of free available CO₂ corrosion prediction models showed that Cassandra 93/95 has good agreement with blank experimental results. Unfortunately, Cassandra 93/95 does not accommodate the presence of HAc. Thus, an empirical model was built which accounts for the effect of HAc species. Corrosion rate of carbon steel in CO₂ corrosion under turbulent flow conditions with the presence of low concentrations HAc can be predicted by following equations:

$$\mathbf{CR = CRb + (0.00105(T) - 0.01) \times [HAc];} \quad (6.1)$$

Where CRb = Corrosion rate of blank solution of any model, T = Temperature (°C), [HAc] = concentration of acetic acid (ppm).

Since Cassandra 93/95 model has good agreement with blank experimental results, it is prefer to calculate the CRb in the equation above using Cassandra 93/95 model. Thus, the equation becomes:

$$\mathbf{CR = Cassandra (DWM 93/95) + (0.00105(T) - 0.01) \times [HAc];} \quad (6.2)$$

The comparison of prediction equation above and Multicorp version 4 model has produced good agreement results. The difference in results of predicted corrosion rate around 20 % were noted almost in most cases.

6.2 Future Work

The prediction equation is built at CO₂ partial pressure of 1 bar. We know that CO₂ partial pressure plays an important role to determine the corrosion rate. Thus, other studies must be done to see the effect of high pressure to the corrosion rate. The studies can be conducted by the use of autoclave or flow loop pipe test.

As based on literature review, the presence of protective film on CO₂ corrosion could decrease the corrosion rate. Some studies have been conducted to see the effect of protective film on CO₂ corrosion, but it was done on static conditions. Thus, further studies must be performed to observe the film formation growth with the presence of HAc under turbulent conditions. The studies can be conducted by the use of Scanning Electron Microscopy (SEM), X-ray Diffraction (XRD), X-ray Photoelectron Spectroscopy (XPS) and other visual morphological methods. SEM and metallurgical microscopy can be used to examine surface morphology. X-ray Diffraction (XRD)

and X-ray Photoelectron Spectroscopy (XPS) can be used to identify the structure and composition of the films.

REFERENCES

1. Moraes F.D., Characterization of Iron Carbonate Scales Developed under CO₂ Corrosion Conditions, Ph.D Thesis, The University of Tulsa, 1999.
2. Nafday O.A., Film Formation and CO₂ Corrosion in The Presence of Acetic Acid, Thesis, Ohio University, 2004.
3. Yang K.S. et al., Numerical Study of Turbulent Flow Around a Rotating Cylinder with Backward-Facing Steps, 39th Aerospace Sciences Meeting and Exhibit, Paper No. 0451, 2001.
4. Crolet J.L., Thevenot, N., and Dugstad, A., Role of Free Acetic acid on the CO₂ Corrosion of Steels, CORROSION/1999, Paper No. 24, Houston, TX: NACE International, 1999.
5. George K.S., Electrochemical Investigation of Carbon Dioxide Corrosion of Mild Steel in the Presence of Acetic Acid, M.Sc Thesis, Ohio University, 2003.
6. Sun, Y., George, K., and Nesic, S., The Effect of Cl⁻ and Acetic Acid on Localized CO₂ Corrosion in Wet Gas Flow, Corrosion/2003, Paper No. 03327, NACE International, Houston, Texas, 2003.
7. George, K., Wang, S., Nesic, S. and C.deWaard, Modeling of CO₂ corrosion of Mild Steel at High Pressures of CO₂ and in the presence of Acetic Acid, Corrosion /2004, Paper No. 04623, NACE International, 2004.

8. George K.S., Nesic.S., Investigation of Carbon Dioxide Corrosion of Mild Steel in the Presence of Acetic Acid – Part 1: Basic Mechanisms, Corrosion/2007, Paper No. 07020178, NACE International, Houston, Texas, 2007.
9. Nafday O.A., Nesic S., Iron Carbonate Scale for motion and CO₂ corrosion in the Presence of Asetic Acid, Corrosion/2005, Paper No. 05295, NACE International, Houston, Texas, 2005.
10. Ismail, M.C., Prediction of CO₂ Corrosion with the Presence of Acetic Acid, Ph.D Thesis, School of Materials, Corrosion and Protection Centre, University of Manchester, UK, 2005.
11. Gulbrandsen, E., and Bilkova, K., Solution Chemistry Effects on Corrosion of Carbon Steels in Presence of CO₂ and Acetic Acid, Corrosion/2006, Paper No. 06364, NACE International, Houston, Texas, 2006.
12. CO₂ Corrosion Rate Calculation Model; Norsok Standard No.M-506, <http://www.nts.no/norsok> (Oslo: Norwegian Technology standards Institution), 1998.
13. Webster, S., McMahon, A.J., BP Report No. 1993-220483, 1993.
14. de Waard, C., Lotz, U., and Milliams, D.E., Carbonic Acid Corrosion of Steel, Corrosion, Paper No. 31(5): p. 13-135, 1975.
15. de Waard, C., Lotz, U., and Milliams, D.E., Predictive Model for CO₂ Corrosion Engineering in Wet Natural Gas Pipelines, Corrosion, Paper No. 47(12): p. 976-985, 1991.

16. de Waard, C., and Lotz, U., Prediction of CO₂ Corrosion of Carbon Steel, Corrosion/93, NACE International, Huston, Texas, 1993.
17. de Waard, C., Lotz, U. and Dugstad, A., Influence of Liquid Flow Velocity on CO₂ Corrosion, Corrosion/95, NACE International, Huston, Texas, 1995.
18. Fatah, M.C., Ismail, M.C., and Kurniawan, B.A., Comparison of CO₂ Corrosion Prediction Models based on Field and Experiment Data, Paper No. PR-03-0, International Conference on Plant and Reliability Management (ICPER), Universiti Teknologi PETRONAS, Malaysia, 2008.
19. Woollam, R.C., and Hernandez, S.E., Assessment and Comparison of CO₂ Corrosion Prediction Models, Paper No. 100673, SPE, UK, 2006.
20. J.K. Heuer, J.F. Stubbins, An XPS Characterization of FeCO₃ films from CO₂ Corrosion, Corrosion Science (1231-1243), 1999.
21. Kermani, M.B., Harrop, D., The Impact of Corrosion on the Oil and Gas Industry, J. SPE Production Facilities 8, Paper No. 186-190, 1996 .
22. Dayalan, E., et al., Modelling CO₂ Corrosion of Carbon Steel in Pipe Flow, Corrosion 95, NACE International, Paper No.118, Houston, Texas, 1995.
23. Pots, D.F.M, Mechanistic Models for The Predictions of CO₂ Corrosion Rates under Multiphase Flow Conditions, Corrosion/ 95, Paper No. 137, NACE International, Houston, Texas, 1995.
24. Kermani M.B, Morshad A, Carbon Dioxide Corrosion in Oil and Gas Prediction – A Compendium, Corrosion/2003; Vol 59, No.8, 2003.

25. Hedges, B. and McVeigh, L., The Role of Acetate in CO₂ Corrosion: The Double Whammy, Corrosion/1999: NACE International, Houston, Texas, 1999.
26. Nesic, S., Postlethwaite, J., and Vrhovac, M., CO₂ Corrosion of Carbon Steel – from Mechanistic to Empirical Modelling, Corrosion Reviews, Paper No. 15 (1-2), 1997.
27. Nyborg, R., Overview of CO₂ Corrosion Models for Wells and Pipelines. Corrosion/2002, NACE International, Houston, Texas, 2002.
28. Wang, H., and Nesic, S., CO₂ Corrosion Model Verification using Field Data, Corrosion/2006, Paper No.06567, NACE International, Houston, Texas, 2006.
29. Ports, B.F.M., et.al., Improvements on De Waard-Milliams Corrosion Prediction and Application to Corrosion Management, Corrosion/2002, Paper No. 02235, NACE International, Houston, Texas, 2002.
30. <http://www.gly.bris.ac.uk>, December 2006.
31. Crolet, J.L., Bonis, M.R., The Role of Acetates Ions in CO₂ Corrosion, Corrosion/1983, NACE International, Houston, Texas, 1983.
32. Kharaka, Y.K., Solmineq 88: A Computer Program for Geochemical Modeling of Water-rock Interactions, Alberta Research Council, Menlo Park, CA, 1989.
33. Wang, S., George, K., and Nesic S, High Pressure CO₂ Corrosion electrochemistry and the Effect of Acetic Acid, Corrosion/2004, Paper No. 04375, NACE International, Houston, Texas, 2004.

34. Abayarathna, A., and Naraghi, A., Inhibition of CO₂ Corrosion of Carbon Steel in the Presence of Acetate, Corrosion/2002, Paper No.291, Houston, TX: NACE International, 2002.
35. Dourghety, J.A., A Review of the Effect of Organic Acids on CO₂ Corrosion, Corrosion/2004, Paper No.04376, NACE International, 2004.
36. Dugstad A, Fundamental Aspects of CO₂ Metal Loss Corrosion Part I: Mechanism, Corrosion/2006, Paper No. 06111, NACE International, Houston, Texas, 2006.
37. Johnson, M.L., Thomson, M.B., Ferrous Carbonate Precipitation Kinetics and Its Impact on CO₂ Corrosion, Corrosion/1991, Paper No.268, NACE International, Houston, Texas, 1991.
38. Paisley, D., Barret, N., and Wilson, O., Pipeline Failure : The Roles Played by Corrosion, Flow and Metallurgy, NACE International, Paper No. 18, NACE International, Houston, Texas, 1999.
39. Van Hunnick E.W.J., B.F.M Pots and E.I.J.A. Hendriksen, The Formation of Protective FeCO₃ Corrosion Product Layers in CO₂ Corrosion, Corrosion/1996, Paper No.6, NACE International, Houston, Texas, 1996.
40. Chiltorn, T.H and Colburn, A.P., Ind.Engineering Chem.26, 1183, 1934.
41. Berger, F.P. and Hau, K.F., Mass Transfer in Turbulent Pipe Flow Measured by the Electrochemical Method, J.Heat Mass Transfer, Vol.20, p.1185-1194, 1977.
42. Silverman, D.C., Corrosion 90, NACE, Paper 13, 1990.

43. Bernardus F.M. Pots, Edwin L.J.A. Hendriksen, and J.F. Hollenberg, What are the Real Influences of Flow on Corrosion, Corrosion/2006, Paper No. 06591, NACE International, Houston, Texas, 2006.
44. Poulson, B., Plat Corrosion, Predictions of Materials Performance, Strutt, J.E and Nickolls, J. (eds) Eihshorward, Chichester, 1987.
45. Mendoza, J.L.M., and Turgoose, S., Influence of Turbulent Flow on the Localised Corrosion Processes of Mild Steel With Inhibition Aqueous CO₂ Systems, Corrosion/2001, Paper No.01063, NACE International, 2001.
46. Gabe, D.R., The Rotating Cylinder Electrode, Journal of Applied Electrochemistry, Volume 4, p. 91 – 108, 1974.
47. PINE, Study of Mass-Transport Limited Corrosion Using Pine Rotating Cylinder Electrode, Technical Note 2006-01, PINE Research Instrumentation, USA, 2006.
48. Gabe, D.R., Walsh, F.C., The Rotating Cylinder Electrode: A Review of Development, Journal of Applied Electrochemistry 13, 1983.
49. Silverman, D.C., The Rotating Cylinder Electrode for Examining Velocity – Sensitive Corrosion – A Review, Corrosion-Vol. 60, No. 11, NACE International, Houston, Texas, 2004.
50. Efird, K.D., Flow Accelerated Corrosion Testing Basics, Corrosion/2006, Paper No.06689, NACE International, Houston, Texas, 2006.

51. Schmit, G., and Bakalli, M., A Critical Review of Measuring Techniques for Corrosion Rates Under Flow Conditions, Corrosion/2006, Paper No. 06593, NACE International, Houston, Texas, 2006.
52. Eisenberg, M., Tobias, C.W., Wilke, C.R., Ionic Mass Transfer and Concentration Polarisation on Rotating Electrodes, J.Electrochem.Soc., 101, p. 306, 1954.
53. Silverman, D.C., Rotating Cylinder Electrode for Velocity Sensitivity Testing, Corrosion/1984, Vol.40 No.5, NACE International, 1984.
54. Turgoose, S., Dawson, J.L., Palmer, J.M., Rizk, T., Corrosion 95, NACE, Paper 112, 1995.
55. Silverman, D.C., Technical Note: Conditions for Similarity of Mass-Transfer Coefficients and Fluid Shear Stresses Between the Rotating Cylinder Electrode and Pipe, Corrosion/2005, Vol.61 No.6, NACE International, 2005.
56. Stern, M, Geary, A.L, Theoretical Analysis of the Shape of the Polarisation Curves, Journal Electrochemical Society, v. 104 (10), p 56-63, 1957.
57. Plummer, L.N. and Busenberg, E., Geochimica et Cosmochimica Acta. 46 1011, 1982.
58. Palmer, D.A., Van Eldik, R., Chem. Rev., 83, p. 651, 1983.
59. Vetter, K.J., electrochemical Kinetics – Theoretical and Experimental Aspects, Academic Press, New York, p.506, 1967.
60. Perry, R.H., Green, D., Perry's Chemical Engineers' Handbook, 50th ed, McGraw-Hill, 1984.

61. Schmitt, G. and Rothmann, B., Studies on the Corrosion Mechanism of Unalloyed Steel in Oxygen-Free Carbon Dioxide Solutions, Part II. Kinetics of Iron Dissolution” in” CO₂ Corrosion in Oil and Gas Production – Selected Papers, Abstracts and References, Newton L.E., Hausler R.H (eds), NACE T-1-3, NACE, USA, p. 163, 1984.
62. Mendoza-Flores, J., Turgoose, S., Corrosion/1995, Paper No.124, NACE International, Houston, Texas, 1995.
63. Atkins, P.W., Physical Chemistry, 5th Ed, Oxford University Press, UK, 1994.
64. Garsany, Y. and Pletcher, D., The Role of Acetate in CO₂ Corrosion of Carbon Steel: Has the chemistry been Forgotten?, Corrosion/2002, NACE International, Houston, Texas, 2002.